OWL-CSR-ESO-00000-0160

Issue: V1.0

Date: 25.10.2005

OWL Instrument Concept Study

COsmic Dynamics EXperiment

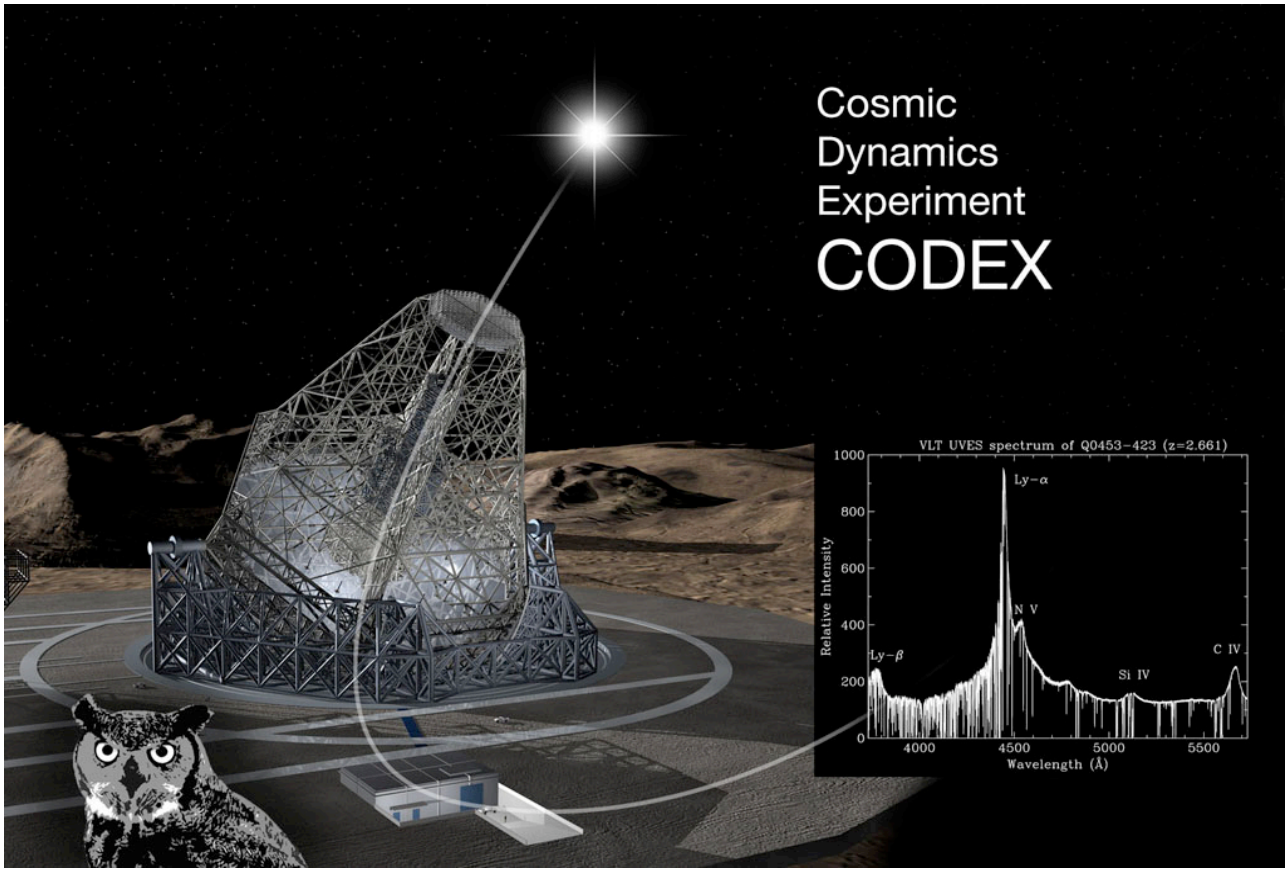

This document has been prepared by

L. Pasquini (Study Coordinator), H. Dekker (ESO), S. Cristiani, P. Molaro (INAF-OAT), F. Pepe (Obs. Geneve), M. Haehnelt (IoA Cambridge)

with inputs from the **CODEX** Team**:**

G. Avila, B. Delabre, S. D'Odorico, J. Liske, P. Shaver (ESO); P. Bonifacio, S. Borgani, V. D'Odorico, E. Vanzella (INAF-OAT); M. Dessagues, C. Lovis, M. Mayor, D. Queloz, S. Udry (Obs. Geneve); M. Murphy & M. Viel (IoA Cambridge); F. Bouchy (OHP and IAP), A. Grazian (INAF-OAR), S. Levshakov (St.Petersburg), L. Moscardini (Bologna University), T. Wiklind (ESA-STScI), S. Zucker (Tel Aviv)

Acknowledgements: We thank **J. Boxheimer** for her help to solve some graphical problems, **E. Janssen** for producing the CODEX logo and **I. Bronnert** for her patient assembly work.

TABLE OF CONTENTS

1. CODEX - Executive Summary

The **COsmic Dynamics EXperiment (CODEX)** is one of the proposed instruments for OWL (the ESO flavor of an ELT). In the framework of the OWL Observatory Concept Study being prepared under assignment by the ESO Council, eight instrument concepts have been explored in collaboration between ESO and various institutes in Europe. The study of CODEX is a collaboration between ESO, the IoA in Cambridge, the Observatoire de Geneve and INAF-Osservatorio di Trieste.

The primary aim of CODEX is to perform for the first time a direct dynamical measurement of the acceleration of the Universe.

Building on the experience that ESO acquired with the High Accuracy Radial velocity Planet Searcher (HARPS), we propose to build an extraordinary stable array of high resolution spectrographs, capable of obtaining a radial velocity precision almost two order of magnitudes more accurate than current capabilities. CODEX will measure the acceleration of the Universe , simply acquiring two series of spectra with a time interval of 10 years or more towards many lines of sight towards z~1 to z~4 Quasars, and measuring directly the shift that has occurred in the intervening Lyα forest and metallic lines due to the change in the cosmic expansion rate (cf. Figure 1-1 for an example of the measurements). This objective is very challenging. It requires a velocity accuracy of around 1 cm/sec over ten years, almost 2 orders of magnitudes better than the best present experiments. Nevertheless the extensive simulations which we have performed show that the goal is attainable if a sufficient S/N ratio is obtained, and that such a S/N ratio can be obtained with a reasonable amount of observing time with OWL.

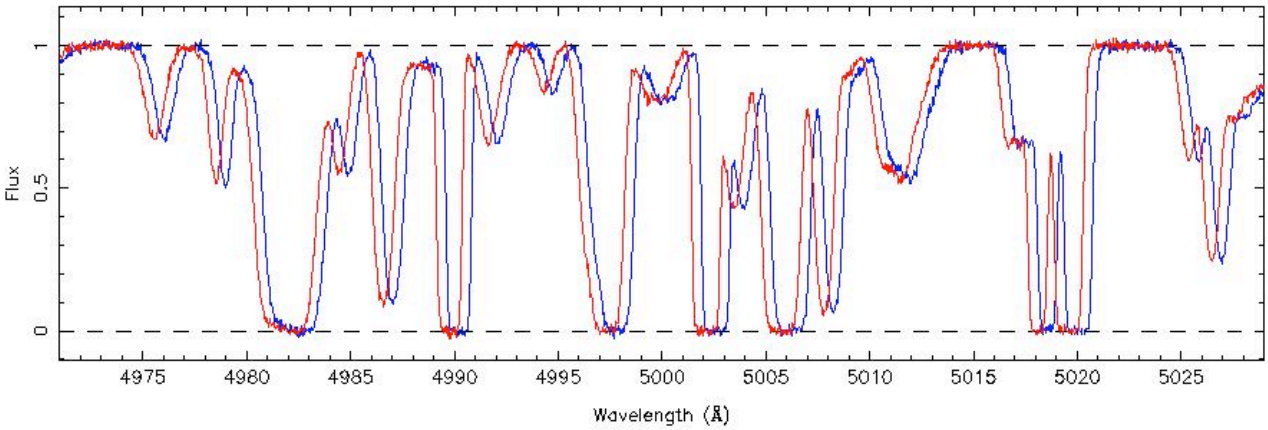

Figure 1-1*: Small portion of a simulated Ly□ forest spectrum. The simulation represents two observations of the same object taken at a time T_0 (Blue curve) and at a time T_0+10^7 years (Red curve). The shift is clearly visible. In the proposed experiment, with a baseline of 10 years, the two spectra would be indistinguishable by eye, and the shift is detected only through a proper statistical analysis of the data.*

While other future experiments are expected to measure cosmological parameters (Ω_m, λ) with high accuracy through measurements of the geometry of the Universe, CODEX will be the only experiment aiming at measuring the dynamics of the Universe directly. CODEX should therefore be considered as a fundamental physics experiment, which does not make specific assumption regarding the underlying theory of gravity. The measurement of the acceleration and the constraints on cosmological parameters will obviously become more accurate, the longer the time baseline of the experiment extends. The main CODEX experiment is therefore also conceived as a legacy program that will produce a suite of extremely well calibrated high resolution spectra of bright QSOs, which can serve as 'first epoch' measurements for future generations of astrophysicists.

It is also worth noting that CODEX will probe the nature of the dark energy and of the dark matter in the redshift range z=1.5-4, which is not easily accessible in other ways.

1. CODEX - Executive Summary

CODEX will produce a set of unprecedented high resolution (R~150000), high S/N (S/N~2000) QSO spectra, which will have a wide range of other ground-breaking applications beyond the main scientific aim of CODEX. The spectra can be used to measure a possible variation of the fine structure constant with a relative accuracy of 10^{-8}, comparable or better to the controversial claims based on the OKLO natural reactor, and at least 2 orders of magnitude more accurate than present astronomical measurements.

A very high resolution spectrograph such as CODEX which combines the collecting power of OWL with the highest stability ever achieved by an astronomical spectrograph will have a tremendous impact on many astrophysical programs, many of which we cannot anticipate. Within this study we have selected a few specific examples only. CODEX will be able to confirm, characterize and eventually discover earth mass planets in habitable zones around other stars. The terrestrial signal will be a few cm/sec/yr, but the most difficult (and time consuming) task will be to eliminate the stellar 'noise' mixed with it. CODEX will also be able to determine with exquisite accuracy the abundances of the primordial elements (and their isotopes), providing the possibility of comparing the physics of the first 20 minutes after Big Bang with that of ~$4x10^5$ years later: CODEX will measure Li^7 and Li^6 /Li^7 abundances for very metal poor stars in our Galaxy and our nearest companions.

A fully exploitation of the unprecedented accuracy of CODEX needs a large amount of photons, and the main experiment will require a substantial number of nights (~500 over 15 years) at the OWL telescope. The most likely strategy foresees the acquisition of first epoch data for about 5 years repeating the measurements 10 years later.

To achieve its outstanding long-term accuracy CODEX will make ample use of Virtual Observatory-type facilities, and will use a novel calibration scheme, based on laser frequency combs, which will achieve the wavelength stability, reproducibility and accuracy typical of an atomic clock. Some of the corrections (e.g. earth rotation, residual systematic trends) will be known only after the experiment has been running for some time. Re-processing of the whole data set will be performed several times.

Building on the very positive experience with HARPS, CODEX will be realized as an array of super stable fibre-fed high-resolution spectrographs (R=150000), which cover the spectral range from 400-680 nm. We propose a concept with an aperture of 0.65 arcsec on the sky for a 100 m. telescope (or 1.1 arcsec for a 60 m. telescope) that uses five spectrographs hosted in a quiet laboratory outside the main telescope structure. The concept is modular and can be adapted to a variety of telescope diameters and sky apertures by changing the number of spectrograph units.

This concept study shows that CODEX, although demanding, is technically feasible with present technology. No show stopper has been identified. Some research and development is required in several areas (fibre feeding, detectors, calibration system), and the project will require extensive prototyping and will benefit from targeted scientific programs, such as preparatory analysis of high resolution, high S/N ratio QSO spectra and surveys increasing the number of bright QSO known.

Part of the study has been devoted to an analysis of possible 'contaminants' of the measurement. We demonstrate that all local (earth and Galactic) sources of noise can be accounted for whereby some synergy with GAIA will be possible. The contamination from astronomical (extragalactic) sources of noise is expected to be one order of magnitude smaller than the cosmic signal. Their contribution will be analyzed and monitored by observing many lines of sight and by comparing the Lyα forest and metal line results.

The estimated HW cost of the whole project is 24 ME, in addition to ~100 FTEs. We foresee development within 12 years, which includes the development of a prototype and 3 years of its operation at the VLT.

2. CODEX Project Overview

2.0 Preface

The concept study presented here has been carried out in the period October 2004 - September 2005 within the framework of the ESO study of OWL instrumentation, with the support of three external Institutes (Institute of Astronomy Cambridge, Observatoire de Geneve, INAF - Trieste). Several team members at other institutions have also contributed.

We stress that the CODEX concept goes beyond the concept of a multi -purpose instrument. CODEX should be conceived as an experiment. Our study covers all aspects of the experiment, from the definition of the optimal instrument parameters and photon collection, to the extraction of the full scientific information. For CODEX an intimate interplay exists between the scientific goals and the instrument characteristics (including HW, SW and operations).

The work has been organized in five Work Packages, which reflect the main aspects of the project. They are listed below, together with the names of the participants.

WP 1000: Coordination and Management: *L. Pasquini (coordinator)*, S. D'Odorico (ESO), M. Haehnelt (Cambridge), M. Mayor (Geneve), P. Molaro (Trieste)

WP2100: Main Science case: *S. Cristiani (coordinator)*, S. Borgani, V. D'Odorico, E Vanzella, (Trieste), M. Haehnelt, M. Murphy, M. Viel (Cambridge), M. Dessagues (Geneve), S. D'Odorico, J. Liske, P. Shaver, (ESO), A. Grazian (Rome), L. Moscardini (Bologna), T. Wiklind (ESA-STScI)

WP2200: Science Methodology: *F. Pepe (coordinator)*, C. Lovis, D, Queloz, (Geneve), F. Bouchy (OHP and IAP), S. Zucker (Tel Aviv)

WP2300: Immediate Science Cases: *P. Molaro (coordinator)*, P. Bonifacio (Ts), M. Murphy (Cambridge), M. Mayor ,S. Udry (Geneve), L. Pasquini,(ESO), S. Levshakov (St. Petesburg)

WP3000: Technical Concept: *H. Dekker (coordinator)*, G. Avila, B. Delabre, J-L. Lizon (ESO), F. Pepe, M. Fleury (Geneve)

2.1 Scientific Goals

Astronomical observations, most prominently those of the CMB, supernovae and the clustering of galaxies are well described within a cosmological standard model -- a flat Friedman-Robertson-Walker (FRW) Universe with a cosmological constant which corresponds to an energy density twice that of the matter in the Universe at the present day.

Current observational constraints are basically geometric in nature as they mainly constrain the angular diameter distance to the last scattering surface (CMB) and the luminosity distance at moderate redshifts (supernovae). The constraints on actual dynamical effects of the cosmological constant as probed by the clustering of the matter distribution are coupled in a complicated way to geometrical constraints and are actually rather weak.

The fact that current observations require a cosmological constant in the framework of a FRW Universe is generally attributed to the presence of a phenomenon called dark energy whose nature is currently completely elusive. The introduction of the concept of dark energy is somewhat reminiscent of the "Ether" in 19th century physics and is arguably the biggest conundrum of present-day physics. It is currently unclear if the solution lies as often assumed in a yet unknown contribution to the total matter energy density of the Universe which can be described in the general framework of General Relativity in a four dimensional space time, whether not yet understood physical phenomena of a higher dimensional space times which nevertheless can be described by General Relativity hold the key to the solution or whether a more radical paradigm shift is necessary to resolve this conundrum. It is thus important to characterize the physical effect of "dark energy" as completely as possible. In particular it is important to establish whether the dark energy

actually has the dynamical effects expected if its evolution is described by General Relativity in four dimensions.

CODEX will measure the small frequency shift in the numerous Lyman-alpha and metal absorption lines in high redshift QSOs which is sensitive to the difference of the expansion rate of the Universe at different observing epochs. CODEX will contribute to establishing the dynamical effect of the alleged dark energy in the following way.

1) By achieving the photon-noise limit for the measurement accuracy of frequency shifts, CODEX will be able to detect the expected dynamical effect of the dark energy on the expansion of the Universe with high significance.

   This requires ambitious but not unreasonable demands regarding
   - total observing time (500 nights)
   - brightness of the observed sources (40 QSO with V~16.5)
   - effective duration of observing campaign (15 Yrs)
   - telescope size and efficiency (see Figure 2-1)

2) By Establishing an absolute frequency standard, it will be possible to assemble a highly accurate legacy measurement which combined with measurements by future generations will give a precise measurement of the dynamical effect of dark matter and dark energy. Within the FRW framework these should translate into constraints on the amount of dark energy and its evolution which are comparable but complementary to those achievable with other methods.

Beside this main, long term objective, CODEX will be a powerful, efficient, super-stable high resolution spectrograph fed by the unprecedented collecting capability of OWL. A wide range of fundamental results will be obtained by this combination. We have selected here three topics for further discussion. The topics were chosen because of their scientific relevance and because they are already well developed in the literature.

The possible variability of physical constants with time would tell us about the existence of so-far uncovered scalar fields or additional dimensions. By observing objects at high redshifts we have the unique opportunity to observe back for several Gyrs in time, and this capability has been used to test if the fine structure constant varied in the past. The results are so far contradictory, as the variability observed by one group has not been confirmed by subsequent studies. This result may challenge the latest interpretation of the natural Oklo reactor data, which concluded that the constant varied in the last 2 Gyrs. Astronomical measurements can be improved by better controlling the systematic effects and by improving the photon statistics. CODEX will be the ideal instrument to pursue this research to the limits, because having a very precise calibration system, having a fibre fed, ADC corrected input, and being super-stable, it will bypass all the shortcomings of present spectrographs. It is shown that, using the OWL photon collecting capability, it will be possible to reach a precision on the variability of the fine structure constant of better than 10^{-8} over several Gyrs. We will therefore be able to confirm the interpretation of the Oklo data, which predicts a variability in excess of $5*10^{-8}$ in the same period.

The discovery and follow–up of earth-mass planets in habitable zones around other stars is one of the major drivers for ELTs. The CODEX accuracy will be more than adequate to detect earth mass planets, but the challenge will be to detect such a small signal on top of the stellar noise, induced by oscillations and stellar activity; this can be done by observing a star for several hundred hours, making the use of OWL for a survey search impractical. It will be, however, essential to use it either to search earth mass planets around stars which have independent evidence of their presence, or to derive the radial velocity curve of transit candidates as provided, for instance, by satellite observations. Radial velocity measurements will be required for all of them to solve the orbit and to determine the planets' mass.

Primordial nucleosynthesis: Accurate measurements of the abundance of the light elements produced in the Big Bang together with the constraints on the baryon density from CMB experiments are an important test of our current modeling of the Primordial nucleosynthesis and the evolution of the Early Universe and whether the physics used is complete. As an example, the detection of Li^6 in several metal poor stars, down to a metallicity of Fe/H=-3, challenges our current understanding of the Early Universe, and may require the decay of exotic particles. With CODEX we will be able to obtain the Li^6 abundance in very metal poor stars of our Galaxy and of other galaxies, providing a fundamental test to theory.

We underline that, even if not studied here, CODEX will bring unique results on many other extremely interesting topics, such as, for instance, asteroseismology, cosmochronometers, first stars, temperature evolution of CMB, chemical evolution of the IGM….

2.2 Technical Design:

The design is based on a variation of the HARPS concept, but we aim at improving the HARPS performances by almost 2 orders of magnitude. As for HARPS, we foresee for CODEX a dedicated laboratory, in a thermally and mechanically quiet environment. This laboratory will be stabilized and each spectrograph will be contained in a vacuum and thermally stabilized tank, each one contained in a box. Our simulations show that a resolving power R ~50000 is sufficient to optimize the signal from the broad Lyα lines, but that higher resolving power (R~150000) is required by the narrow metal lines; these are less numerous, but being narrower carry almost half of the information. A resolving power of about 150000 is also required to obtain the appropriate wavelength calibration accuracy. As far as spectral range is concerned, the information from the high redshift lines is wiped out by the excessive number of absorbers, while at low redshift their number become so small that the information from them also rapidly decreases. The selected optimal spectral range is therefore between 400 and 680 nm. An extension towards the blue would still add some information, but it does not seem worth at present, given the very limited system efficiency in the blue and the possible problems induced by enlarging the detector area further. The product of large telescope diameter and high resolving power in a seeing limited situation poses a formidable challenge. We present an innovative concept which solves this problem:

a) By building several spectrographs (5 are proposed), in a modular concept

b) By using new techniques that have not been used so far on this scale in astronomical spectrographs:
i) pupil slicing,
ii) use of anamorphic beams,
iii) use of Volume Phase Holographic Gratings as crossdisperser and beam expander.
In this way a resolving power of 150000 with a 100 m. telescope and an 0.65 arcsec aperture can be obtained by using a reasonable 0.2x1.6 m. mosaic of echelles, that is the combination of 2 UVES gratings.

c) A new wavelength calibration system is needed to achieve the accuracy, stability and reproducibility required by the science cases. We need a system which can provide an absolute repeatable calibration, which can be guaranteed for the duration of the whole project and beyond. A system based on the development of laser frequency combs is planned. The laser comb will provide equally spaced lines of similar intensity with a frequency difference calibrated and known to better than one part in $10^{\sim 14}$

2.3 Performance Assessment and Critical areas

Our extensive simulation program has shown that the main goal of CODEX can be attained. It has also identified a number of critical areas which need to be carefully monitored and developed. Namely:

- **Photon Flux**: Our simulations show that our main scientific goal requires an equivalent S/N~13600 per 0.0125 A pixel. As seen in Figure 2-1, this requires that a minimum of photoelectrons/second is recorded in order to keep a reasonable observing time. The product of system efficiency, target magnitude and telescope diameter must converge to a minimum flux. Telescope and fibre transmission must be optimized. Optimized optical coatings and high CCD QE are needed as well, but for the CODEX limited spectral range the performances of commercial products are already excellent.

- **'Local' Astronomical source of noise**: Local sources of noise and corrections have been analyzed in detail; the earth orbit is known at the required level; the acceleration of the Sun in the Galaxy can be measured by CODEX, and, in addition, it will be measured exceedingly well by GAIA. The observatory position and earth rotation are the most unpredictable contributors, and corrections will only be possible a

posteriori. Great care is required in determining the effective time barycenter of observations, which can be determined by use of an exposimeter (or time resolved spectroscopy).

- **Instrumental sources of noise** : We propose to start from an as stable as possible environment. We consider this strategically superior to an 'active' system because of, among others reasons, the long duration of the experiment, which would put strong requirements on any active system. A proper calibration is essential. The behavior of the detectors is also critical. While most "noise" effects are equivalent of having a time variable PSF, not all possible effects can be fully simulated; we have issued preliminary CCD requirements, but a complete study will be needed in future phases of development.

2.4 Feasibility and Costs

We could not identify any specific show stopper and the project is feasible with present technology, although some R&D is required and some developments are desirable (cf. Next sections). Costs have been briefly analyzed, mostly through a comparison with UVES and HARPS, which are our closest examples to one CODEX unit. CODEX will not have moving parts (as HARPS) but will have a large (20 x 40 cm.) pupil , twice the one of UVES.

The full HW costs are estimated as 24ME (including the prototype). This figure is larger, but comparable with the costs of large VLT instruments. The full development of the instrument will require a manpower of about 100 FTE's. The development of HARPS (no moving parts, 'well known' design.) took a total of 3 years. To build a full CODEX prototype for the VLT, four years will be needed. After three years of testing at the VLT, we will be able to have the CODEX FDR, and to start the production of the 5 units, to be at the OWL telescope by 2017. This is just a preliminary plan, not optimized, and it could be modified if required. Detector production may require some special agreement with the manufacturers.

2.5 Required Technology Developments

The development of a new calibration system is an essential requirement for the main scientific aim of CODEX. ESO is already pursuing the development of such a system in collaboration with the group at MPQ awarded the 2005 Nobel prize for physics (laser frequency comb). Alternative solutions (e.g. stabilized Fabry-Perot) might be considered.

The availability of detectors with very low RON, excellent QE, CTE, extremely low thermal dissipation is also important. The merit of time resolution capabilities, possibility of reading simultaneous calibration and science spectra independently (at different rates..), or other special features of advantage needs to be evaluated.

The feasibility of the proposed novel concept for the Crossdisperser needs to be proven.

A very efficient system to bring the light to the spectrographs, with a high transmission in the blue, must be explored.

2.6 Required Scientific Developments

It will be essential to have a complete census of bright QSO in the range of redshifts of interest. Several all sky surveys (STARRS. GAIA) are planned. We shall ensure that they produce the data we need.

Characterization of QSO spectra: obtain high resolution (R=150000), high S/N ratio spectra of a few QSO's to analyze the Lyα and metal profiles, line frequency, broadening statistics. This could be done for a few objects with a prototype at the VLT.

About the immediate science cases, it is very important to attempt the 'decomposition' of the stellar noise, to reach the highest precision and to test the limits of this technique. Could be done with a prototype at the VLT.

2.7 Areas of possible improvement

While the present document is adequate for a conceptual study, we are conscious that several key issues need to be addressed in more depth in future study phases. Targets for improvements include:

- More complete simulations, including realistic 2D spectra, spectra extraction and additional noise sources, as, for instance, sky and atmosphere shall be developed.
- The present study is based on existing technology or simple extensions of it. Possible technological breakthroughs have not been considered here on purpose, since the aim was to prove feasibility. The possibility of technological breakthrough should be considered in the future phases.
- The design presented should be considered as a 'prove for existence', rather than a final design. A detailed trade-off analysis between costs, size, location, number of spectrographs etc. is beyond the scope of the present phase and has not been attempted.

2.8 Feedback Requirements to OWL

Some requirements have been identified and given to the OWL project.

CODEX needs a lab in a quiet place outside of the telescope area.

The length of fibres (over 200 m) from the proposed OWL focus to the CODEX lab would be prohibitively long. It produces too large losses, in particular in the blue. We do not see an obvious way of improving fibre transmission. We therefore need a coudé focus that can be reached through highly reflective surfaces.

We must be able to position and maintain our sources with an accuracy of ~0.02 arcseconds in the fibre centre, which corresponds to 40 m/sec before scrambling.

2.9 Prototype

For HARPS, since the step from the previous generation of instruments required an improvement of less than a factor 10, it was decided to proceed directly to the construction of the spectrograph, knowing the weakness of the previous instruments and improving them. Since for CODEX we aim at improving the accuracy by almost two orders of magnitude, some critical aspects (thermal stability, fibre performances..) will not only benefit, but also demand extensive testing. Perhaps most important are the system aspects, for which CODEX will need a full system prototype, to test the full chain, from instrument HW to data reduction and analysis.

We therefore suggest that the possibility of building a CODEX prototype for the VLT, with characteristics as similar as possible to the OWL instrument should be seriously considered. With a 1.0 arcsecond aperture in the sky, a resolving power of 200000 will be reached. With this system we will be able to use an extensive set of calibrations to verify instrument stability, calibration accuracy and all instrumental noise. It will be possible to obtain high S/N ratio observations for a few very bright QSOs and to prove that we can reach the photon noise limit. Several of the 'immediate' science cases will benefit from this prototype; the precision that will be obtained at OWL will not be reached, but we will be able to improve substantially the current (UVES, HARPS) performances. The full set of test data will be used at the CODEX FDR to prove the concept and to improve the design.

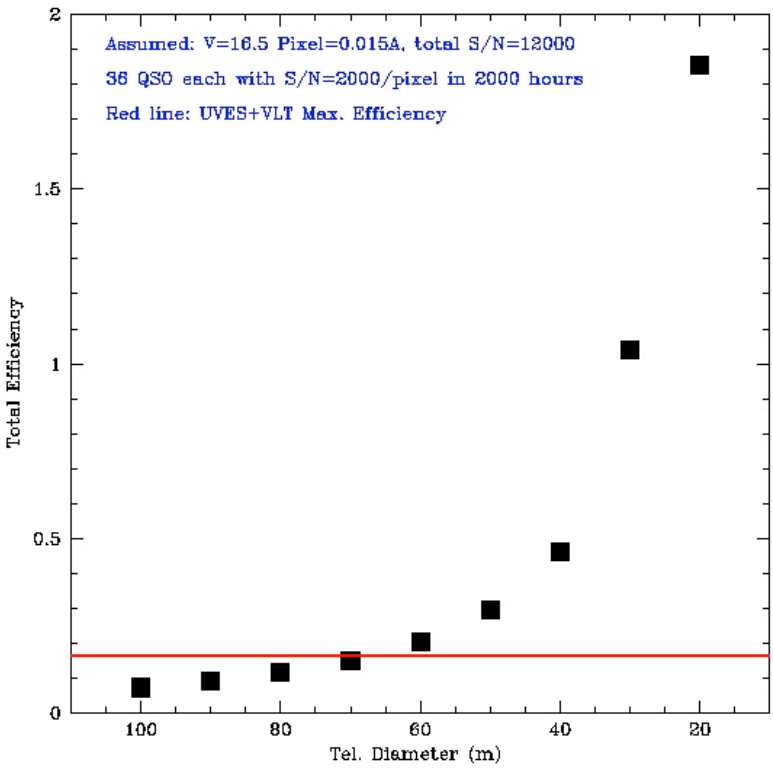

Figure 2-1: *Telescope+CODEX efficiency vs. telescope diameter. The total S/N ratio of 12000, the integration time of 2000 hours and a QSO magnitude of V=16.5 has been fixed. The plot shows the total efficiency that the system should have to reach the goal within the above assumptions. This Figure shows as, for given scientific strict balance needs to be maintained between telescope diameter, instrument efficiency and magnitude to stay within a reasonable observing time. The red horizontal line shows the UVES + VLT measured efficiency.*

3. CODEX Main Science Case

3.1 The Expanding Universe and the Hot Big Bang -- Historical Background

One if not ***the*** major milestone in modern Cosmology is the discovery of the expansion of the Universe. Established in the late 1920s by Edwin Hubble it brought to an end the cherished belief held by most Physicists of the time including Albert Einstein that the Universe is static and not evolving. Hubble's early discovery of the expansion of the Universe enabled by the new observational facilities on Mount Wilson has later been impressively confirmed by a vast range of astronomical observations. It eventually led to the now widely accepted Hot Big Bang Theory which predicts that the Universe was very dense and hot at early times. With the detection of the relic Cosmic Microwave Background (Penzias & Wilson 1965) and the experimental verification of the prediction for the synthesis of light elements (Alpher et al. 1948) the Hot Big Bang is now an essential aspect of the cosmological standard model.

Around 1916 Einstein had introduced General Relativity (GR), which led to the description of the Universe as a homogeneous and isotropic four-dimensional space time, the so-called Friedman-Robertson-Walker (FRW) Universe. In 1922 Friedman (and independently Lemâitre in 1927) found that Einstein's original equations did not allow static solutions. Ironically this prompted Einstein to ``spoil'' his new theory of gravity by introducing a cosmological constant to allow static solutions in his field equations. Even more ironically this same cosmological constant which Einstein in his later years considered as “the biggest blunder” of his life has now become another pillar of the modern cosmological standard model.

In the Early Universe a large vacuum energy density acting like a cosmological constant is believed to have been responsible for the rapid expansion of the Universe in a phase called *Inflation*. Furthermore, recent observations of the luminosity distance of moderate and high redshift supernovae of type Ia have established the presence of a form of *Dark Energy* which appears to have a very similar effect to that of Einstein's cosmological constant within the framework of a FRW Universe.

We should, however, not forget to mention that there has been a long and on-going discussion on the cosmological interpretation of the redshift of spectral features in astronomical objects (see e.g. Arp(2001) and Arp et al. 2002 and references therein). Other high-profile dissenters critical of the Big Bang Theory include Nobel laureate Hannes Alfvén, Geoffrey Burbidge, and Sir Fred Hoyle. Bondi & Gold (1948) proposed the model of Steady State Cosmology (SSC), which was recently revived in the form of a Quasi Steady State Cosmology (QSSC, Hoyle et al. 1995).

The vast majority of practitioners of Observational Cosmology nevertheless feel that there is little room for doubt that the Universe is expanding and was hot and dense at early times.

3.2 “Dark energy” and the current standard cosmological model

The majority if not all “cosmological” astronomical observations, most prominently those of the CMB, supernovae, Lyman-α forest and the clustering of galaxies are consistent with a Friedman-Robertson-Walker Universe with no curvature and a cosmological constant which corresponds to an energy density about twice that of the matter in the Universe at present.

The fact that current observations require a cosmological constant in the framework of a Friedman-Robertson-Walker Universe is generally attributed to the presence of a phenomenon called dark energy to which we already briefly alluded in the last section and whose nature is currently completely elusive. The introduction of the concept of dark energy is somewhat reminiscent of the "Ether" in 19th century physics and

is arguably the biggest conundrum of present-day physics. It is currently unclear if the origin of the cosmological constant has to be attributed, as often assumed, to a yet unknown contribution to the total energy density of the Universe that can be described in the general framework of GR in a 4-D space time, whether not yet understood physical phenomena of higher dimensional spacetimes - still describable by GR - hold the key to the solution, or whether a more radical paradigm shift is required.

It is thus important to characterize the physical effects of "dark energy" as completely as possible and in particular it is essential to establish whether the dark energy actually has the dynamical effects expected if its evolution is described by GR in four dimensions. Current observational constraints are basically geometric in nature as they mainly constrain the angular diameter distance to the last scattering surface (CMB) and the luminosity distance at moderate redshifts (supernovae). The constraints on actual dynamical effects of the cosmological constant as probed by the clustering of the matter distribution are coupled in a complicated way to geometrical constraints and are actually rather weak.

We propose here to revitalize an old idea - **to use the expected wavelength shifts of spectral features of light emitted at high redshift to probe the evolution of the expansion of the Universe directly. If GR is the correct theory of physics on large scales, then there is a differential equation that relates the Hubble expansion function, inferred from measurements of angular diameter distance and luminosity, to the variation of the redshift as a function of time. Deviations from this consistency relationship could be the signature of the breakdown of GR on cosmological scales.** The measurement of the change of cosmological redshifts with time is a dream already discussed by Sandage (1962), and more recently reconsidered by several authors (Harrison 1976, Davis & May 1978, Rudiger 1980, Lake 1981, Phillipps 1982, Loeb 1998, Freedman 2002, Barbachoux and Le Denmat 2002, Davis and Lineweaver 2004). With the notable exception of Loeb (1998) the general conclusion was that the measurement of the cosmological change of redshifts would be out of the reach of the measuring accuracy of available astronomical instruments and/or would be swamped by peculiar accelerations.

As we will show here, **for QSO absorption spectra obtained with an ultra-high precision spectrograph on a next generation 100m-class telescope, a direct measurement of the redshift change of spectral features with time will become feasible. This opens up the exciting possibility to directly measure the dynamical evolution of the Universe and probe the effect of the elusive dark energy.**

3.3 The cosmological change of redshifts as a dynamical probe of the Friedman-Robertson-Walker Universe

3.3.1 ż and the evolution of the Hubble parameter

As discussed in the previous section the necessity to attribute the major fraction of the energy density of the Universe to some form of dark energy with an equation of state similar to that of a cosmological constant casts some doubt on the validity of the framework of FRW Universes in which we generally describe astronomical observations. It is thus important to check extensively if this description leads to any serious internal inconsistency.

In an expanding FRW Universe the light of a source which is emitted at time t_e and received at time t_0 is redshifted by a factor

$$1 + z(t_o, t_e) = \frac{a(t_o)}{a(t_e)} = \frac{a_o}{a}, \qquad (1)$$

For a source at fixed coordinate distance the change of t_e and t_0 are related by $dt_e = dt_0/(1+z)$. The total change of redshift is given by

$$dz = \frac{\partial z}{\partial t_o} dt_o + \frac{\partial z}{\partial t_e} dt_e \tag{2}$$

Dividing by dt_0 yields,

$$\dot{z} = \frac{dz}{dt_o} = \frac{\partial z}{\partial t_o} + \frac{\partial z}{\partial t_e}\frac{dt_e}{dt_o} = \frac{\dot{a}(t_o)}{a(t_e)} - \frac{\dot{a}(t_e)a(t_o)}{a(t_e)a(t_e)}\frac{1}{1+z}$$

or simply

$$\frac{dz}{dt} = (1+z)H_o - H(t_e) \tag{3}$$

The time derivative of the redshift of light emitted by a source at fixed coordinate distance is thus related in a simple manner to the evolution of the Hubble parameter between the epoch of emission and receiving. As mentioned previously a number of authors have pointed out that the measurement of wavelength shifts of astronomical objects can thus be used to measure the change of the expansion rate of the Universe. In a FRW Universe the Hubble parameter $H=\dot{a}/a$ is related to the energy content of the Universe as

$$H = H_o\left[\Omega_{mat}\left(\frac{a_o}{a}\right)^3 + \Omega_R\left(\frac{a_o}{a}\right)^4 + \Omega_{de}\left(\frac{a_o}{a}\right)^{3(1+w)} + (1-\Omega_{tot})\left(\frac{a_o}{a}\right)^2\right]^{1/2} \tag{4}$$

where $\Omega_{tot} = \Omega_{mat} + \Omega_R + \Omega_{de}$ and Ω_{mat}, Ω_R, Ω_{de} are the energy density of matter, radiation, and dark energy expressed in terms of the critical density, respectively. The dark energy density is characterized by an equation of state of the form $p_{de} = w\rho_{de}c^2$, and w=-1 corresponds to the case of a cosmological constant. Note that the redshift dependence of the contribution of the dark energy could well be more complicated than parameterized here by a simple equation of state. At the relevant redshifts the radiation energy density is small $\Omega_R << \Omega_{tot}$ and we will neglect it in the following. Note that the expected wavelength shift is of order unity in a Hubble time.

3.3.2 The relation of ż to the Cosmological Parameters describing FRW Universes

It is convenient to express the expected wavelength shift over a period Δt in terms of the velocity of the equivalent Doppler shift, $v=(\Delta\lambda/\lambda)c$. For a FRW Universe with no curvature and neglecting the radiation energy density this gives

$$\begin{aligned}\Delta v = \dot{v}\Delta t &= \frac{\dot{z}}{1+z}c\Delta t = (1-E(z))H_o c\Delta t \\ &\approx 30.68h(1-E(z))\left(\frac{\Delta t}{10yr}\right)cm/s\end{aligned} \tag{5}$$

where c is the speed of light and $E(z) = [\,\Omega_{mat}(1+z)^3 + \Omega_{de}(1+z)^{3(1+w)}]^{\{0.5}\,/(1+z)$.

Figure 3-1 shows the expected change of redshift for a range of FRW models with no curvature as a function of redshift. There are a few things to note. The wavelength shift has a very characteristic redshift dependence. At some redshifts the wavelengths are ``stretched'' while in others they are “compressed”. **The wavelength shift corresponds to a Doppler shift of about 1-10 cm/s over a period of 10 yrs. Measuring the wavelength shift therefore requires a about a factor 10-100 times improved wavelength calibration compared to that currently achievable with an instrument like HARPS at the ESO 3.6m (Mayor et al. 2002). In asteroseismology a comparable sensitivity is already obtained for**

bright sources and short periods. For an Einstein-de-Sitter Universe the redshift of an object at fixed coordinate distance *decreases* with time independent of the redshift of the object. However, for flat models with a contribution of dark energy to the total energy density the redshift increases for objects at low redshift and decreases at high redshift. This is the tell-tale sign of the accelerating effect of the dark energy.

The characteristic redshift dependence of ż is very important as it will help to discriminate against systematic uncertainties and random errors. Note further that the signal is actually largest for the Einstein-de-Sitter model and that the redshift where ż becomes zero does not depend on the value of H_0 (see Figure 3-2). In the framework of the currently discussed FRW Universes measuring ż as a function of z will put constraints on Ω_{mat}, Ω_{de}, H_0 and w. We will discuss this in more detail in section 3.6.

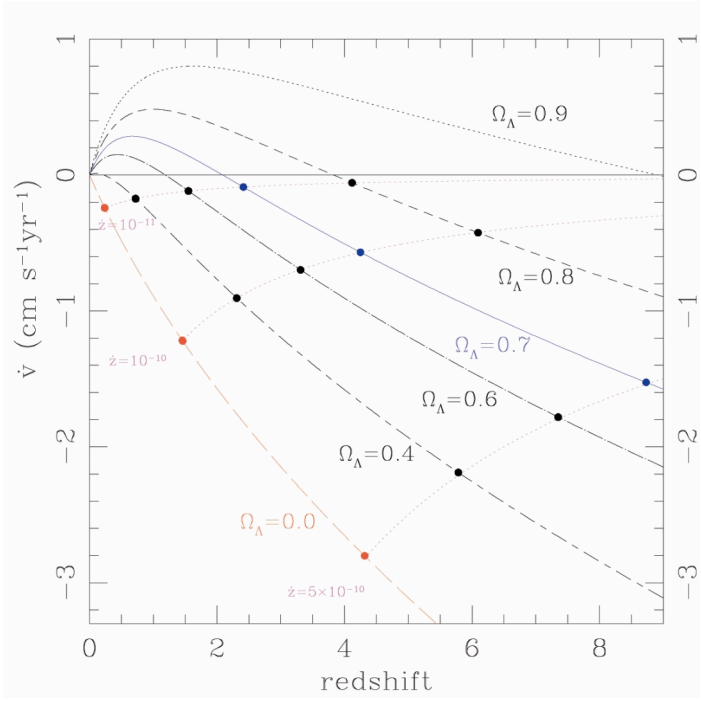

Figure 3-1: *Evolution of $\dot{v}$ as a function of redshift. The cosmological parameters have been fixed to Ω_{tot}=1, H_0=70 and different values of Ω_Λ have been considered. The lines represent the behavior of the Equation 3. The Ω_Λ=0.7, Ω_M=0.3 cosmology is shown with a blue solid line, while the EdS model is plotted with a red long-dashed line. The filled circles connected by dotted lines show loci of constant ż, in units of yr^{-1}.*

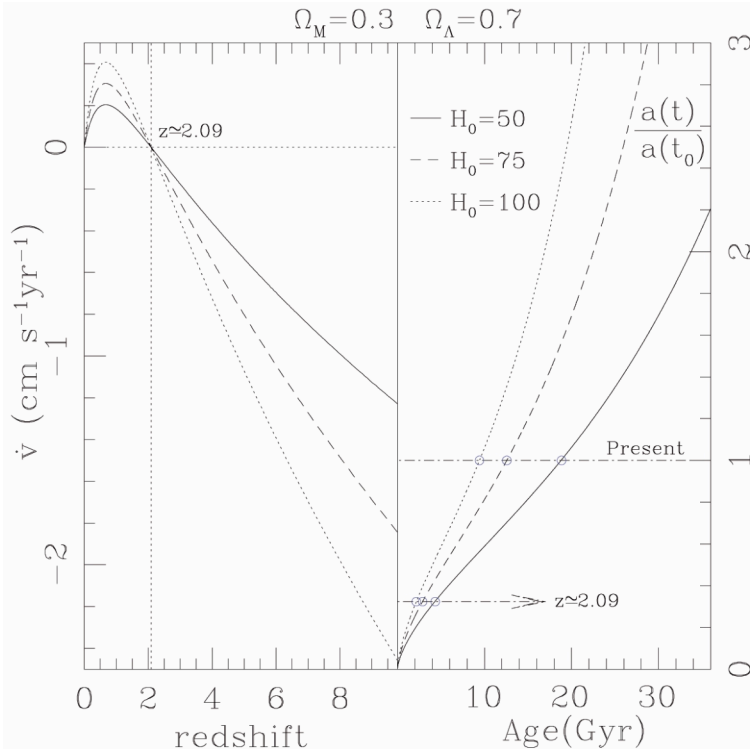

Figure 3-2: *Evolution of ύ with redshift (left panel). In the right panel the behavior of a(t)/a(t_0) is shown from t≈10^5 yr until z= -2/3. Ω_M and Ω_Λ have been fixed to 0.3 and 0.7, respectively, while 3 values of H_0 are shown (50, 75 and 100 km s^{-1} Mpc^{-1}). Note that the redshift value at which ż=0 is independent of H_0.*

3.4 Measuring the wavelength shift in high redshift objects

3.4.1 General considerations

As discussed in the previous section the wavelength shift due to the changing redshift of sources at fixed coordinate distance is of order $\Delta\lambda/\lambda \sim 10^{-10}$ per year, which corresponds to a Doppler shift of about 3 cm/s. Most spectral feature in astrophysical objects are much wider than this. With a sufficiently high S/N and accurate wavelength calibration it is, however, possible to measure wavelength shifts much smaller than the widths of the corresponding spectral features. A prime example is the measurement of radial velocity modulations of the spectral features in nearby stars which has led to the detection of numerous planets. Currently an accuracy in radial velocity as small as ~ 40 cm/s can be achieved with HARPS (Santos et al. 2004). The wavelength calibration has not yet met any fundamental limit and with a sufficient number of photons (as can be obtained by co-adding many spectral features observed with a next generation 100m telescope) the sensitivity to frequency shifts can be substantially improved. The experiment proposed here has thereby to achieve:

1) Sufficient wavelength accuracy to measure the expected signal

2) Sufficient S/N to measure the wavelength shift which is much smaller than the width of the observed spectral features.

For a given cosmology the wavelength shift has a well defined pattern of compression/stretching as a function of redshift (viz. wavelength). The signal is isotropic and it is thus possible to observe many different sources all over the sky. A priori it is not obvious which objects and which spectral features are best suited for a measurement of ż. For a given energy flux the S/N of the final measurements will increase with the sharpness of spectral features (less noise) and increasing wavelength (more photons). Another important

consideration is the expected peculiar acceleration associated with peculiar motions relative to the Hubble flow which will act as additional noise.

3.4.2 Possible targets for the measurement of ż

3.4.2.1 Emission lines objects: Masers, HI 21 cm

Masers (e.g. Miyoshi et al. 1995) and/or HI 21 cm (e.g. Murphy et al. 2001, Davis and May 1978) with their very sharp emission/absorption features would seem to be very well suited to measure small wavelength shifts. Due to their rather long wavelength, noise is also much less of a problem than at optical wavelengths. However, the emitting/absorbing regions typically reside in deep potential wells and should be subject to strong peculiar accelerations which will swamp the expected cosmological change of the redshift of spectral features (see section 3.8 for more details). This is a general problem as sharp features require the emitting/absorbing material to be cold. Cold material is generally found in rather dense regions of the Universe in which the peculiar accelerations are expected to be large.

3.4.2.2 Molecular absorption line systems

In Appendix 1 we explore in detail the possibility of using ALMA to measure cosmic acceleration through rotational molecular transitions seen in absorption. The mm/submm regime has the potential for very high frequency resolution with already existing instruments. With dedicated spectrometers, an even higher resolution could be obtained. An advantage of the use of molecular lines is their accessibility at redshifts were the cosmic acceleration shows the largest effect and that they could at least in principle be used to measure the acceleration as a function of redshift. There are, however, several problems that need to be addressed before using molecular absorption lines for ultra-high precision redshift measurements. The first problem is that a much larger number of absorption line systems would be required than are presently known. Another concern is that the molecular gas is typically situated deep in a galaxy potential and therefore are expected to experience peculiar accelerations, which are larger, or of the same order of magnitude, as the cosmic acceleration. These peculiar accelerations will probably be the main obstacle to using molecular absorption lines to measure the cosmic acceleration. The estimated number of available absorption line systems will not be sufficient to overcome this limitation by statistical analysis.

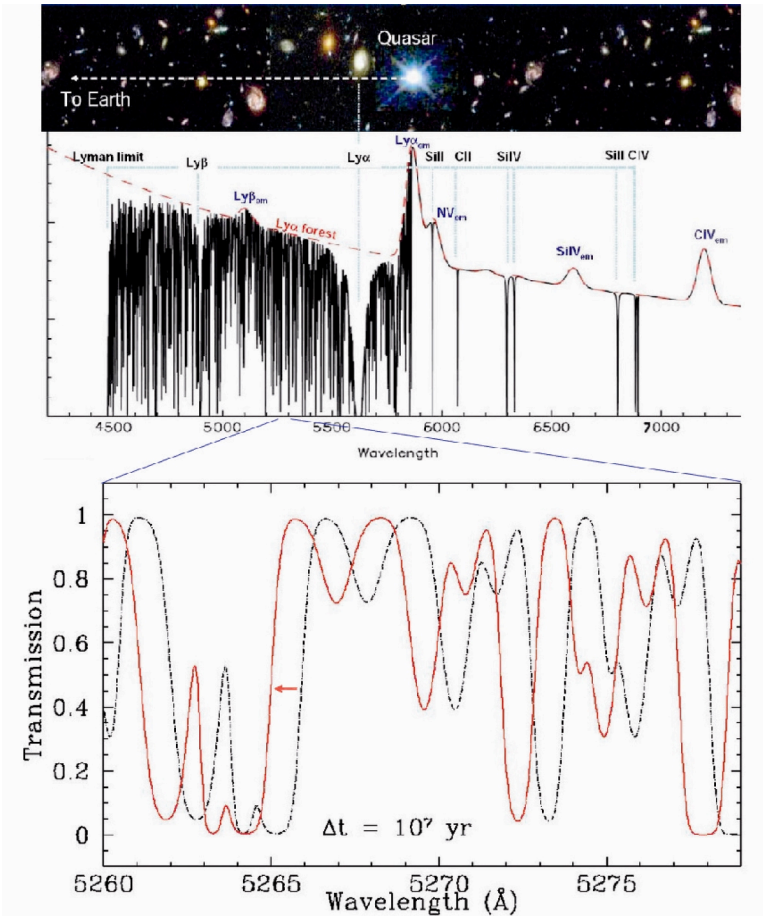

Figure 3-3: *The displacement of the absorption features due to the intergalactic medium as a function time. The lowest panel shows a small portion of the simulated Lyman-α forest of a z ~ 3.5 quasar observed today (black, dashed-dotted line) and in 10^7 years from now (red continuous line). The red arrow shows the direction of the effect. The interval of time has been chosen to be 10^7 years for the sake of visualization. In the real experiment it will be about six orders of magnitude shorter. The displacement of the spectral features will be correspondingly smaller.*

3.4.2.3 Absorption lines in the spectra of high-redshift QSOs

The numerous absorption lines in the spectra of high-redshift QSOs, which make up the so called Lyα forest, appear to be the most promising targets for a measurement of ż. The most striking feature of the Lyα absorption is the large number of lines in a single spectrum. Figures 3-3,4 show typical Lyman forests at z ~ 3.5 - 4. Most of the absorption features are caused by Lyman series transitions of hydrogen and the lines contributing most to the signal of ż are those with an optical depth of 1-2. There are about one hundred such features in a single spectrum which have a typical width $\Delta \lambda_{line}$ of 30 km/s. With QSO absorption spectra we can probe a wide redshift range from z ~ 1.5 up to 4 and beyond. There is a generally accepted paradigm for the origin of the Lyα forest absorption and the associated metal absorption which has been established by extensive comparison of cosmological hydrodynamical simulations (Miralda-Escude' et al. 1996, Hernquist et al. 1996, Theuns et al. 1998,2002, Dave' et al. 1999, Meiksin et al. 2001) and analytical calculations (Bi & Daidsen 1997, Viel et al. 2002) with the exquisite data which have become available from 10m class telescopes (see Rauch (1998) for a review; Kim (2002)). We can thus be confident that the Lyα absorption lines with optical depth of order unity arise from moderate density fluctuations in a warm photo-ionized Intergalactic Medium which closely follows the Hubble flow (Smette et al. 1992, 1995). The Lyman series absorption lines are thus ideally suited to measure the global evolution of the Hubble parameter. The narrower metal lines are normally associated with hydrogen lines of larger optical depth and arise predominantly in denser regions.

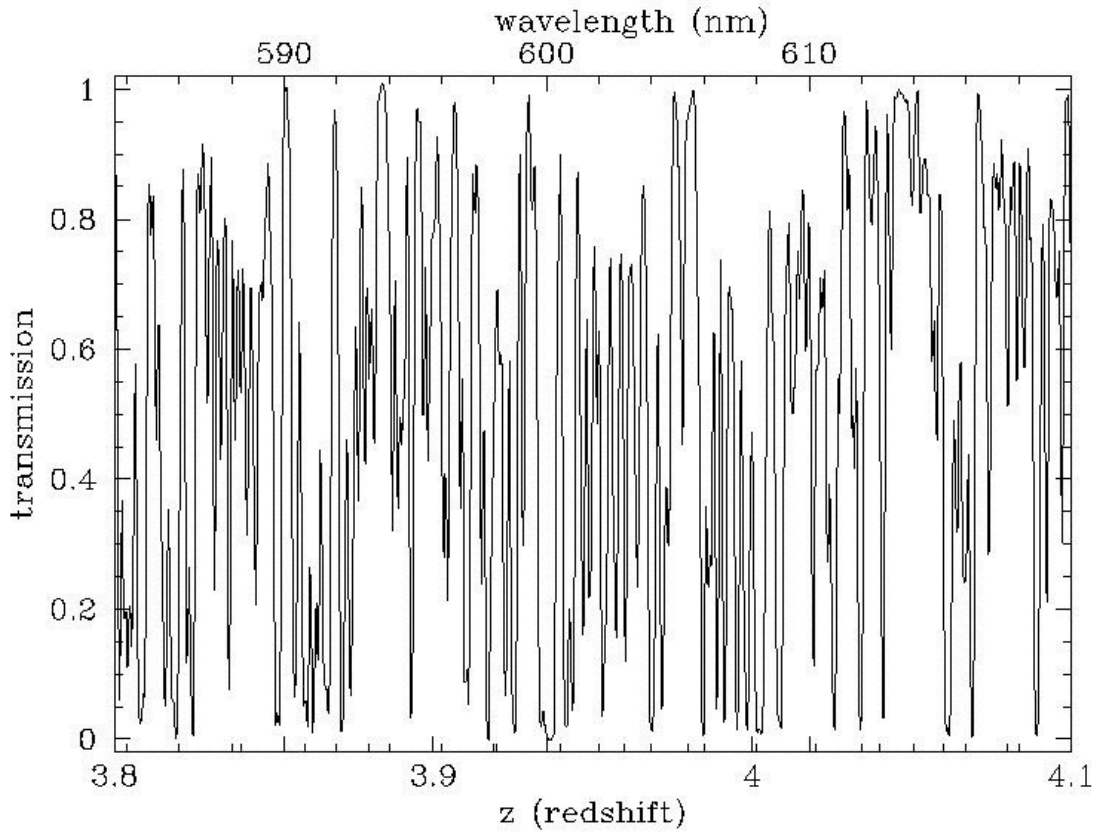

Figure 3-4: *The transmission of the intergalactic medium at redshift z ~ 4, observed along the line of sight to the QSO Q0000-26. The average transmission is about 0.5 and hundreds of features modulate the signal between 0 and 1.*

3.5 Achievable accuracy for a photon noise limited experiment using QSO absorption spectra

3.5.1 Monte Carlo simulations of the Lyman-α forest

In section 3.3 (Figure 3-1) we have seen that the detection of the redshift drift, ż, requires a radial velocity accuracy of order $\sigma_v \sim 1$ cm/s. Given the properties of the Lyα forest, how many spectra of which resolution and signal-to-noise ratio (S/N) are required to achieve this accuracy? How does σ_v depend on redshift?

High-resolution observations have demonstrated that, to first approximation, the Lyα forest can be decomposed into individual absorption lines. One way to answer the questions above is to generate *simulated* spectra with the desired instrumental characteristics from lists of absorption lines which have previously been derived from *real* observations. However, at any given redshift there are only few spectra for which line lists are available over the entire Lyα forest region and therefore it is difficult to investigate realistic error distributions induced by sightline-to-sightline variations using this method.

In this section we explore an alternative approach: Monte Carlo simulations allow us to quickly generate any number of realizations of the Lyα forest at any redshift and hence to fully explore how well the cosmic signal can be recovered as a function of the basic parameters of the experiment. In future, the tools developed here may also be used to investigate the effects of potential systematic errors as well as calibration issues.

3.5.1.1 Line lists

As noted above, the Lyα forest can be decomposed into a collection of individual absorption lines. These are usually taken to be Voigt profiles and so each line is characterized by three parameters: redshift z, neutral hydrogen gas column density N_{HI}, and velocity width b. Reversing the decomposition we can simulate a Lyα forest spectrum by simply randomly drawing values for the above parameters from the observed distributions (e.g. Kim et al. 2001):

$$f(z, N_{HI}, b) \propto (1+z)^{2.2} N_{HI}^{-1.5} \exp\left(-\frac{(b-\bar{b})^2}{2\sigma_b^2}\right), \quad (6)$$

where $\bar{b}$ = 30 km/s, σ_b = 8 km/s and we impose limits of 15 < b < 100 km/s. We also restrict N_{HI} to the classical Lyα forest regime and hence exclude Lyman limit and damped Lyα systems: 12 < log N_{HI} (cm^{-2}) < 16. The above distribution is normalized to give 100 lines with 13.64 < log N_{HI} (cm^{-2}) < 16 per unit redshift at z = 2 (Kim et al.2001).

Note that we make no assumptions about the underlying physics of the intergalactic medium in which the absorption occurs. We simply use the observational fact that Lyα forest spectra can be well represented as a random collection of Voigt profiles.

The most significant difference between our Monte Carlo line lists and the real Lyα forest is clustering: the real Lyα forest is not randomly distributed in redshift but shows significant redshift-space correlations on scales of at least 100 km/s. However, experiments with line lists derived from real data indicate that the systematic effect introduced by clustering is smaller than the sightline-to-sightline variations.

3.5.1.2 Generating spectra

Given an absorption line list a normalized spectrum is generated by

$$s(\lambda) = \exp\left(-\sum_{i}^{N} \tau(\lambda_{Ly\alpha}(1+z_i), N_{HI,i}, b_i)\right), \quad (7)$$

where N is the number of absorption lines in the spectrum, τ is the optical depth of a Voigt profile and $\lambda_{Ly\alpha}$ = 121.567 nm is the rest wavelength of the Lyα transition. This spectrum is then pixelized and convolved with an assumed line-spread function. In this section, unless otherwise stated, we will use a pixel size of 0.00125 nm and a resolution element four times this size, corresponding to a resolution of R =100,000 at 500 nm and a sampling of 4 pixels per resolution element. We then add random noise to the spectrum assuming Poisson statistics and all S/N values quoted in the rest of this section refer to the S/N per pixel in the continuum. Finally, for a given spectrum we only consider the spectral range between the assumed background QSO's Lyα and Lyβ emission lines, i.e. the classical Lyα forest region. Figure 3-5 shows an example of a simulated spectrum.

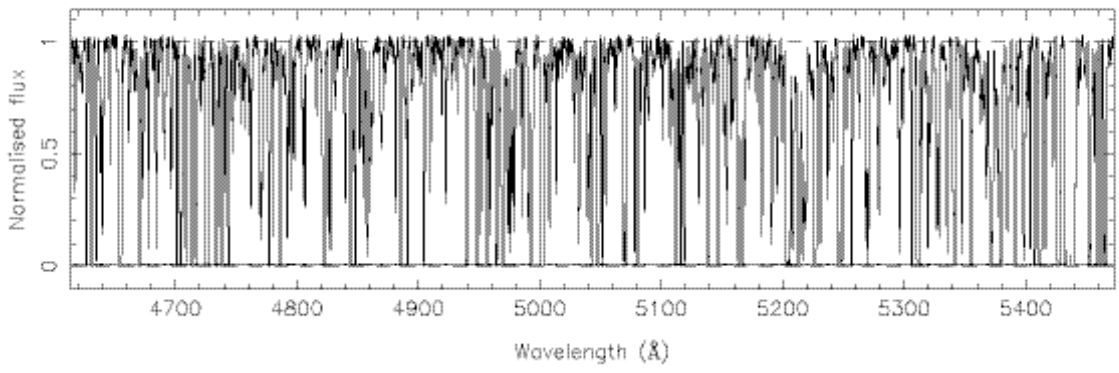

Figure 3-5: *Simulated Lyα forest spectrum for a QSO at z = 3.5 with S/N = 100. The line near zero flux is the 1σ error array.*

3.5.1.3 The second epoch

Simulating a ż measurement requires a second epoch observation' of the same spectrum: first we generate a second epoch absorption line list from the original line list by simply shifting the redshift of each line according to a given cosmological model:

$$\Delta z_i = \frac{dz}{dt}(z_i; H_o, \Omega_M, \Omega_\Lambda)\Delta t, \tag{8}$$

where Δt is the assumed time interval between the first and second epochs. We use H_0 = 70 km/s/Mpc, Ω_M = 0.3 and Ω_Λ = 0.7 unless stated otherwise. The second epoch spectrum is then generated from the new line list in the same manner as before. Figure 3-6 shows the flux difference of two simulated (noiseless) spectra taken Δt = 10 years apart.

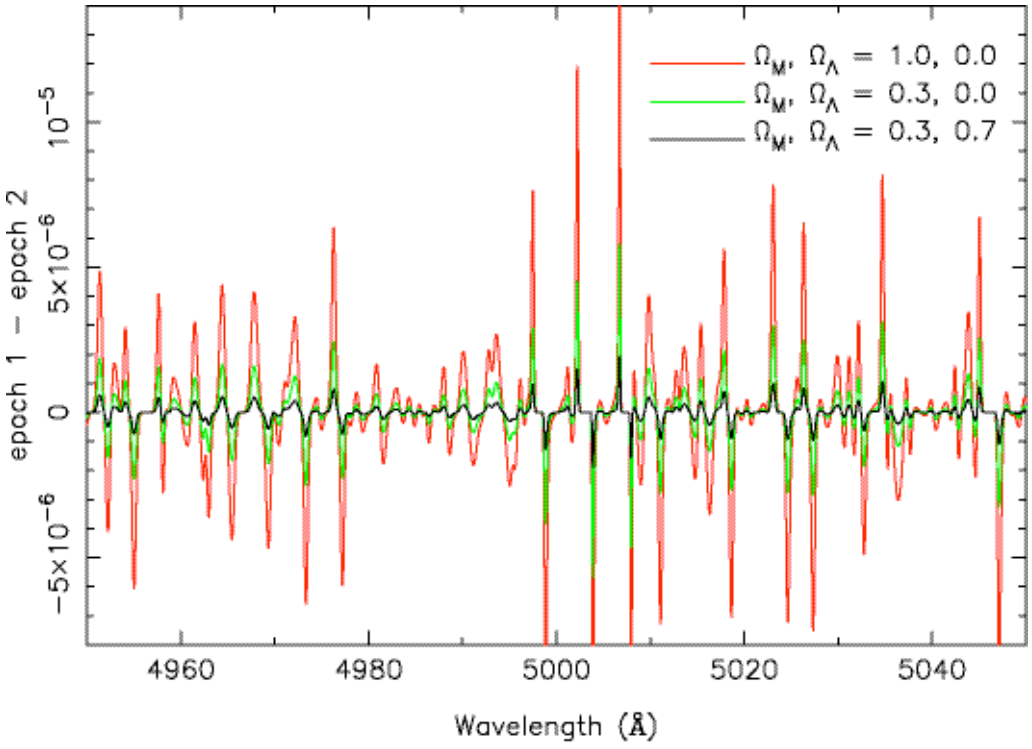

Figure 3-6: *Flux difference of two simulated, noiseless Lyα forest spectra at z = 3.1 taken Δt = 10 years apart for different cosmological parameters as indicated and H_0 = 70 km/s/Mpc.*

3.5.2 Defining σ_v

In practice, a ż determination will involve the measurement of a radial velocity difference between a pair of spectra of the same object taken several years apart. We now need a method to estimate σ_v, the accuracy to which this difference can be determined. We follow Bouchy et al. (2001) and express the flux observed in pixel i at the second epoch as a small perturbation on the first epoch flux in the same pixel:

$$s_i^2 = s_i^1 + \frac{ds_i^1}{d\lambda}\frac{\Delta v_i}{c}\lambda_i, \tag{9}$$

which defines a small velocity shift Δv_i for each pixel. Averaging this shift over all pixels in a spectrum, using weights w_i, we have:

$$\Delta v = \frac{\sum_i \Delta v_i w_i}{\sum_i w_i} \tag{10}$$

and hence

$$\sigma_v = \frac{1}{\sum_i w_i} \tag{11}$$

Clearly, the weight for the i-th pixel should be chosen as the inverse variance of Δv_i. Here we must differ from Bouchy et al. (2001) because in our case both spectra have noise. We find:

$$\sigma_{v,i}^2 = \left(\frac{c}{\lambda_i \frac{ds_i^1}{d\lambda}} \right)^2 \left[(\sigma_i^1)^2 + (\sigma_i^2)^2 + \frac{(s_i^2 - s_i^1)^2}{\left(\frac{ds_i^1}{d\lambda} \right)^2} (\sigma_{v,i}^1)^2 \right], \tag{12}$$

where σ^1_i/σ^2_i are the flux errors in the i-th pixel of the first and second epoch spectra and $\sigma^1_{s,i}$ is the error on the slope of the flux in pixel *i*.

3.5.3 Scaling behavior of σ_v

In Figure 3-7 we show σ_v as a function of spectral resolution. Note that σ_v does not depend on resolution as long as the absorption lines are resolved. Figure 3-8 shows the behavior of σ_v as a function of QSO redshift (dots). The scaling of σ_v can be summarized as follows,

$$\sigma_v = 2 \left(\frac{S/N}{2350} \right)^{-1} \left(\frac{N_{QSO}}{30} \right)^{-1/2} \left(\frac{1+Z_{QSO}}{5} \right)^{-1.8} cm/s, \tag{13}$$

where σ_v referes to the accuracy obtained by the experiment, S/N to the S/N ratio of each single epoch measurement and N_{QSO} is the number of QSO spectra. The scaling relations with S/N and N_{QSO} are those expected for a photon-noise limited experiment. The dependence on z_{QSO} is only valid for $z_{QSO} < 4.4$. For higher redshifts σ_v remains approximately constant. The redshift dependence of σ_v is a combination of several factors:

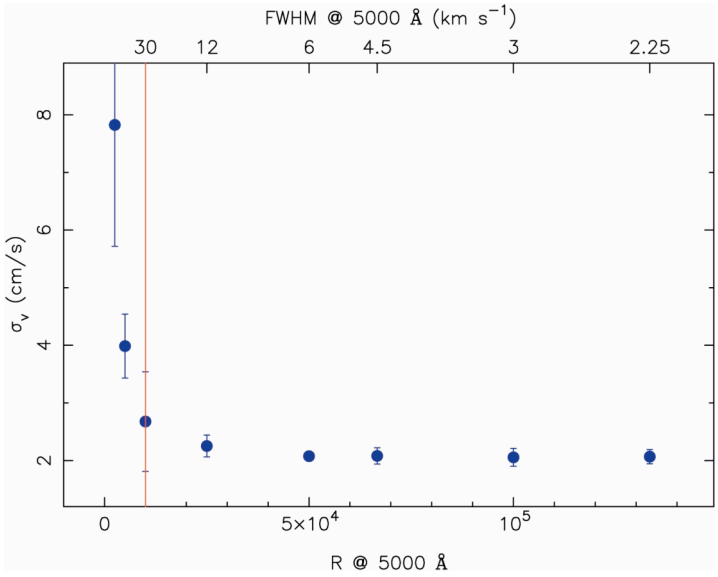

Figure 3-7: *σ_v as a function of spectral resolution. Note the lack of improvement of the sensitivity at R > 50000. The pixel size is kept constant at 0.00125 nm so that a resolution element at the highest resolution is still sampled by 3 pixels. Each point is the mean of 10 simulations at z = 3.5 and S/N = 15000. The error bars show the rms of the 10 simulations, increased by a factor of 2 for clarity. The vertical line shows the mode of absorption line width distribution ($\overline{b}$ =30 km/s).*

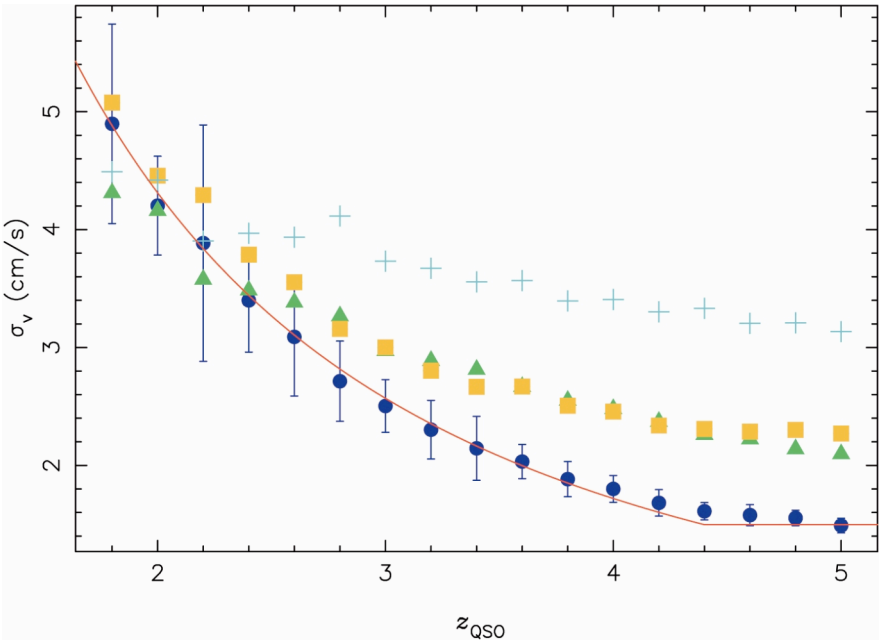

Figure 3-8: *The blue dots with error bars show σ_v as a function of QSO redshift. Note the quasi-saturation of the sensitivity at z > 4.4. The red line goes as $(1+z)^{-1.8}$ for z < 4.4 and is constant for z > 4.4. The orange squares show the evolution of σ_v when using a constant redshift interval of z =0.4 instead of the full Lyα forest region between the QSO's Lyα and Lyβ emission lines. The green triangles show the results for simulations where the redshift evolution of the Lyα forest line density has been switched off, i.e. where γ = 0 (cf.equation 6). Finally, the cyan crosses show the combined case, Δz = 0.4 and γ =0. Each point is the mean of 10 simulations at S/N = 15000, and the error bars show the rms of the simulations, shown only for the original set and increased by a factor of 2 for clarity.*

(i) The observable redshift range of the Ly□ forest (i.e. the region between the QSO's Lyα and Lyβ emission lines) is given by $\Delta z = 0.156\ (1+z_{QSO})$. Hence the number of independent pixels entering the analysis also increases as $(1+z_{QSO})$. The squares in Figure 3-8 show the result of using a constant $\Delta z = 0.4$ at all redshifts.

(ii) The redshift evolution of the Lyα forest line density (cf. equation 6). As the line density increases towards higher redshift, more spectral features are available for determining a velocity shift and so σ_v decreases. However, from z ~ 4 the absorption lines severely blanket each other and a large fraction of the spectrum is absorbed. Thus the number of steep spectral features does not increase any further, causing the `saturation' of σ_v at $z_{QSO} > 4.4$. The triangles in Figure 3-8 show the result of switching off the Lyα forest redshift evolution, i.e. of setting the evolutionary index γ to 0 (cf. equation 6). Indeed we can see that now σ_v continues to decrease even at z > 4.4.

(iii) In wavelength space the widths of the absorption lines decreases as 1/(1+z), making the edges of the lines less steep and hence decreasing the spectrum's sensitivity to velocity shifts.

(iv) Finally, we can see from equation (12) that, all else being equal, σ_v goes as $1/\lambda \propto 1/(1+z)$. This actually over-compensates the previous effect and leads to the behavior shown by the crosses in Figure 3-8, where we have set $\Delta z = 0.4$ and $\gamma = 0$.

Comparison of Figure 3-1 and equation 13 makes it immediately clear that beating the photon noise will make substantial demands on the typical apparent brightness of the observed sources, the product of collecting area of the telescope and the total efficiency of the optical system, the amount of observing time and the effective duration of the observing epoch.

3.6 Measuring ż

Analogous to equation (9) we can define and measure a Δz_i for each pixel of a pair of Lyα forest spectra taken Δt years apart and these measurements can be directly compared to a model $\dot{z}(z)$. This is shown in Figure 3-9: the (binned) `data' points come from 30 simulated spectra of S/N =3000, where the background QSOs were randomly assigned a redshift in the range $2 < z_{QSO} < 4.5$, and we assumed $\Delta t = 20$ years. The deviations from $\Delta z = 0$ are clearly visible at z > 3 and in this particular case the cosmic signal is detected at the >99 % confidence level.

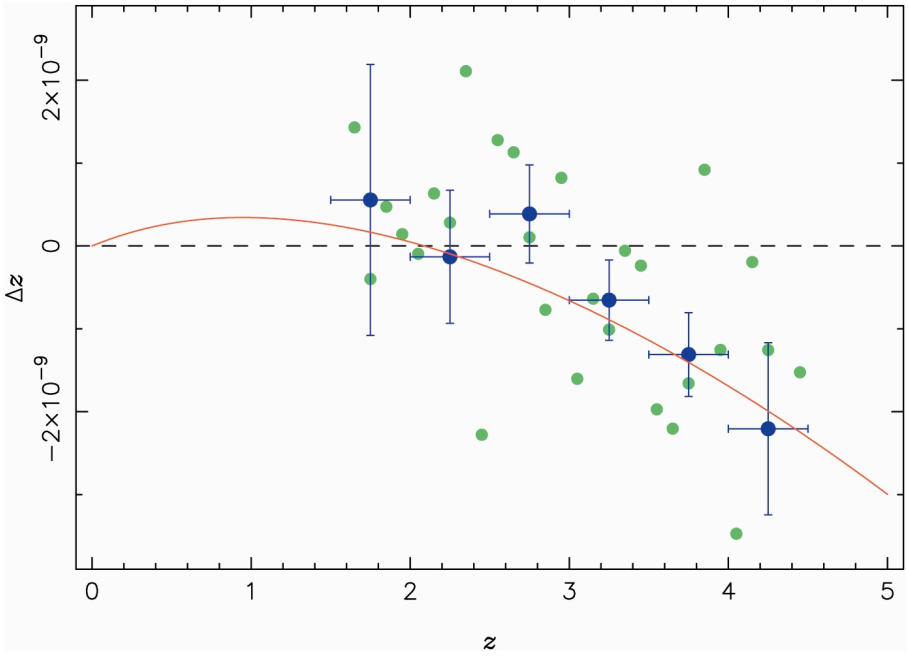

Figure 3-9: *Monte Carlo simulation of a ż measurement using 30 pairs of Lyα forest spectra with S/N = 3000 per pixel in the range $2 < z_{QSO} < 4.5$, where the pairs are separated by $\Delta t = 20$ years. The green points show the simulated data in bins of 0.1, the blue points with error bars show the same data in bins of width 0.5. The solid line shows the expectation for the input cosmological model of $H_0 = 70$ km/s/Mpc, $\Omega_M = 0.3$ and $\Omega_\Lambda = 0.7$.*

3.6.1 Metal lines

Unfortunately, a parametrisation analogous to equation (6) does not exist for metal lines. Hence we cannot perform Monte Carlo simulations of sightline-to-sightline variations as we have done for the Lyα forest, and we have no choice but to resort to absorption line lists derived from real data. Here we will use the line list of Q1101-264 at z_{QSO} =2.145, which was derived from a VLT/UVES spectrum, and we will consider the metal lines red-wards of the QSO's Lyα emission line as well as those lying in the Lyα forest region. Naturally, the additional absorption lines increase the sensitivity of the spectrum to radial velocity shifts, especially since metal lines are generally significantly narrower than Lyα absorption lines. Applying the formalism of section 3.6.4 to the line list of Q1101-264 we find that the metal lines decrease σ_v by a factor of 0.7 compared to the Lyα-forest-only case.

However, when it comes to actually measuring $\dot{z}$ (cf.Fig.3-9) one needs to consider that in general the optical depth in a given pixel may be contributed by multiple absorbers with very different rest-wavelengths and hence very different redshifts. Thus the Δv_i of equation (9) may contain multiple contributions, each of different magnitude and possibly even of different sign. Taking this effect into account is particularly important in the Lyα forest region. From the simulations of Q1101-264 we find that the presence of unidentified metal lines in the Lyα forest significantly biases the determination of $\dot{z}$ by ~20 %.

3.7 The Quasar Sample

An important input for the feasibility of the project is a knowledge of the brightest QSOs - their numbers and redshifts in the surveys made to date. *The numbers* will help to decide on the observing strategy to adopt to make the CODEX experiment successful.

The redshift interval on which we have focused our QSO selection is 1 to 5. As shown by the simulations (e.g. Figure 3-8) beyond redshift z=4.4 a saturation of the sensitivity to the cosmic signal takes place (and less and fainter QSOs are available), while at redshifts lower than about 2 only the metal-lines will be accessible in the optical spectra (redwards of the Lyα QSO emission). Hence, the QSOs with redshifts between 2 and 4.5 are the most promising for our experiment, since their spectra will provide information on both the metal-lines and the Lyα forest. Consequently, the critical wavelength range for the CODEX spectrograph is identified to lie between 380 and 700 nm.

3.7.1 Quasar catalogues

The QSO sample presented here has been assembled from two QSO catalogues: the Véron-Cetty & Véron (2003) catalogue and the Sloan Digital Sky Survey Data Release 3 (SDSS DR3, Abazajian et al. 2005). These are the richest QSO catalogues in the current literature. We describe in Appendix 2 how the QSO selection from each of these catalogues has been carried out. In total 4639 QSOs turn out to be suitable for the CODEX experiment with redshifts between 1 and 5 and magnitudes < 18.5.

3.7.2 Redshift and magnitude distributions

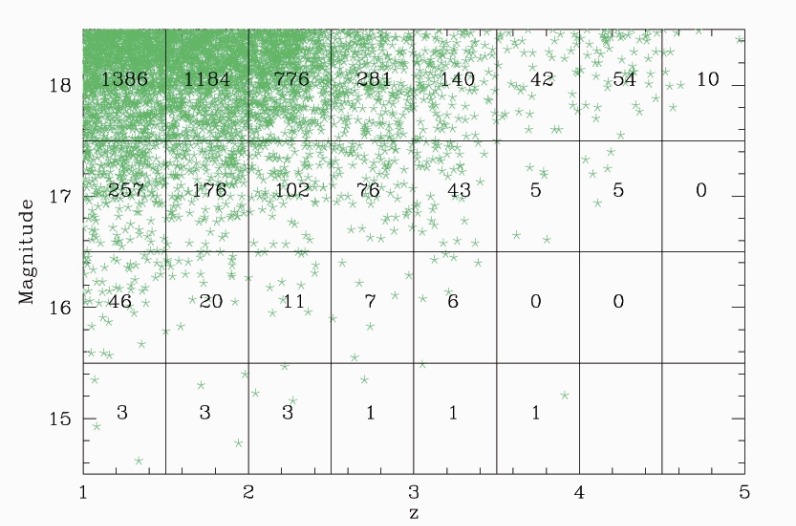

Figure 3-10: *The redshift and magnitude distribution of the 4639 QSOs in our sample. The number of QSOs found in each 0.5 redshift and 1 magnitude bin is shown.*

The 4639 QSOs satisfying our selection criteria clearly show a peak toward low redshifts, $z_{QSO} < 2$, and toward faint magnitudes, > 18, in their respective distributions. The number of high redshift QSOs and the number of bright QSOs are both steeply decreasing, as illustrated in Figure 3-10 showing the redshift-magnitude distribution of QSOs in our sample. **The sample contains a total of 91 QSOs brighter than magnitude 16.5 with a redshift up to 4 and 25 QSOs brighter than magnitude 16.5 with a redshift between 2 and 4.**

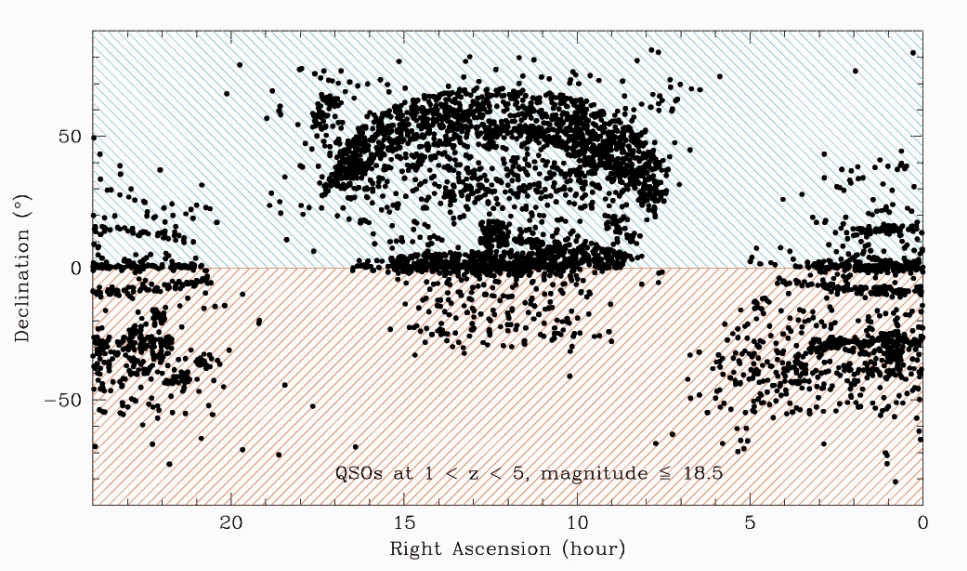

Figure 3-11: *Sky distribution of the selected 4639 QSOs at redshifts between 1 and 5 and with magnitudes < 18.5.*

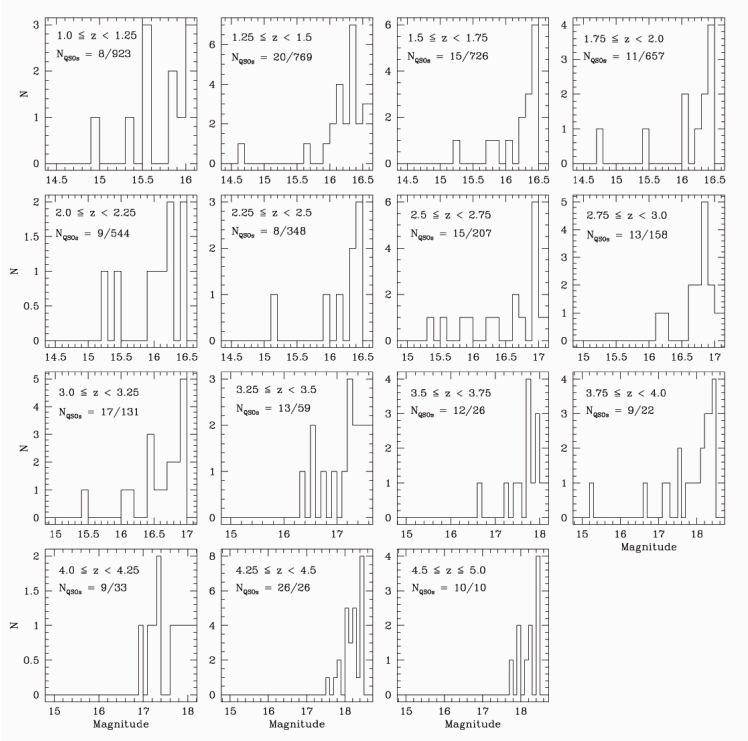

Figure 3-12: *Magnitude distributions of QSOs in our sample plotted in redshift bins of 0.25. N_{QSOs} corresponds to the number of QSOs in a chosen magnitude interval over the total number of QSOs found in the redshift bin.*

We have also investigated the spatial distribution of the 4639 QSOs in our sample. In Figure 3-11 we show the sky distribution of bright QSOs with magnitudes <18.5 and redshifts between 1 and 5 found in the current QSO surveys. The sparcely populated regions, aside from the zone of avoidance corresponding to the galactic equator, are expected to be filled up with future QSO surveys. There should thus be significantly more bright QSOs available when OWL will be in operation. We further notice that the majority of the known bright QSOs are in the northern hemisphere. This reflects the bias of the sky coverage of existing QSO surveys. Future surveys can thus significantly increase the number of bright QSOs available in the southern hemisphere.

Finally, we present the magnitude distribution of the QSOs in redshift intervals of 0.25 (see Figure 3-12). At lower redshifts, one easily finds more than 10 QSOs brighter than magnitude 17.5 in each redshift bin, while from z_{QSO} = 3.5 it is necessary to extend the magnitude interval up to 18.5 to find at least 10 QSOs per redshift bin. The coordinates, redshifts and magnitudes of the 10 brightest QSOs per redshift bin of 0.25 are listed in Table 1 in Appendix 2.

3.8 Peculiar accelerations and other contaminants for measurements of ż from QSO absorption spectra

3.8.1 General considerations

A possible contaminant for measurements of ż are peculiar accelerations of the emitting/absorbing material. Let's start with a simple estimate of the effect. The expected velocity shift scales with the peculiar acceleration of the absorber and the duration of the experiment Δt_{obs} as

$$\delta v_{shift} = g_{acc}\Delta t_{obs} \approx 1\left(\frac{g_{acc}}{3\times10^{-9}\,cm/s^2}\right)\left(\frac{\Delta t_{obs}}{10\,yr}\right)cm/s$$
$$= \left(\frac{\Delta v_{aoc}}{t_{aoc}}\right)\Delta t_{obs} \approx 1\left(\frac{\Delta v_{acc}}{100\ \ km/s}\right)\left(\frac{t_{aoc}}{10^8\,yr}\right)^{-1}\left(\frac{\Delta t_{obs}}{10\,yr}\right)cm/s \quad (14)$$

Other possible contaminants are changes of the absorbers due to changes in the ionization state or the underlying continuum emission. We will discuss these in more detail in turn.

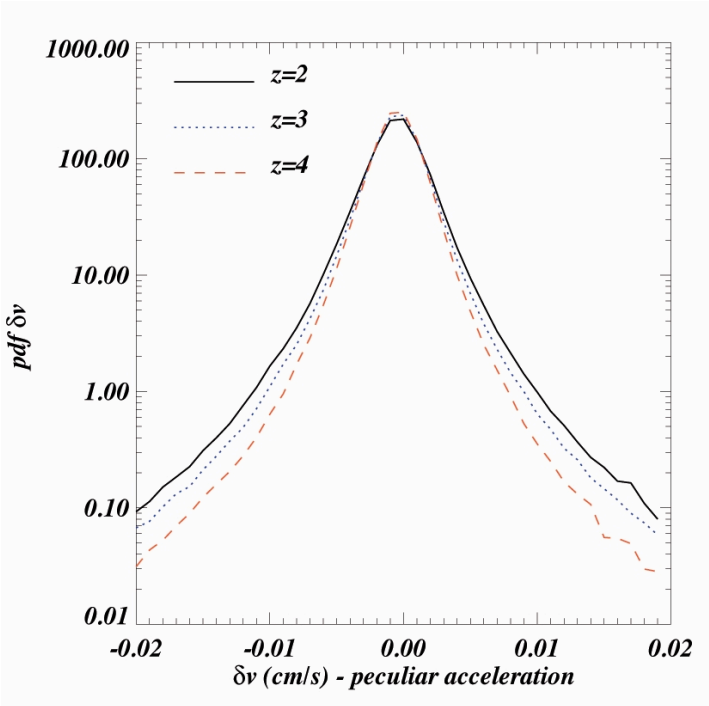

Figure 3-13: *The distribution of expected velocity shifts due to peculiar acceleration over a period of 10 yrs as estimated from a state-of the art numerical hydro-simulations of the Lyα forest based on the measured peculiar velocity and a local estimate of the dynamical time.*

3.8.2 Peculiar accelerations in the Lyman-α forest and metal absorption systems

Typical peculiar velocities of the gas responsible for the Lyα forest absorption with optical depth of order unity are about 100 km/s. The characteristic timescale on which these peculiar velocities change is of order the dynamical timescale of the absorbing gas which is 10^9/yr or larger. Peculiar acceleration of the Lyα forest can therefore be safely neglected. This is further demonstrated in Figure 3-13 which shows the distribution of expected velocity shifts due to peculiar acceleration over a period of 10 yrs as estimated from a state-of the art numerical hydrosimulations of the Lyα forest based on the measured peculiar velocity and a local estimate of the dynamical time. The peculiar velocities of metal absorption systems can be larger (up to a few hundred km/s) and the typical times on which they change can be 10^8/yr or shorter. For the narrowest metal absorption systems originating deep in galactic potential wells velocity shifts due to peculiar accelerations are thus expected to be larger than the cosmic signal. The peculiar velocities will, however, not change coherently over large wavelength ranges. The peculiar accelerations of metal absorption systems therefore just act as additional noise.

The effect of peculiar accelerations will average out for the large number of metal absorption systems which are necessary to beat the photon noise for a ż experiment that works in the optical wavelength range. This is different from observations at radio wavelengths (masers, molecular absorption lines etc.) in which the peculiar accelerations are expected to completely swamp the cosmic signal.

3.8.3 Variations of the ionization state

The UV background responsible for the highly ionized state of the gas making up the Lyα forest absorption is due to a superposition of a large number of sources. The typical attenuation length at z=4 is a few hundred (comoving) Mpc and becomes larger than the Hubble radius at z=2. Global changes of the amplitude of the UV background and the temperature of the IGM are of order unity over a Hubble time. For absorption systems with a typical width of 30 km/s the apparent shifts which can be caused by variations of the ionization state are thus two order of magnitudes smaller than the cosmic signal. The situation is different for metal absorption systems which arise from deep in galactic potential wells. The flux of UV photons could there easily vary by factors of order unity on timescales of 10^7 yr. This may thus lead to velocity shifts of order the comic signal.

3.8.4 Intrinsic variability of the QSO and its effect on the "continuum" of QSO absorption spectra

Typical QSOs show variations of luminosity and spectral shape from a few percent to order of unity on timescales of years. An important step in obtaining an absorption spectrum is the determination of the "continuum" emission of the QSO which is a superposition of emission lines and and power-law emission from non-thermal processes in the vicinity of an accreting black hole. Errors in the determination of the continuum also act as noise on the measurement of ż.

3.9 Conclusions

In order to detect the systematic wavelength displacement of spectral features of light emitted at high redshift and probe **directly** the evolution of the expansion of the Universe an accuracy corresponding to a Doppler shift of a few cm/s over a period of 10 years has to be achieved.

The most promising targets for a measurement of this ż appear to be the numerous absorption lines observed in the spectra of high-redshift quasars: mainly the so-called Lyα forest, but also the rarer but sharper metal absorption lines, provided that the responsible transitions are properly identified.

The optimal redshift range for the observation of the Lyα forest, $2 < z < 4.5$ translates into a requirement on the wavelength range to be observed with CODEX: $380 < \lambda < 700$ nm.

The accuracy of the measurement does not depend on the resolution of the spectra as long as the spectral features are resolved. The goal of using metal lines to improve on the sensitivity of the Lyα forest observations and extending the redshift range over which the cosmic signal is sampled down to $z \sim 1$, therefore sets a lower limit on the resolution $R > 100.000 - 150.000$.

Obtaining spectra of ~30 quasars with a S/N at the continuum of the order of 2000 per 0.00125 nm pixel between redshift 2 and 4.5 would provide an accuracy sufficient for the detection of the cosmic signal. A total of 91 QSOs brighter than magnitude 16.5 with a redshift up to 4 and 25 QSOs brighter than magnitude 16.5 with a redshift between 2 and 4 is known in the literature, which provides a suitable sample of targets for observations with a 100m class telescope. These numbers are likely to increase significantly with planned future surveys. This will make it possible to use even brighter sources for CODEX and to reduce the required observing time.

Figure 3-14 summarizes the present situation and demonstrates that a sufficient number of targets is available to carry out the program with reasonable assumptions. Figure 3-14 shows the redshift of known bright QSOs vs. the QSO magnitude. Only the five brightest QSOs in each 0.25 redshift bin are shown. The dashed lines represent iso-accuracy curves corresponding to 1, 1.5 and 2 cm/sec respectively. The curves have been computed assuming the photon noise resulting from 2000 hours of observations with CODEX and an 80 meter telescope, a global efficiency of 14% and a redshift dependence of the accuracy as found in our simulations (cf. equation 13). All the objects as bright or brighter than the iso-accuracy curves will be suitable

to complete the program with a σ_v (on the single epoch) as labeled on the plot and within the above mentioned observing limits.

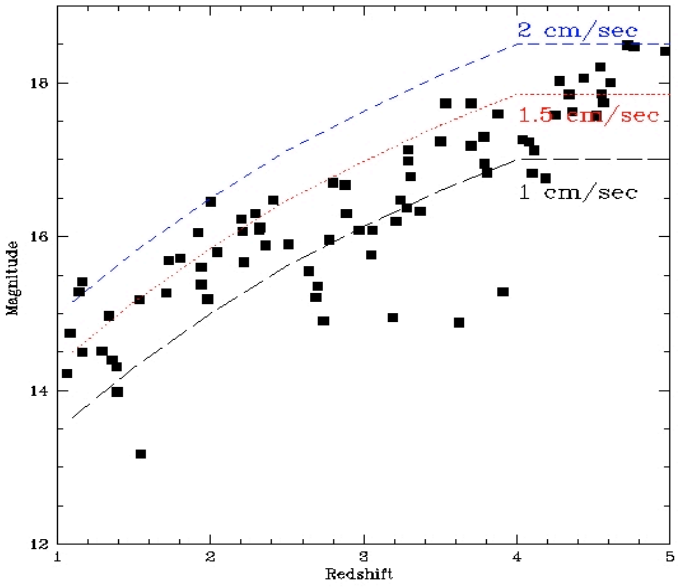

Figure 3-14: *Diagram showing redshift and magnitudes of known bright QSOs (5 brightest in each 0.25 redshift bin). Overimposed are the iso-accuracy curves for 1,1.5 and 2 cm/sec respectively. The curves have been computed by assuming the photon noise for 2000 hours of observations with CODEX on an 80 meter telescope with a total efficiency of 14%. The curves also take into account the dependence of the measurement accuracy on the redshift as found from our simulations, given in Equation (13).*

From the analysis of the peculiar accelerations and other contaminants of ż in the Lyα forest we could not identify any obvious show stopper: their level is significantly lower than the cosmic signal. This is no surprise since hydrodynamical simulations have convincingly demonstrated that the Lyα absorption lines with optical depth of order unity, those contributing most to the detection of the ż signal, arise from moderate density fluctuations in a warm photo-ionized Intergalactic Medium, which closely follows the Hubble flow.

References:

- Abazajian K., Adelman-McCarthy J. K., Agueros M. A., et al. 2005, AJ 129, 1755
- Alpher, R. A., Bethe, H. A., Gamow, G., 1948, Physical Review 73, 803
- Arp H. 2001 ApJ 549, 780
- Arp H., Burbidge E. M., Chu Y., Flesch E., Patat F., Rupprecht G.2002 A & A 391, 833
- Barbachoux C., and Le Denmat G., astro-ph/0209158
- Begeman, K. G., Broeils, A. H. and Sanders, R. H. 1991 MNRAS 240, 523
- Bento, M. C., Bertolami, O. & Sen, A. A.2003 astro-ph/0303538; General Relativity and Gravitation Vol. 35, 11, p. 2063
- Bi H.G., Davidsen A.F., 1997, ApJ, 479, 523
- Boughn, S. P., Crittenden, R. G., 2005, NewAR 49, 75
- Bondi H. \& Gold T. 1948 MNRAS 108, 252
- Croom S. M., Smith R. J., Boyle B. J., Shanks T., Miller L., Outram P. J., Loaring N. S. 2004, MNRAS 349, 1397
- Dave' R., Hernquist, L., Katz, N., Weinberg, D. H., 1999, ApJ, 511, 521
- Davis M. M. & May L. S. 1978 ApJ 219, 1

- Davis T. M. and Lineweaver C. H. 2004 PASA 21, 97
- Einstein, A., 1916, Annalen der Physik, 49
- Fan X., Strauss M. A., Schneider D. P., et al. 1999, AJ 118, 1
- Freedman, W. L. 2002 astro-ph/0202006
- Fukugita M., Ichikawa T., Gunn J. E., Doi M., Shimasaku K., Schneider D. P. 1996, AJ 111, 1748
- Harrison, E. R. 1976 Nature 260, 591
- Hernquist L., Katz N., Weinberg D.H., Miralda-Escude', 1996, ApJ, 457, L51
- Hoyle F., Burbidge G. & Narlikar J. V. 1995 MNRAS 277, 1
- Kim, T.-S., Carswell, R. F., Cristiani, S., D'Odorico, S., Giallongo, E. 2002, MNRAS, 335, 555
- Lake K. 1981 ApJ 247, 17
- Loeb A. 1998 ApJ 499, 111L
- Mayor, M., Pepe, F., Queloz, D. and Rupprecht, G. 2002 The ESO Messenger No. 110
- Meiksin A., Bryan G., Macachacek M., 2001, MNRAS, 327, 296
- Miralda-Escude' J. et al. 1996, ApJ, 471, 582
- Miyoshi, M., Moran, J., Herrnstein, J., Greenhill, L., Nakai, N., Diamond, P., Inoue M., 1995, Nature, 391, 51
- Murphy, M. T., Webb, J. K., Flambaum, V. V., Drinkwater, M. J., Combes, F., Wiklind, T., 2001, MNRAS, 327, 1244
- Penzias, A. A., Wilson, R. W., 1965, ApJ 142, 419
- Perlmutter S. and the Supernova Cosmology Project team 1999 ApJ 517, 565
- Phillipps, S. 1982 ApJ 22, 123L
- Rauch M., 1998, ARA&A, 36, 267
- Riess A. G. and the High-z Supernova Search team 1998 AJ 116, 1009
- Rudiger, R. 1980 ApJ 240, 384
- Sandage, A. 1962 ApJ 136, 319
- Santos, N. C., Bouchy, F., Mayor, M., Pepe, F., Queloz, D., Udry, S., Lovis, C., Bazot, M., Benz, W., Bertaux, J.-L., Lo Curto, G., Delfosse, X., Mordasini, C., Naef, D., Sivan, J.-P., Vauclair, S., 2004, A&A 426, L19
- Smette, A., Surdej, J., Shaver, P. A., Foltz, C. B., Chaffee, F. H., Weymann, R. J., Williams, R. E., Magain, P., 1992, ApJ, 389, 39
- Smette, A., Robertson, J. G., Shaver, P. A., Reimers, D., Wisotzki, L., Koehler, T., 1995, A&AS, 113, 199
- Spergel D. N. and the WMAP collaboration 2003 ApJS 148, 175
- Theuns T. et al. 1998, MNRAS, 301, 478
- Theuns T., Viel M., Kay S., Schaye J., Carswell B., Tzanavaris P., 2002, ApJ, 578, L5
- Véron-Cetty M.-P., Véron P. 2003, A&A 412, 399
- Viel M., Matarrese S., Mo H.J., Haehnelt M.G., Theuns T., 2002, MNRAS, 329, 848

4. CODEX IMMEDIATE SCIENCE CASE

4.1 Summary

CODEX, being an excellent, super-stable high resolution spectrograph at OWL, will bring fundamental results in many areas of astrophysics. Among many possibilities we opted to concentrate on only three well established cases for which smaller telescopes have been extensively used and where major breakthroughs are expected.

4.1.1 Search for variability of fundamental constants

Fundamental constants cannot be deduced from first principles and are supposedly universal and invariable quantities. They play an important role in our understanding of nature, since they *capture at once our greatest knowledge and our greatest ignorance about the universe* (J. Barrow). Testing for their variability probes fundamental physics. Measured variations would have far reaching consequences for the unified theories of fundamental interactions, for the existence of extra dimensions of space and/or time and for the existence of scalar fields acting in the late universe. Only astronomical observations hold the potential to probe the values of fundamental constants in the remote past, and in remote regions of space. In 2001, observations of spectral lines of distant astronomical objects brought the first hints that the fine-structure constant, α - the central parameter in electromagnetism - might change its value over time, but recent observations are consistent with a null result. The debate over the variability of α is nevertheless still completely open and makes strong demands for a high resolution spectrograph for significant progress. We show that an effective two-order-of-magnitude precision gain is foreseen with a spectrograph with $R \approx$ 150000 at OWL, stemming equally from the higher resolving power of the spectrograph and from the larger photon collecting area of OWL.

4.1.2 Search for other earths

Exo-planets and, in particular, terrestrial planets in habitable zones will be one of the main scientific topics of the next decades, and one of the main OWL science drivers. CODEX@OWL will lead the discoveries in at least three main cases in exo-planetary science, providing with unique capabilities and observations: i) discovery and confirmation of rocky planets, ii) search for long-period planets, iii) Jupiter mass planets around faint stars.

The need for a ground based follow-up facility capable of high radial velocity accuracy has been stressed in the recent ESO-ESA working group report on solar planets, which states in the Summary of Follow-Up facilities required (p. 63): *a) high precision radial velocity instrumentation for the follow-up of astrometric and transit detections, to ensure the detection of a planet by a second independent method, and to determine its true mass. For Jupiter-mass planets, existing instrumentation may be technically adequate but observing time inadequate; for Earth-mass candidates, special purpose instrumentation (like HARPS) on a large telescope would be required.* The concept is re-iterated in the first recommendation to ESO by the committee, which reads: *Support experiments to improve radial velocity mass detection limits, e.g. based on experience from HARPS, down to those imposed by stellar surface phenomena (ESA-ESO report, Section 5, p. 72).*

4.1.3 Primordial nucleosynthesis

Standard Big bang nucleosynthesis presents a pressing cosmological conundrum. There is some evidence suggesting a cosmological origin for ^{6}Li and the stellar value for primordial ^{7}Li does not agree with primordial D from QSOs and with WMAP Ω_b. Although Li observations in low metallicity Galactic halo stars are plagued with possible systematic uncertainties due to modelling of stellar atmospheres and the treatment of

convection, it is appealing that both the discrepancies can be reconciled with physics beyond the standard model during the Quark-Hadron phase. CODEX will allow first observations of ^{7}Li and ^{6}Li in dwarf stars in galaxies of the Local Group and it will make possible to measure for the first time the interstellar ^{7}Li/^{6}Li ratio in unprocessed material of HVC or DLA. The latter is a direct and robust probe of BBN yields providing important insights on whether new physics is playing a role in early universe nucleosynthesis.

4.2 Variability of Fundamental constants

The universality and constancy of the laws of nature rely on the space-time invariance of fundamental constants. The Principle of Equivalence states that “in any free falling local reference frame, the result of a non-gravitational measurement should not depend upon when and where it is performed”, implying the stability of fundamental constants. A great diversity of theoretical and experimental explorations of possible space-time variations in fundamental constants has been pursued (e.g.see review in Uzan 2003).

In particular, much research was focused on the fine-structure constant (or Sommerfeld fine-structure constant), usually denoted α. This is the fundamental physical constant characterizing the strength of the electromagnetic interaction and is defined as $\alpha = e^2/\hbar c 4\pi\varepsilon_0$ where *e* is the elementary charge, $\hbar = h/(2\pi)$ is the reduced Planck's constant, *c* is the speed of light in vacuum, and ε_0 is the permittivity of free space. In electrostatic cgs units, the unit of electric charge is defined in such a way that the permittivity factor $4\pi\varepsilon_0$ is dimensionless and so $\alpha = e^2/\hbar c$. The fine-structure constant is a dimensionless quantity: its numerical value is independent of the system of units used. The value recommended by CODATA as of December 2003 is α = 1/13703599911(46). In quantum electrodynamics, the fine-structure constant plays the role of a coupling constant, representing the strength of the interaction between electrons and photons. Its value cannot be predicted by the theory, and has to be determined experimentally: it is one of the twenty-odd "external parameters" in the Standard Model of particle physics.

Milne and Dirac in the 1930s first suggested the time-variation of the Newton gravitational constant. Today this hypothesis is no longer considered, but many modern theories predict variations of various fundamental constants. The number of fundamental particles, their masses and the coupling constants of their interactions were determined in processes in the early universe. Thus the fundamental constants can be different in different parts of the universe, or they vary in cosmological time. Within inflationary models only a small part of the space-time can inflate to produce our universe, and other parts of the universe may evolve in different ways with different laws and constants of nature. There is a class of theoretical models in which a cosmological scalar field, which may be closely related to the cosmological acceleration, manifests itself through a time-dependent fine structure constant.

String theory unifies physics by producing all known forces and particles as different vibrations of a single substance called superstrings. The strings are too tiny to be observed directly, but string theory makes a number of testable predictions. It implies supersymmetry and predicts seven undiscovered dimensions of space, dimensions that would give rise to much of the mysterious complexity of particle physics. In such higher dimensional theories, the constants' values are defined in the full higher-dimensional space, and the values we observe in the four-dimensional world are not fundamental and do not need to be constant. The effective values of the constants in our 4D space depend on the values of certain scalar fields and on the structure and sizes of the extra dimensions. Any evolution of these sizes, either in time or space, would lead to dynamical constants in the 4D space. If the scalar fields are extremely light, they could produce variations of constants only on cosmological time scales. Thus, any change in the scale of extra dimensions would be revealed by a change in the constants of our 4D space.

According to the renormalization group theory, the value of the fine-structure constant depends on the energy scale and it grows logarithmically as the energy increases. The observed value of α is associated with the energy scale of the electron mass. Since the electron and the positron are the lightest charged objects, the present value for α is the value of the fine-structure constant at zero energy. As the energy scale increases, the electromagnetic interaction approaches the strength of the strong and weak nuclear interactions, which is important for the theories of grand unification. Thus, any variations in α are likely to imply variations in the other coupling constants of the standard model of particle physics.

The functional dependence of the gauge-coupling constants on cosmological time is not known and even oscillations might be possible during the course of the cosmological evolution (Marciano 1984, Fujii 2005). In this regard, astronomical observations are the only way to test such predictions at different space-time coordinates.

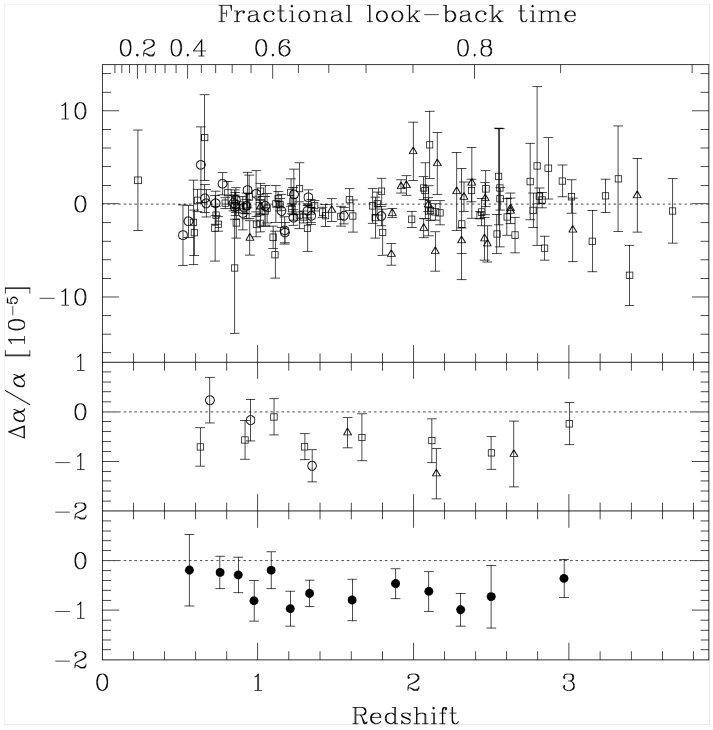

Figure 4-1: Results of Murphy et al. (2004) from 143 absorption systems with HIRES-Keck. A variation in α is found at 5-σ significance at the level of -6 x 10^{-6}.

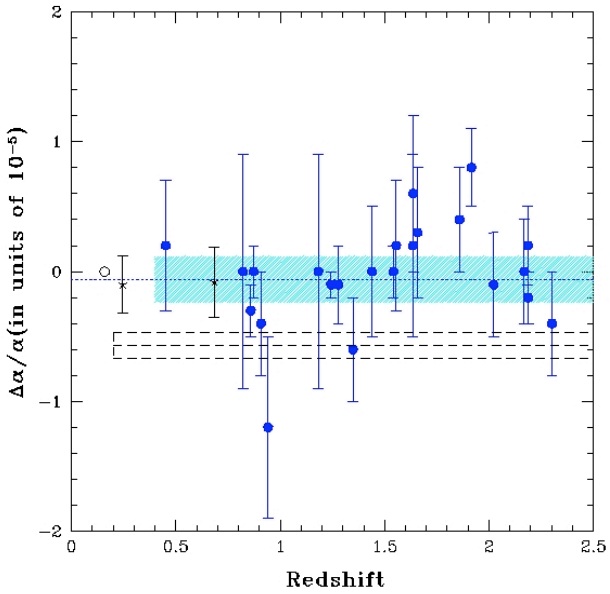

Figure 4-2: Results of Chand et al. (2004a) in 23 absorption systems with UVES-VLT. The shaded region is the $\pm 3\sigma$ error range for the combined results. The Keck results with $\pm 1\sigma$ error range are also shown with the dashed line rectangle.

4.2.1 Measurements and constraints on variability

The mere existence of nucleons, atoms and stars constrains $\delta\alpha/\alpha \leq 10^{-2}$ where we define $\delta\alpha/\alpha=(\alpha_z - \alpha_o)/\alpha_o$, with α_z and α_o the values of α at an epoch z and in the laboratory, respectively. A change by 4% shifts the key resonance level energies in the C and O nuclei which are needed for C and O synthesis from He nuclei. Stable matter, and therefore life and intelligent beings, could not exist if the value were different by as much as 1%. Similar limits are imposed by Big Bang nucleosynthesis (BBN) at $z \approx 10^{10}$ and the cosmic microwave background (CMB) power spectrum at $z \approx 1100$.

Constraints on the present day variation of α in laboratory experiments are based on the comparison of atomic clocks using different types of transitions in different atoms, such as ^{87}Rb and ^{133}Cs. The time-dependence of α is restricted at the level of $(\dot{\alpha}/\alpha)_{t0} \approx 10^{-15}$ y^{-1}. This limit transforms into $|\Delta\alpha/\alpha| < 10^{-5}$, at a cosmological time-scale of $t \sim 10^{10}$ yr, ($z > 1$), assuming α_z is a linear function of t.

The ACES (Atomic Clock Ensemble in Space) project, foreseen to fly on the International Space Station in 2007, will operate several cold atomic clocks in microgravity to test General relativity and search for a possible drift of the fine-structure constant. Neutral atomic clocks in microgravity have the potential to surpass ground based clocks both in the microwave and optical domains. Rubidium clocks should enter the 10^{-17} stability range with a gain of two orders of magnitude with respect to present laboratory constraints.

Meteoritic data on the radioactive β-decay of ^{187}Re place a bound around $\delta\alpha/\alpha \leq 10^{-7}$, but this somewhat model dependent. An intriguing geophysical constraint comes from the Oklo uranium mine in Gabon, Africa, where a fission reaction took place about 1.8 Gyrs ago ($z \approx 0.14$), naturally self-sustained and moderated for about 200,000 years. The isotopic abundances in the rock surrounding the mine provide information about the nuclear rates and therefore about the value of α at that time. A key quantity is the ratio of two light isotopes of samarium which are not fission products. This ratio is 0.9 in normal Sm but about 0.02 in Oklo samples due to the transformation of Sm after neutron capture while the reactor was active. Recent analysis of the isotopic abundances in the Oklo samples provides a hint for a variation at a very low level: $\delta\alpha/\alpha \geq 4.5 \times 10^{-8}$ (Lamoreaux & Torgerson, 2004).

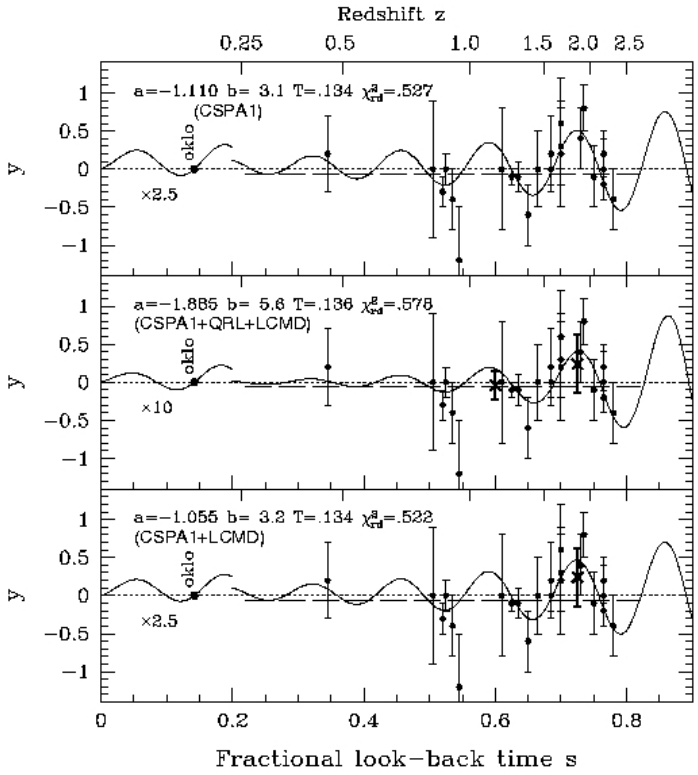

Figure 4-3: *The oscillating α model of Fujii (2005) compared with the UVES-VLT measurements*

The astronomical measurements of the fine-structure splittings of emission lines in galaxies provide $\delta\alpha/\alpha = 10^{-4}$ at relatively low redshift $0.4 < z < 0.8$. Early high resolution spectroscopy of distant absorption systems lying along the lines-of-sight to background QSOs focused on the alkali-doublets (AD) such as C IV, Si II, Si IV, Mg II and Al III, since the comparison between AD separations in absorption systems with those measured in the laboratory provides a simple probe of the variation of α. The best current constraints come from the analysis of Si IV absorption systems in $R \approx 45\,000$ spectra: $\delta\alpha/\alpha = (0.15 \pm 0.43)\ 10^{-5}$ (Chand et al. 2004b, 15 systems; $1.6 < z_{abs} < 3$).

The many-multiplet (MM) method generalizes the AD method by utilizing many transitions from different multiplets and different ions associated with each QSO absorption system (Dzuba, Flambaum & Webb 1999 and Webb et al. 1999). This is because the energy of each transition depends differently on changes in α. The relativistic correction to the frequency of each transition is expressed by the coefficient *q* (Dzuba et al. 1999, 2002). The MM approach compares the line shifts of the species particularly sensitive to a change in α to those with a comparatively minor sensitivity, which are referred to as anchor-lines. Mg, Si and Al act as anchors against which the larger expected shifts in Cr, Fe, Ni and Zn transition wavelengths can be measured. The method holds an effective order-of-magnitude precision gain with respect to the AD method due to the large differences in sensitivity of light and heavy ions to the varying α.

Applied to HIRES-Keck QSO absorption spectra the MM method has yielded the first tentative evidence for a varying α by Webb et al. (1999), which has become stronger with successively larger samples. The most recent value $\delta\alpha/\alpha = (-0.57 \pm 0.11)\ 10^{-5}$ comes from the analysis of 143 absorption systems over the range $0.2 < z_{abs} < 4.2$ (Murphy et al. 2004). The deduced variation of α at about 5 σ significance, if proved correct, would have extraordinary implications. However, the result has not been confirmed by other authors. Chand

et al. (2004a) have analysed 23 Mg/Fe absorption systems in higher signal-to-noise ratio (S/N) spectra from a different telescope and spectrograph, the UVES-VLT, claiming a precise, null result over the range 0.4 < z_{abs} < 2.3, $\delta\alpha/\alpha$ = (-0.06 ± 0.06) 10^{-5}. The validity of both results are still under intense scrutiny in the literature, and the final conclusion from QSO absorption lines is still far from clear.

Another methodology makes use only of pairs of FeII lines observed in individual high resolution exposures. This approach avoids the influence of possible spectral shifts due to ionization inhomogeneities in the absorbers or non-zero offsets between different exposures (Levshakov 2004, Levshakov et al. 2005 and Quast, Reimers & Levshakov 2004). Applied to the FeII lines of the metal absorption line system at z_{abs} = 1.839 in the spectrum of Q1101-264, and to the z_{abs} = 1.15 system in the spectrum of HE0515-4414, this methodology provides $\Delta\alpha/\alpha$ = (0.4±1.5$_{stat}$) x 10^{-6}. This value is shifted with respect to the HIRES-Keck mean at the 95% confidence level. This discrepancy between UVES-VLT and HIRES-Keck results is yet to be resolved. Problems are likely to exist in both datasets and any significant improvement in the future will require higher precision, as we explain below.

Though we have focused here on variations of α, we note in passing that the observation of ro-vibrational transitions of H2 in damped Lyman-α systems provides constraints on variations in the proton-to-electron mass ratio $\mu = m_p / m_e$. The most accurate measurement is at $z \approx 3$ by Ubachs & Reinhold (2004), $\delta\mu/\mu$ = (-0.5 ± 1.8) x 10^{-5} (1σ).

4.2.2 The gain with CODEX

A measure of $\Delta\alpha/\alpha$ is essentially a measurement of the wavelength for a pair of lines with different sensitivity coefficients. Therefore the accuracy of a $\Delta\alpha/\alpha$ measurement is determined by the precision with which a line position can be determined in our spectrum. The best estimate of $\Delta\alpha/\alpha$ has an uncertainty of $\sigma_{\Delta\alpha/\alpha} = 1/(Q1-Q2)\delta_\lambda$, where Q1 and Q2 are dimensiless sensitivity coefficients. For current spectrographs with $R \approx 4 \times 10^4$ the observed line positions can be found with an accuracy of about $\sigma_\lambda \approx 1$ mÅ (or Δv = 60 m s^{-1} at 5000 Å). Thus, $\delta_\lambda \sim 2 \times 10^{-7}$ and we obtain $\sigma_{\Delta\alpha/\alpha} \sim 2 \times 10^{-5}$ for a typical $|Q_1 - Q_2| = 0.01$, in a single measurement.

Any improvement with respect to this figure is related to the possibility to measure more accurately line positions. According to the theory of error analysis, the determination of a line center in presence of photon noise can be improved by increasing the resolving power to resolve the narrowest intervening physical clouds. When this is achieved, accuracy scales with the signal-to-noise ratio per pixel (Bohlin et al. 1983). The Bohlin formula gives a relatively simple analytical expression which has also been tested by means of Monte Carlo analysis: $\sigma_\lambda = \Delta\lambda_{pix}\ (\Delta\lambda_{pix} / W_{obs})\ (1 / \sqrt{N_e})\ (M\sqrt{M} / \sqrt{12})$, where $\Delta\lambda_{pix}$ is the pixel size or the wavelength interval between pixels, W_{obs} is the observed equivalent width, N_e is the mean number of photoelectrons per pixel at the continuum level, and M is the number of pixels covering the line profile. The expression shows that the error σ_λ decreases with decreasing the wavelength bin per pixel, with the total number of pixels that sample the line profile, and with the square-root of N_e.

The metal lines which are observed in QSO absorption systems have intrinsic widths (or b values) of a few km s^{-1}, rarely of less than 1 km s^{-1}. Thus the optimal spectral resolution for the QSO metal lines is the one which resolves lines of $b \sim 1$ km s^{-1} (or FWHM = 1.6 km s^{-1}) and this implies a spectrograph with a resolving power R ≈ 150,000.

The number of photoelectrons which arrive at the detector is given by $N_e = (F_\star s_{tel}\ \varepsilon_{tot}\ t_{exp}\ \Delta\lambda_{pix})/10^{0.4\ mv}$, where s_{tel} is the telescope area in cm^2, ε_{tot} the overall detection efficiency of the telescope, spectrograph and detector corrected for the contribution of the atmosphere, t_{exp} is the exposure time in seconds, mv the visual magnitude of the quasar. The specific flux of a $mv = 0$ star outside the Earth's atmosphere is $F^V = 1.05 \times 10^3$ photon $cm^{-2}\ s^{-1}\ Å^{-1}$. In figure 4-4 an estimate of the accuracy for a spectrograph with R=150,000 is shown for

a line with an equivalent width of W=0.2 Å in the spectrum of a *mv* = 15 QSO with a 100-m telescope.

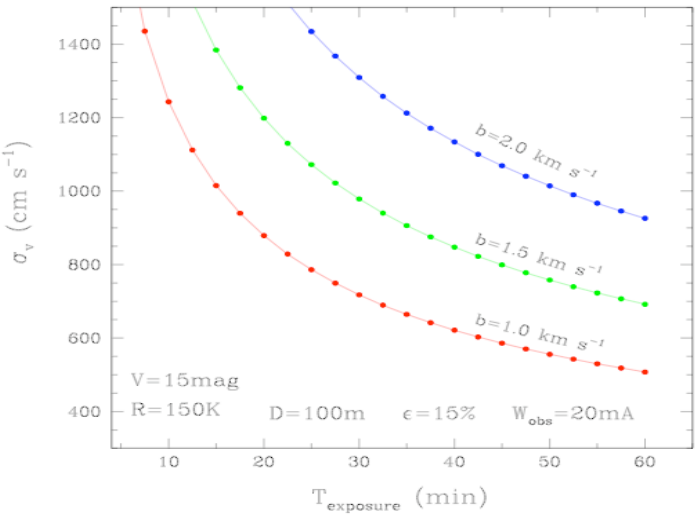

Figure 4-4: *Wavelength precision measurement of a single metal line with intrinsic broadening of 1, 2 and 3 km^{-1}, with a spectrograph with R = 150,000 at a 50-m telescope. See text for details.*

Considering a perfect wavelength calibration, the accuracy in the line position measurement is of the order of σ_λ^{lim} ~10^{-5} Å. Compared with UVES-VLT or HIRES-Keck, this is an improvement of about 2 orders of magnitude. This will allow a precision level in $\Delta\alpha/\alpha$ measurements higher than ~10^{-8}, equivalent or better to the Oklo sensitivity.

Such an improvement is crucial for a definitive and reliable test of the variability of α at the level of, or even better than that found in Oklo and comparable to the limits which are expected from space-borne atomic clock experiments like ACES. An ELT with high resolution spectroscopic capability would therefore act as an important probe of fundamental physics at remote times and distances.

4.3 Immediate Science: Exo-planets with CODEX.

Exo-planets and, in particular, terrestrial planets in habitable zones will be one of the main scientific topics of the next decades in Astronomy, and one of the main OWL science drivers: OWL will have a tremendous impact in this field.

CODEX, with its unprecedented high accuracy, coupled to the unprecedented photon collecting capability of OWL, will lead the discoveries in at least three main aspects of exo-planetary science, providing with unique capabilities and observations:

- Confirmation and possibly discovery of very low mass planets
- Search for long-period planets

- Jupiter mass planets in faint stars

The need for a ground based follow-up facility capable of high RV accuracy has been recently stressed in the **ESO-ESA working group report on solar planets,** which states (at p. 63 of the Summary of Follow-Up facilities required):

a) *high precision radial velocity instrumentation for the follow-up of astrometric and transit detections, to ensure the detection of a planet by a second independent method, and to determine its true mass. For Jupiter-mass planets, existing instrumentation may be technically adequate but observing time inadequate; for Earth-mass candidates, special purpose instrumentation (like HARPS) on a large telescope would be required.* "

The same concept is reiterated in the recommendations of the same committee, whose first recommendation on ESO reads:

b) *Support experiments to improve radial velocity mass detection limits, e.g. based on experience from HARPS, down to those imposed by stellar surface phenomena" (ESA-ESO report, Section 5, p. 72).*

4.3.1 Low mass Planets:

The detection of Earth mass planets in the habitable zone of a star with RV techniques will indeed require a long term RV accuracy of 3-10 cm/sec, well within the CODEX capabilities. In the case of stars, however, the main limitations will be given by the additional stellar 'noise', which must be filtered out in order to clean the planet signal.

There are three main sources of noise when observing solar-type stars in search for RV variations induced by terrestrial mass planets: photon noise, stellar acoustic noise, and stellar activity noise. Each of them is separately discussed in the following.

Photon Noise: Given that the main CODEX aim is measuring the cosmological redshift on faint QSO, we expect that photon noise is not a problem. However, we shall consider that for stellar observations high accuracy must be obtained in a short time and on a single star, without observing a large number of QSOs as in the main CODEX science case. We can evaluate the CODEX performances in this application by extrapolating the HARPS experience. HARPS represents a good approximation for CODEX, because CODEX spectral coverage and resolution is comparable to HARPS, though it will have a much higher intrinsic stability. Considering that for a given spectrograph, RV precision scales linearly with the S/N ratio, going from 1 m/sec to 1 cm/sec will require 10^4 more photons. Part of the flux will be provided by the larger OWL collecting area (about 700 times larger than the 3.6 meter feeding HARPS). Taking at face value the above numbers, this implies that to obtain a photon noise of 1 cm/sec, a S/N ratio of about 8000/pixel for a slowly rotating G star is needed. This requires 15 minutes of integration on a V=7.5 magnitude star with the 100m OWL. This clearly shows that even for a giant telescope, the highest accuracy can be reached only on relatively bright stars, if a short integration time only can be used. However, each individual measurement will be affected by activity – induced and oscillation – induced stellar noise, likely at the 10 cm/sec level (see below) or higher. So, it will not be useful to pursue an accuracy much below such level on a single measurement.

The best strategy is to obtain the aimed precision by accumulating many measurements. To clarify this point it is however needed to look in some detail at the stellar noise: the 'activity' noise and the 'oscillation' noise.

Stellar Activity Noise:

The noise signal (jitter) related to 'stellar activity' is produced by the transit of inhomogeneities across the stellar surface, or by the net effect of asymmetric convective motions. The observations show as the jitter decreases with chromospheric activity; i.e. it is lower in old, slowly rotating, inactive stars. As far as spectral type is concerned, this noise seems to increase at the two ends of the 'solar-type' dwarfs, that is, among the dMe stars and the F stars (Saar et al. 1998, Santos et al. 2000). In addition to these pioneering works, not many more data have been published, but it is worth mentioning that the danger of taking the chromospheric

signal as a planet signal is a serious one, in particular if a long, multi-season campaign is not carried out (see e.g. the detection claimed and then disclaimed by Desidera et al. 2004). A positive aspect, on the other hand, is provided by the analysis of the HARPS GTO data, which indicates that this jitter can be much lower than what predicted by these early works, and that it may stay well below 1 m/sec (Lovis et al. 2005). These HARPS observations show as stars with as little as 1.8 m/sec overall long term variability can be found, and as, after the known source of noise are eliminated, a residual noise of less than 1 m/sec is left. This is an important point which needs to be better understood and characterized; it would benefit from an 'ad hoc' observational program and from further, dedicated studies.

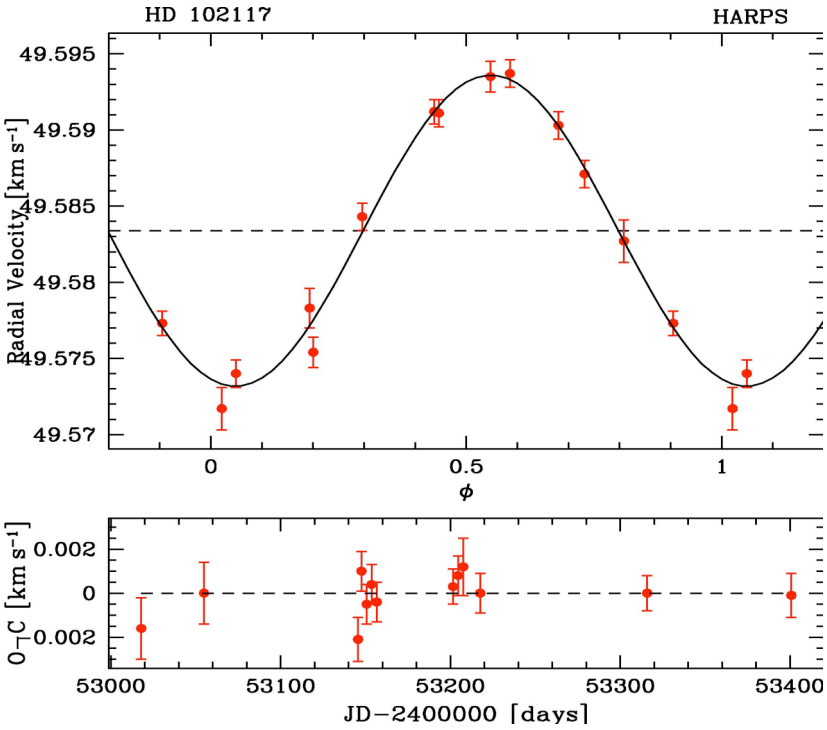

Figure 4-5: *Observations and orbital solution for a planet orbiting around a star, as observed with HARPS. The O-C for the 3 last exo-planets discovered (and published) by HARPS is below 2 m/sec and it is only of 0.9 m/sec for the star in the picture (Lovis et al. 2005). This O-C scatter includes all source of noise: photon noise, spectrograph, operations and calibration instabilities, stellar noise (oscillations and noise induced by chromospheric activity).*

If the activity-induced jitter is related to the migration of surface inhomogeneities, its signal is most probably not really periodic in the long term. Active regions and spots are created and destroyed at different phases, and in addition their locations migrate on the stellar surface at different latitudes, which implies also different periods, due to stellar differential rotation.

A strategy to overcome this noise is to gather many random – epoch measurements over a time longer than the typical Jitter timescale to average out the effect. It seems reasonable that if the effect is less than 1 m/sec, with many observations it will be possible to reduce it down by a factor 10 or more.

A detailed study of the relationships between stellar activity and observed RV jitter seems rather urgent. This does not require CODEX at OWL, and could be carried out easily with HARPS or with an 8m facility

Acoustic (pulsation) Noise

RV variations due to stellar acoustic modes might not be negligible, and HARPS has clearly shown as they can be clearly revealed even in a simple observational sequence (Mayor et al. 2003), and also that they depend on the spectral type of the star: Figure 4-6 shows a series of HARPS observations of stars of different absolute magnitude, from a K dwarf to a G subgiant: oscillations are clearly visible, they have frequencies from a few minutes to 15 –20 minutes and their amplitude grows for the lower gravity stars

(Mayor et al. 2003, see also Figure 4-7). Their amplitude is given by the single acoustic modes, and by their combination (beats). In dwarfs the typical timescale of the modes is of the order of a few minutes, and they can be easily averaged, while the interference between modes induces variations of these averages over longer timescales of the order of hours. Figure 4-7 shows the temporal behavior of a long series of HARPS observations of μAra, where the short period oscillations and the beating are clearly visible (Bouchy et al. 2005).

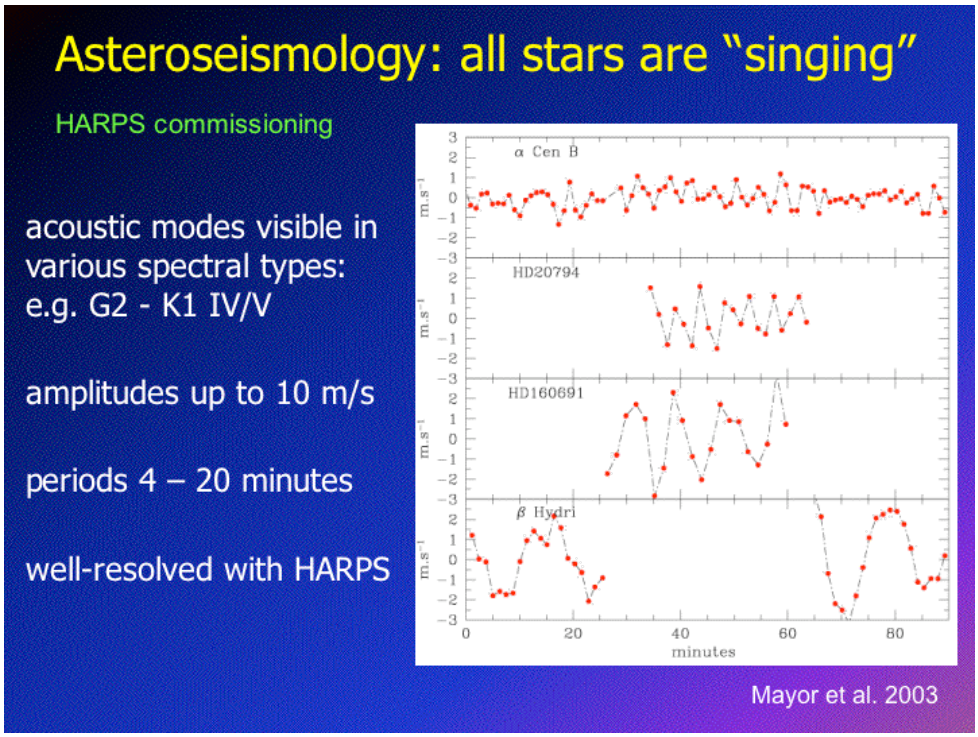

Figure 4-6: *Temporal series of HARPS observations of solar-type stars of different spectral type. Stars are ranked by decreasing surface gravity, from a K2V dwarf (α CenB to a G subgiant (β Hydri): the increase of the pulsation period and of the amplitude with decreasing gravity is evident from the HARPS observations (Mayor et al. 2003)*

Since asteroseismology is a branch still in its infancy, not much statistics on stellar pulsations are available. Scaling the results of the best observations (μ Ara, α Cen) the peak to peak variations of the 'quiet' star are well below 1 m/sec and the beat induced variations are probably

i) Of the order of 20 cm/sec when averaging the measurements over a timescales corresponding to timescale of the modes (10-15 minutes)
ii) Of the order of a few cm/sec if the average is done over several hours.

In the case of μAra, the 14 earth mass planet has been deduced after that all the spectra taken in one night were averaged to give a single point, and the long term trend due to the first planet was subtracted. After these two operations the O-C shows an overall scatter of 0.9 m/sec.

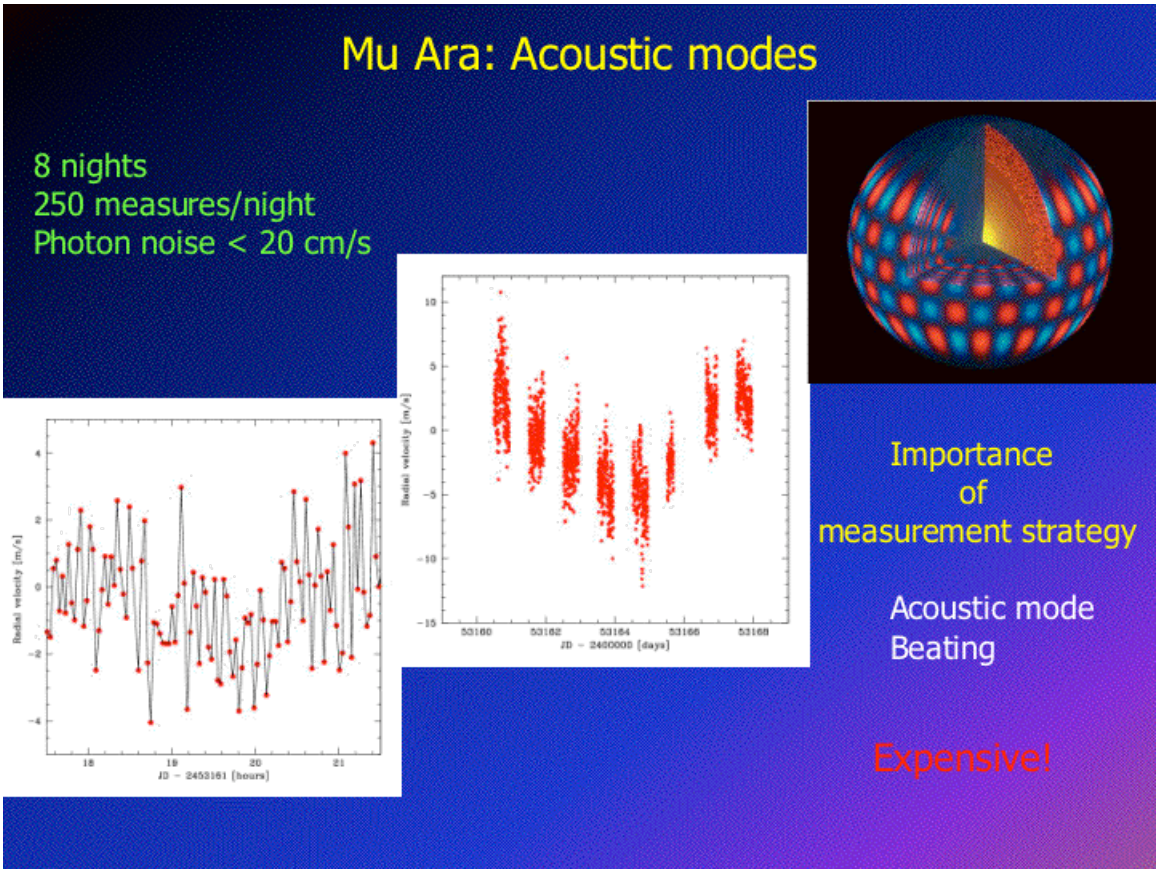

Figure 4-7: *summary of the HARPS observations of μ Ara: the star has been observed for oscillations, and a 14 Earth mass planet found, in addition to a long term trend due to another companion. Each set of observations/night has been averaged to provide one RV value. By using these average points the O-C is better than 0.9 m/sec*

4.3.2 High Priority Planet – search programs

All the above is showing that, if on the one side there are excellent perspectives to beat the stellar noise to a few cm/sec, on the other hand this cannot be obtained with a simple series of observations, rather it will require a continuous monitoring of the stars for long periods. It will therefore be demanding as far as observing time is concerned.

On the positive side, recent theoretical calculations predict the existence of a large number of objects with masses below 15 earth masses spread over a large range of separations (e.g. Lin and Ida 2004). Figure 4-8 shows the predictions of these authors.

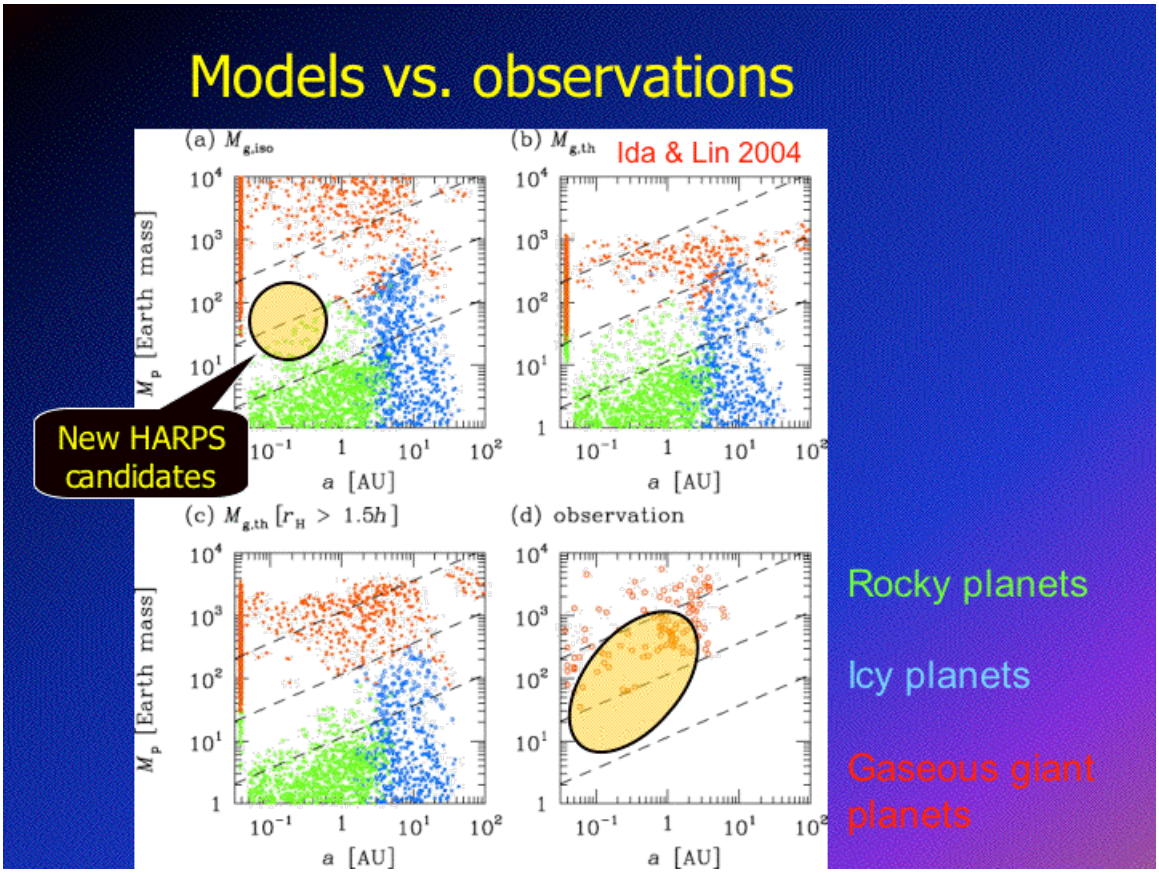

Figure 4-8: *Expected distribution of planets in the Mass-separation diagram (adapted from Ida and Lin 2004). The picture indicates the new 14 Earth mass planet found around μ Ara. The precision is approaching the regime where rocky planets are observable, and what is relevant, while the present HARPS accuracy corresponds to a fairly low density region of the diagrams, with the accuracy of CODEX we will enter in the rocky planet regime, and many of them are predicted by theory.*

These predictions strongly argue for a dedicated search for very low mass Earth-type planets. As far as low mass planets are concerned, two main programs are analyzed; the search for Earth analogues and the follow-up characterization of Earth-size planets discovered by other techniques and instruments.

Detection of Earth analogs

The detection and characterization of Earth-like planets in the habitable zone is the driver for an enormous effort in the next decades. As for radial velocities, an accuracy of a few cm/sec over many years will be required. As shown above, CODEX will have the needed accuracy, provided that a proper observational strategy is adopted and enough observing time is allocated. A possible strategy would consist of

a) several exposures/night to average out the acoustic modes, for a total of about 1 hour/night for each star (limiting ourselves to solar-type dwarfs)

b) A few hundreds of such nights over a few years (i.e. 100 nights over 4 years) to average the jitter and cover the period

With a total telescope time of about 100 hours/star, clearly this technique cannot be applied to large surveys, but it can only be conceived for a limited number of objects. A program with 10 stars would require about 25 nights/year over 4 years. A prototype of CODEX at the VLT would be very useful to prototype the program and the method.

This program should be run only on a restricted number of stars which have been pre-selected because they show very high probability of hosting low mass planets (or very high probability of detecting them) on the basis of independent observations.

Characterization of earth-size planets

This use is emphasized in the ESA-ESO report: Kepler space mission will provide transit candidates as faint as V=14-15. Among them, several tens will be earth-size candidates or smaller. Experience with transit surveys so far has shown the relevance of radial velocity follow up: not only without radial velocities the full orbital solution cannot be obtained, but, in addition, photometric transit observations will always require the RV observations to validate the nature of the companion (cf. Melo et al. 2004). A short period planet (15 days) of earth mass will produce a reflex motion of 24 cm/sec in the RV of the star, which shall be easily observable with CODEX. In fact, once the orbital period and phase are known, the noise introduced by the potential jitter and the oscillations will not be a stopper, since it will have different frequency and phase.

The combination of the CODEX measurements with transit photometry will provide the radius, mass and mean density of the Earth-like planets (rocky? Icy?) on short period orbits. They will provide information on the diversity of the structure and if these objects potentially formed at different locations of the system. The off-eclipse and the on-eclipse spectra could also be combined separately to obtain very high S/N spectra, and to investigate the presence of subtle spectral features related to the planet.

At present there is no instrument able to reach the accuracy needed and to gather enough photons from the faint stars. We shall notice that the Kepler field has been chosen at +44 degrees of declination, so that in order to observe Kepler targets, CODEX should be located in the northern hemisphere, or not too far from the equator.

This scientific case is extremely interesting and complements beautifully other OWL instruments and other space facilities, to the extent that is indicated as a first priority in the ESA-ESO report. It requires a number of preliminary steps to be fulfilled, both on the theoretical and on the observational side, such as :

a) Understanding the nature of the stellar noise
b) Measuring and subtracting the stellar noise
c) Find stars with the highest probability of hosting earth planets, in which the planets are best detectable.

Jovian-type Planets around faint objects

In addition to the search of very low mass planets, we should not forget that CODEX will be able to exploit the tremendous photon collection capability of OWL. Considering that with a S/N ratio of ~80/pixel a photon noise of 1 m/sec is reached with HARPS on a slow rotating G star, this implies that with CODEX it will be possible to obtain an accuracy of 1 m/sec on a 17.5 magnitude star in 10 minutes and an accuracy of 10 m/sec on a 22.5 magnitude star in the same time (negligible RON is assumed).

This opens the prospect of investigating and studying Jupiter size exo-planets in different environments. The study of exo-planets it is in fact until now limited to the nearest stars with RV techniques and it will be enlarged by photometric transit surveys. Locations as far as the nearest galaxies (Magellanic Clouds), the Galaxy Bulge and Globular Clusters will be out of reach until CODEX is in use. It is difficult at the moment to anticipate the demand and the amount of future interest in studying planets in environments far from the solar neighborhood. However, to study other environments characterized by different star formation history, chemistry and dynamical state seems a natural step once our surroundings have been fully exploited and statistically characterized. The search for planets in open clusters with Keck (Paulson et al. 2004) and with UVES-fibre has started, but is still in its infancy.

4.4 BBN and the early universe

The abundances of the light elements ^{4,3}He, D and ^{7}Li measured in a variety of metal poor environments or extrapolated to zero metallicity are in fairly good agreement with the predictions of Big Bang Nucleosynthesis in a homogeneous Robertson-Walker-Friedman cosmology, and they have been succesfully used to impose

important constraints on the number of light particles species. However, precision cosmology opens new avenues to study the physics of the early Universe.

The WMAP measurement of the cosmic background anisotropies have provided a new and very precise constraint on Ω_b, 380000 years from Big Bang (Spergel et al 2003) challenging the value obtained of the same quantity from primordial nucleosynthesis, a few minutes from the Big Bang.

As shown in Figs 4-9 and 4-10, the WMAP measurement of Ω_b shows a spectacular agreement with that inferred from the primordial Deuterium as derived in high z clouds, but on the other side reveals a discrepancy with ^{7}Li and ^{4}He. A recent reanalysis of the ^{4}He data led to a significant enlargement in the statistical uncertainty, and an upwords shift of the mean value of what shown in figure 4-9 removed the discordance with WMAP, leaving Li alone in discordance (Cyburt et al 2004, and refrences therein). The prediction by WMAP for ^{7}Li is higher by a factor of 2 or 3 than the primordial abundances deduced from halo population II stars.

Moreover, a *plateau* in the ^{6}Li abundances has been detected in halo stars at very low metallicity (see Fig. 4-11). This plateau is paralleling the one of ^{7}Li and possibly requires some primordial synthesis which is not envisaged by the standard big bang nucleosynthesis.

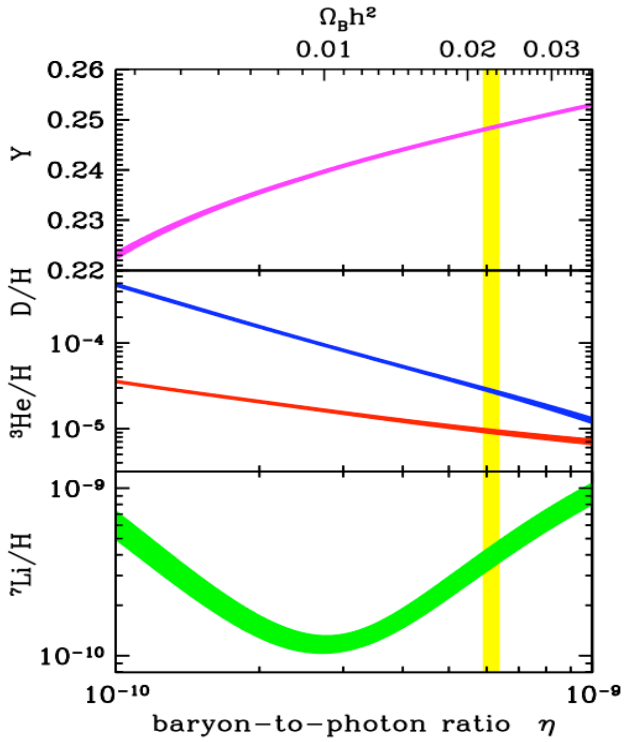

Figure 4-9: *Predictions of SBBN compared to the WMAP measurement. Figure from Steigman (2004)*

The WMAP measurement of the universal baryonic mass calls for new and refined measurements of the abundance of elements cooked in the Big Bang. It is rather pressing to understand if and to which extent the disagreement is real or due to systematic errors. A real disagreement in the absence of astrophysical explanations could reflect aspects of physics occuring in the processes in the very early universe. CODEX would bring new and unique contributions to the solution of this cosmological conundrum. CODEX will allow an extensive survey of ^{6}Li measures, which are presently limited to the handful of brightest halo stars, and possibly also first ^{6}Li ^{7}Li in F and G metal poor stars of the nearest galaxies. This will allow us to understand whether the "floor" in the ^{6}Li has a cosmological nature. CODEX will also make it possible to detect the first interstellar LiI in the metal poor high velocity galactic clouds (HVCs) or other extragalactic clouds. The abundance measure in the interstellar gas phase is free from the systematic uncertainties that abundance

measurements in halo stars suffer due to modeling of stellar atmospheres and convection. In particular the measure of the ^{7}Li /^{6}Li ratio will provide a direct check of the BBN ratio for these two elements.

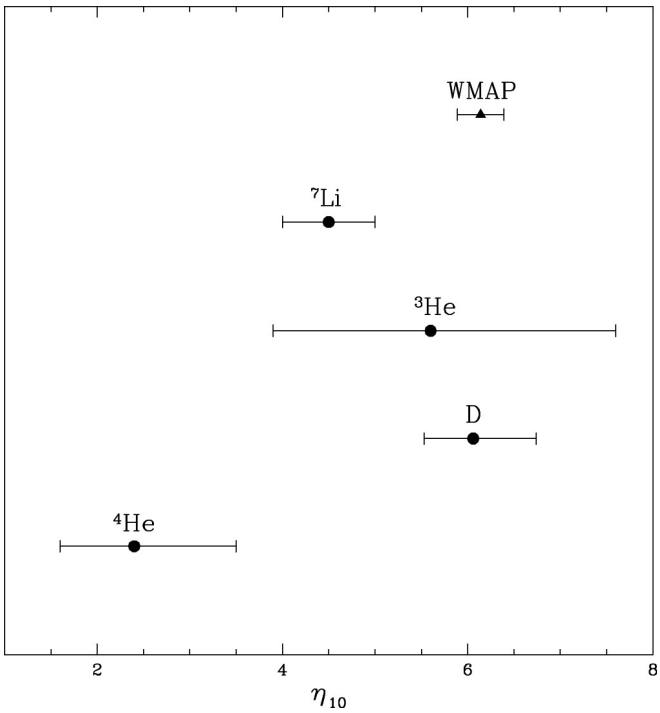

Figure 4-10: *Predictions of SBBN compared to the measurements of different primordial nuclei. Note that the error for ^{4}He is underestimated in the figure according to Cyburt et al. (2004)*

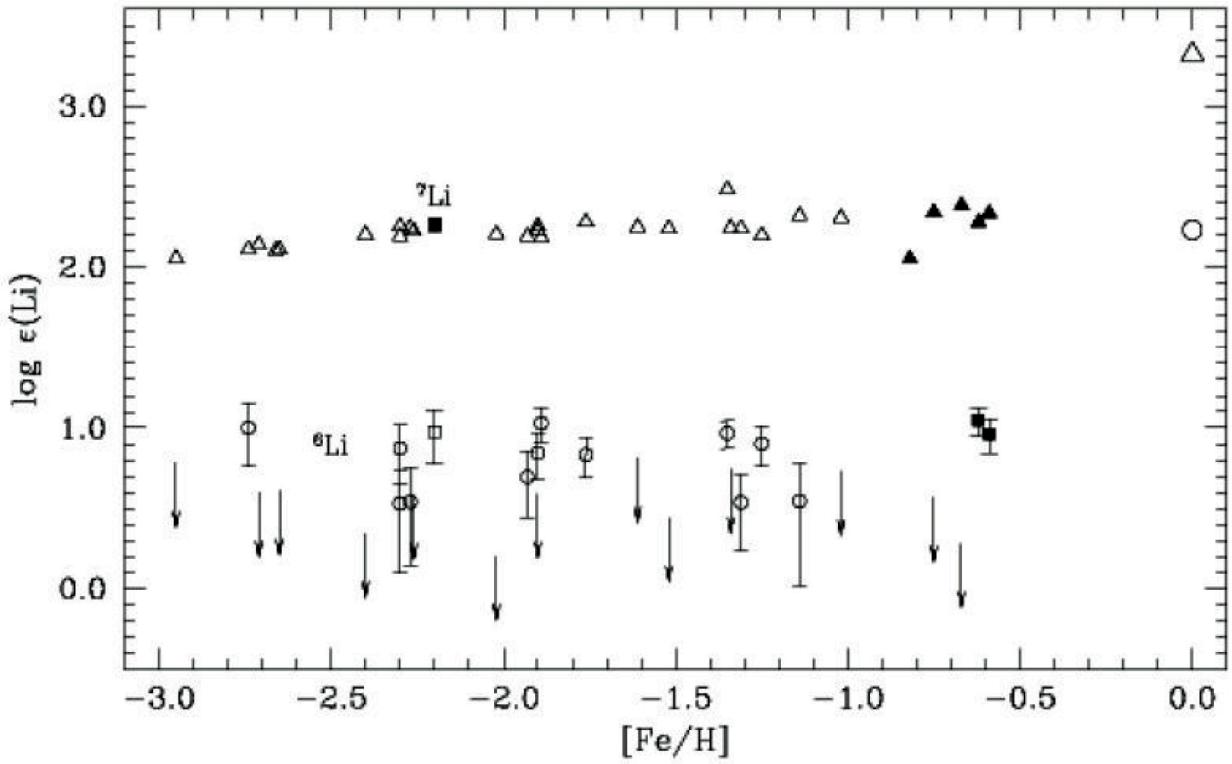

Figure 4-11: *^{7}Li and ^{6}Li plateaux from Lambert (2004) and references therein.*

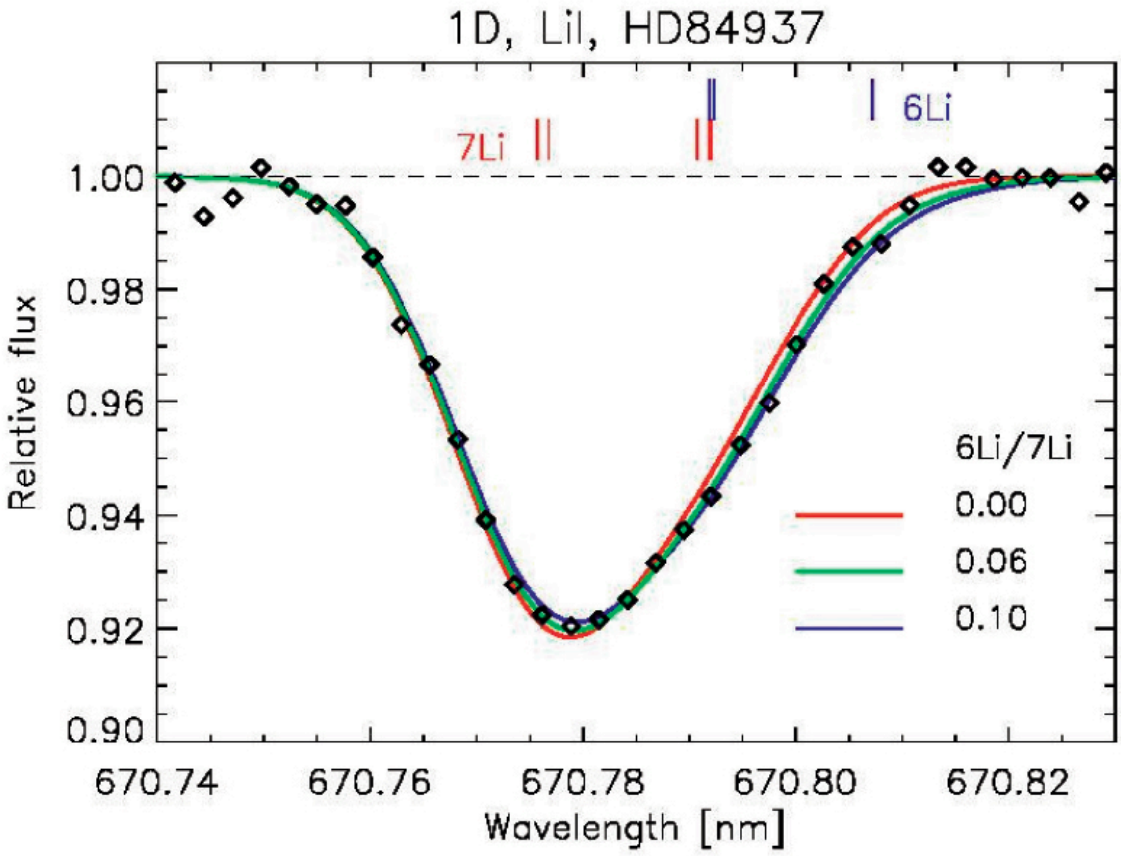

Figure 4-12*: The profile of the Li doublet in HD 84937 (Lambert 2004).*

4.4.1 Primordial ^{6}Li?

Standard BBN does not foresee production of ^{6}Li in measurable amounts, and theoretical predictions are at about 5 orders of magnitude below ^{7}Li. The ^{6}Li observed in nature is supposed to be produced by spallation processes induced by galactic cosmic rays with ions in the interstellar medium, which produce also Be and B.

Recent VLT observations of ^{6}Li in stars as metal poor as [Fe/H]=-2.8 are suggestive of a *plateau* level of ^{6}Li/H ~ 10^{-11} paralleling the Spite plateau. The ^{6}Li plateau is shown in Fig 4-11. The measurement of ^{6}Li in stellar atmospheres is quite difficult because the ^{6}Li and ^{7}Li doublets are separated by almost the same amount which separate the two lines of the dominant ^{7}Li. Presence of ^{6}Li is revealed by a tiny shift towards the red of the barycent of the line and by an increased asymmetry of the doublet profile (Fig. 4-12). High resolution and high signal-to-noise are a prequisite of this analysis. After the first upper limit, the first detection was given by Smith,Lambert and Nissen (1993) for HD 84937 with ^{6}Li /^{7}Li =0.06 ± 0.03, further confirmed by Cayrel et al. (1999) who found ^{6}Li/^{7}Li =0.052 ± 0.019. The mere detection of ^{6}Li has important bearings on the stellar structure and on the amount of ^{7}Li burned by warm protons in the stellar interior. In fact, being ^{6}Li more fragile than ^{7}Li, the presence of ^{6}Li shows that Pop II plateau stars cannot have gone through ^{7}Li burning. Standard models of metal poor stars predict a slight depletion of ^{6}Li and negligible depletion of ^{7}Li in turn off stars.

The presence of ^{6}Li in halo stars poses the problem of its origin. The extension of the Galactic cosmic rays spallation reactions to the metal poor stars fail to reproduce the observed light element ratios. There is no existing GCR mechanism which is able to produce such a level of ^{6}Li. A *plateau* implies that either the ^{6}Li

was a Big Bang product or was produced in a pregalactic phase. Suzuki & Inoue (2002) suggested that the assembly of our Galaxy by infalling and merging of subgalactic clumps produced gravitational shocks and ^{6}Li through $\alpha + \alpha$ fusion reactions. The cosmological origin is very intriguing and might be related to one of the most fundamental particle: ^{6}Li could be produced by primordial spallation produced by the decay or annihilation of neutralinos (Jedamzik 2004). None of the theories have yet a satisfactory status. However, they show the need to firmly establish the existence of a ^{6}Li plateau and whether this has a galactic or a primordial origin.

CODEX could significantly contribute to this by measuring ^{6}Li/^{7}Li in most metal poor environments and in extragalactic turnoff stars, either in the Magellanic Clouds or in the Sagittarius galaxy. These will be demanding observations even for CODEX. The limiting magnitude of stars observed at the required S/N ratio (~400) with the VLT at a resolving power of R>100000 is V~15. The ratio of the collecting areas between OWL/VLT is of ~120, which translates in about 5 magnitudes gain, or an OWL limiting magnitude at V~20. Given that the scenarios in which these galaxies formed is different from that of the Milky Way, a primordial ^{6}Li should be detected at the same levels observed in the Galaxy, while it would be different if local nucleosynthetic processes were at its origin.

4.4.2 Interstellar ^{7}Li /^{6}Li ratio in metal poor clouds

Presently, halo stars are the only site suitable for observations of primordial Li, and it is critical to identify other independent sites in which Li can be measured. An important crosscheck could be performed with CODEX in unprocessed material such as that belonging to high velocity clouds or to Damped Lyα galaxies observed along the line of extragalactic sources. Measuring Li in these environments will provide an important test of the Li problem. If the measurement is consistent with the WMAP+BBN Li abundance, it would indicate that the low Li abundance observed in halo stars is a convection problem.
Lithium measurements in the diffuse gas are particularly challenging due to the low column density. Interstellar ^{7}Li was first detected in the early 1970s and since then there have been relatively few observations. The detections show weak interstellar LiI absorptions with equivalent widths on the order of a few mÅ at most. The equivalent width of the ISM lines depends also critically on the depletion on grain and on the ionization of the gas. The ionization corrections are rather large and only a small percentage of Li is in the form of Li I. A gas-phase observation of the ratio of the Li isotopes reflects the true nucleosynthetic ratio of the elements since no differential depletion or differential ionization processes are expected between the two isotopes. The ratio is therefore a crucial one for Galactic chemical evolution models. The isotopic ratio has been measured towards several bright stars in the solar neighborhood with high resolution (R~360000) observations. However, a smaller resolution of the kind proposed for CODEX would be sufficient for measuring the elemental lithium isotope abundances. The observations show that the ^{7}Li /^{6}Li ratio is about 12, a value close to the solar system value of 12.3, implying that the relative ratio has not changed significantly since the formation of the solar system (cfr. Knauth et al 2003, and references therein). One exception is the line of sight towards *o* Per, where the ratio is about 2, namely the value expected for pure GCR spallation. However, an enhancement of total LiI is not detected in this case and such a low value remains a puzzle.

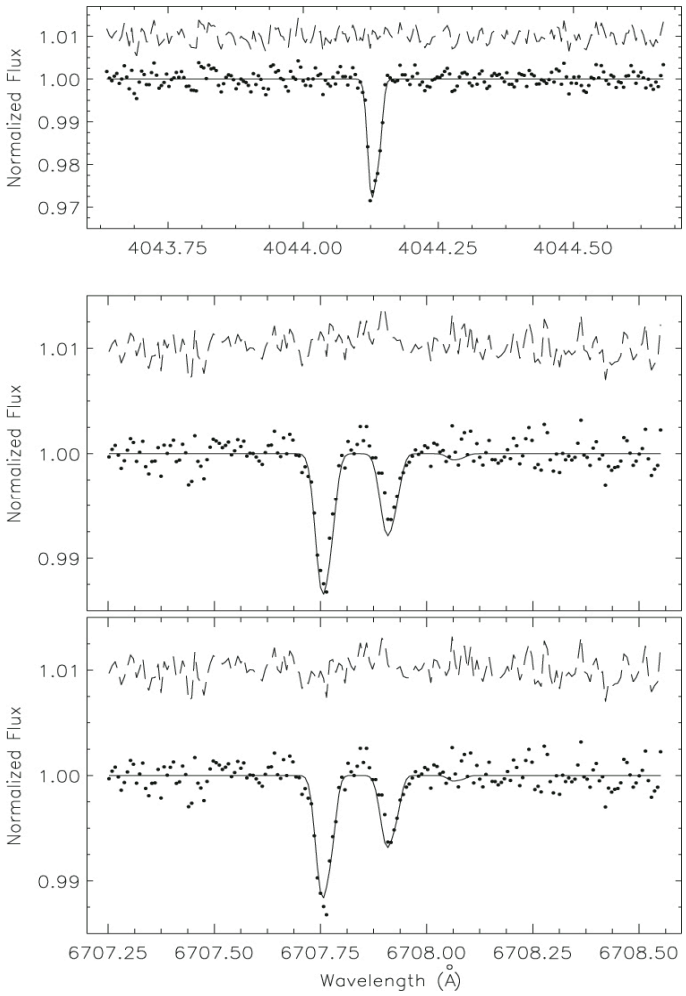

Figure 4-13:
The interstellar ^{7}Li /^{6}Li ratio towards ζ Oph (Knauth et al. 2003). A similar ratio measured in a low metallicity cloud would reveal the primordial isotopic ratio

High Velocity Clouds falling onto our Galaxy or extragalactic neutral gas forming the Damped Lyα galaxies show metallicity of about 10% solar or less and little depletion into dust and are therefore very promising sites for testing primordial lithium. Deuterium close to the actual estimate of the primordial value has been measured in DLA towards distant quasars (D' Odorico et al 2001) and recently in a metal poor high velocity cloud in the complex C by using a QSO as background source (Sembach et al. 2004). This latter line of sight has been proposed for future attempts to detect interstellar ^{7}Li (Prodanovic and Fields 2004). In the ISM of our Galaxy the N(LiI) ~ $5x10^{9}$ cm^{-2} measured typically towards sources which are 6 mag. By using the galactic observation as a reference, an exposure of about 3 hours can be estimated to measure the Li isotopic ratio in the complex C towards QSO PG 1259+593 (m_v ~ 15). Then, detection of the ^{7}Li/^{6}Li would be a direct probe of the primordial ratio between these two isotopes.

References:

- Bohlin, R. C.; Jenkins, E. B.; Spitzer, L., Jr.; York, D. G.; Hill, J.K.; Savage, B. D.; Snow, T. P., Jr. 1983 ApJS 51, 277
- Bouchy et al. 2004: A&A 426, L19
- Chand, H., Srianand, R., Petitjean, P., & Aracil, B. 2004, A\&A, 417, 853
- Cayrel, R., Spite, M., Spite,F., Vangioni-Flam, E. Casse', M., Auduze, J. 1999 A&A 343, 923
- Cyburt, R., H., Fields, B.D., Olive, K.A., & Skillman, E. 2005, Astrop. Phys. 23, 313
- Desidera, A. et al. 2004: A&A 420, l27
- D'Odorico, S., Dessagues-Zavadsky, M., Molaro, P. 2001, A&A 368, L21
- Dzuba, V. A., Flambaum, V. V., Kozlov, M. G., & Marchenko, M. V. 2002, Phys. Rev. A, 66, 022501

- Dzuba, V. A., Flambaum, V. V., \& Webb, J. K. 1999, Phys. Rev. A, 59, 230
- Fujii, Y. 2005, Physics Letters B 616, 141 astro-ph/0502191
- Jedamzik, K 2004, PhRvD 70, 3510
- Knauth, D. C., Federman, S.R., and Lambert D. L., 2003, ApJ, 586, 26
- Lambert, D.L. 2004 AIP Conference Proceedings 743, p. 206
- Lamoreaux S. K., Torgerson, J. R. 2004 PhRvD 691,1701
- Levshakov, S. A., Centuri\'on, M., Molaro, P., & D'Odorico, S. 2005, A&A, 434, 827
- Levshakov, S. A. 2004, in Astrophysics, Clocks and Fundamental Constants, eds. S. G. Karshenboim and E. Peik (Springer-Verlag: Berlin, Heidelberg), p.151
- Levshakov, S. A., & D'Odorico, S. 1995, in QSO Absorption Lines, ed. G. Meylan, p.202
- Levshakov, S. A. 1994, MNRAS, 269, 339
- Lin, D.N.C., Ida, S. 2004: in " Star formation in the Interstellar Medium", ASP Conf. 323, p. 339
- Lovis, C. et al. 2005: A&A 437, 1121
- Marciano, W. J. 1984, Phys. Rev. Lett., 52, 489
- Mayor, M. et al. 2003: The Messenger 114, 20
- Melo, C. et al. 2004: The Messenger 116, 32
- Murphy, M. T., Flambaum, V. V., Webb, J. K., Dzuba, V. V., Prochaska, J. X., \& Wolfe, A. M. 2004, in Astrophysics, Clocks and Fundamental Constants, eds. S. G. Karshenboim and E. Peik (Springer-Verlag: Berlin, Heidelberg), p.131
- Murphy, M. T., Webb, J. K., & Flambaum, V. V. 2003, MNRAS, 345, 609
- Paulson, D.B., Cochran, W.D, Hatzes, A.P. 2004, AJ 127, 3579
- Prodanovic, T. & Fields, B. D. 2004 ApJ 616 L115
- Quast, R., Reimers, D., \& Levshakov, S. A. 2004, A&A, 415, L7
- Quast, R., Baade, R., \& Reimers, D. 2002, A&A, 386, 796
- Reimers, D., Baade, R., Quast, R., \& Levshakov, S.~A. 2003, A&A, 410, 785
- Reimers, D., Hagen, H.-J., Rodriguez-Pascual, P., \& Wisotzki, L. 1998, A&A, 334, 96
- Saar, S. et al. 1998: ApJ 498, L153
- Santos, N. C. et al. 2000: A&A 361, 265
- Spergel, D. N., et al 2003, ApJS, 148, 175.
- Sembach, K.R., et al 2004, ApJS 150, 387
- Smith, V.V., Lambert, D.L., Nissen, P.E. 1998 ApJ 506, 405
- Steigman, G., 2004 Cosmochemistry. The melting pot. Cambridge Contemporary Astrophysics p. 1-30
- Suzuki, T.K., & Inoue, S, 002, ApJ 573, 70
- Ubachs, W., \& Reinhold, E., 2004, Phys. Rev. Lett., 92, 101302
- Uzan, Jean-Philippe 2003 RvMP 75, 403
- Webb, J. K., Flambaum, V. V., Churchill, C. W., Drinkwater, M. J., &Barrow, J. D. 1999, Phys. Rev. Lett. 82, 884

5. CODEX Instrument Design

5.1 Summary

CODEX is a set of high-resolution, seeing-limited crossdispersed echelle spectrographs. The diameter of the entrance aperture is 1 arcsec. The instruments are fed using a 200 – 300 m optical fiber or a Coude feed, followed by a fiber slicer. The design of a unit spectrograph does not depend on the size of the telescope; only the number of spectrographs must be increased. The instruments are vacuum spectrographs that are located in a thermally stabilized underground facility.

The following table summarizes the main characteristics:

Table 5-1. *Main characteristics of CODEX*

Acceptance aperture on the sky	1 arcsec
Location	Underground in nested thermally stabilized environment
Feed	Fiber or Coude feed
Peak DQE including injection losses (with GLAO)	9% (Fiber feed) 14% (Coude feed)
Number of unit spectrographs	5 for 60-m OWL 11 for 100-m OWL
Unit Spectrograph dimensions	Dia. 2.4 x 4 m (vacuum vessel)
Spectral resolution	150 000
Wavelength coverage	446 - 671 nm in 35 orders
Spectrograph layout	White pupil
Echelle	41.6 l/mm, R4, 170 x 20 cm, 4 x 1 mosaic
Crossdisperser	VPHG 1500 l/mm operated off-Littrow
Camera	Dioptric F/2.3 image quality 30 um
Detector	CCD mosaic 8K x 8K, 15 um pixels Stabilized to a few mK
Noise performance	Photon shot noise limited for Mv = 16.5 in 10 minutes
Sampling	4 pixels per FWHM

5.2 Grating and detector size

CODEX relies heavily on the experience made with HARPS. A description of this instrument is given in F. Pepe et al (2000) SPIE. 4008. Like HARPS, CODEX is designed as a crossdispersed echelle spectrograph. The required entrance aperture in arcsec, the spectral range and resolution are very similar. The main design modifications stem from the fact that while HARPS is fed by a 3.6 m telescope, CODEX will be fed by a 60 – 100 m telescope. This has important implications for the size of the grating and the detector area; these will be explored in this section.

The spectral resolution of a grating spectrograph is given by:

$$\Re = \frac{OPD_{gr}}{OPD_{tel}} = \frac{2.\tan\vartheta_B.D_{col}}{\tan s.D_{tel}}$$

where *OPD* denotes the optical path length difference associated with the grating or the telescope, ϑ_B is the grating blaze angle, *s* the angular slit width and *D* the diameter of the telescope or spectrograph collimated beam.

For a given resolution and aperture on the sky, the collimated beam size scales with the telescope diameter: a factor 28 when going from a 3.6-m to a 100-m telescope. The HARPS echelle would scale from 0.20 x 0.80 m to 5.6 x 22.5 m. This increase is a direct result of the unavailability of Adaptive Optics (AO) in the foreseen wavelength range.

Since gratings this size are not feasible, the only solution then is to reduce the size of the entrance aperture (image slicer in the telescope focal plane) or the effective size of the telescope seen by the spectrograph (pupil slicer). Such slicing leads to longer slits that require additional interorder space. Since interorder space is limited by crossdisperser technology, this implies that the number of spectrographs must be increased.

The first conclusion is that *CODEX must be designed as a multi-instrument spectrograph cluster.*

The required detector area follows from the main design parameters and can be computed without detailed knowledge of the spectrograph design:

$$A_{\det} = \frac{A_{img}.\lambda\lambda}{\Delta\lambda.\varepsilon_p} = \frac{A_{img}.\lambda\lambda.\Re}{\lambda_c.\varepsilon_p} = \frac{(Fno.D_{tel}.s)^2\,\lambda\lambda.\Re}{\lambda_c.\varepsilon}$$

where *A* denotes detector or image area, $\lambda\lambda$ the wavelength range, λ_c the central wavelength, $\Delta\lambda$ a spectral resolution element, $\Re$ the spectrograph resolution, *Fno* the camera F-number, D_{tel} the telescope diameter and *s* the angular width of the entrance aperture.

The parameter ε measures how efficiently the detector area is used and is equal to the ratio between the number of pixels receiving “relevant” (science) photons to the total number of pixels in the array. In other ESO fiber echelle spectrographs this number lies between 0.061 (HARPS) and 0.078 (FEROS). The reason for this low efficiency is that in HARPS, only 10% of the slit height is used for the object fiber. Another 10% is used for the simultaneous calibration fiber while 80% is dead space necessary to prevent crosstalk between object and calibration spectra.

With $\lambda\lambda$ = *200* nm, λ_c = 550 nm, $\Re$ = 150 000, *Fno* = 2, D_{tel} = *100* m, *s* = 1” and ε = 0.06, the required detector area is 0.85 m^2 or about 475 E2V chips of 2k x 4k with 1800 mm^2 each. While these numbers follow from a rather arbitrary example, it is clear that *CODEX will have to use a fast camera and make an efficient use of the detector area in order to contain cost. This may require to modify the concept of simultaneous reference as used in HARPS.*

5.3 Interface with OWL

5.3.1 Location and Instrument Facility

As in HARPS, a CODEX unit spectrograph will be located inside a temperature-stabilized vacuum vessel, which in the case of CODEX has an estimated size of dia. 2.5 m x 4 m. As will be shown later on, the number of unit spectrographs in the cluster is about 5 for 1 arcsecond aperture at a 60-m telescope and 11 for a 100-m.

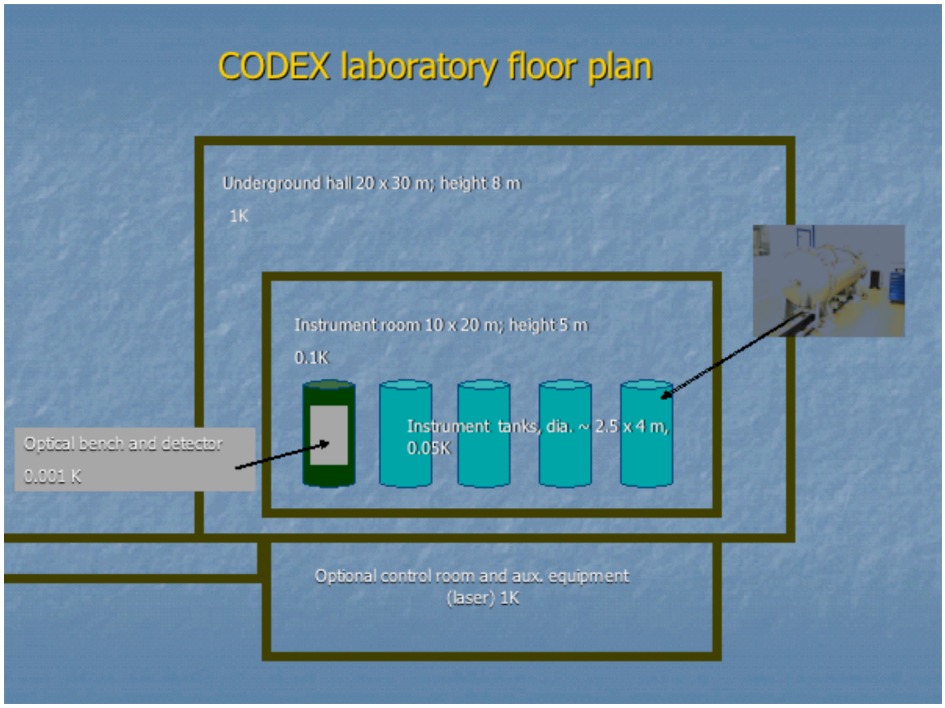

Fig. 5-1. *Conceptual floor plan of the CODEX underground laboratory. Day to day access using the underground corridor on the left; large pieces can be entered through doors located in the wall located near the top of the figure.*

Stability requirements and the experience with HARPS dictate that the vessels be stationary with respect to gravity and are located in a temperature-controlled facility, well isolated from diurnal temperature variations and vibrations due to wind buffeting. We estimate that the air temperature in this facility must be held stable to 0.1 K, more stringent requirements apply for the temperature stability of the optical bench and the detector assembly. The possible impact of frequent human access, should the instrument be placed at a common instrument location, will be critical to the success of the experiment. All this implies that the instrument must be located underground.

The cover of this report shows a 3-D view of the facility, with an access ramp to the mountain top. Figure 5-1 shows a tentative floor plan of the facility, and identifies nested thermal regimes, needed to achieve the required stability. Human access will normally be restricted to the outer hall, the access corridors and the control room.

5.3.2 Fiber feed or Coude feed

We estimate that on a 100-m telescope, 300 m of fiber will be needed to deliver the photons from the telescope focal plane to the underground facility. On a 60-m the required length scales to 200 m. These are lower-limit estimates based on the height of the focal station above the ground and the three cable wraps needed (adaptor/rotator, elevation, azimuth). For comparison: the FLAMES fiber feed from NasA to NasB on the 8-m UT2 has a length of 55 m and requires only a single cable wrap at the Adapter/Rotator.

With Silica fibers the efficiency of such a feed is quite poor, especially in the blue, as can be seen in the following figure.

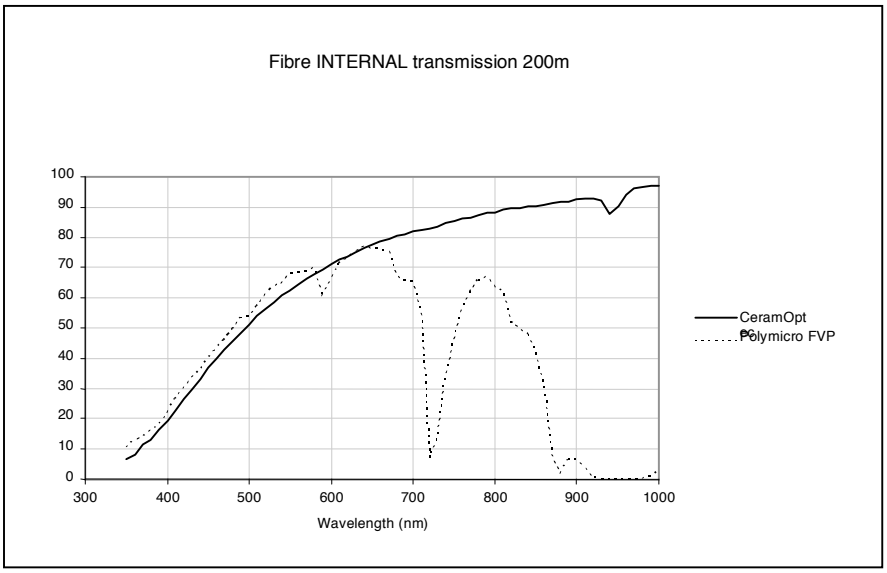

Fig. 5-2. *Internal transmission of 200 m of optical Fused Silica fiber. The CeramOptec is a water-free IR fiber. By using the "wet" Polymicro, the efficiency in the UV can be somewhat enhanced at the expense of an OH dip at 580 nm, but the net gain is not large since the fundamental limit is presented by Rayleigh scattering in Fused Silica.*

We have looked at fiber alternatives that might be a solution to this problem. Recently, fibers with a silica core but holey cladding have become available. They have big numerical apertures (0.6 – 0.7) because of the high ΔN between core and cladding. Because of this, the manufacturer claims that they have an excellent focal ratio degradation. Two fibres are under test in the ESO Fiber Laboratory and first FRD results are very promising. Since the light transport still takes place through the Silica, this does not help to solve the main problem which is absorption in the Silica. We have also explored air-guiding photonic band-gap fibres, where an air core acts as a waveguide. This type of fibre could go beyond the theoretical Rayleigh scattering limit of Fused Silica. The attenuation of the best commercially available NIR fibres is 10-20 dB/km over a 80 nm range around 1500 nm, corresponding to an internal transmission of 80 - 60% per 200 m.

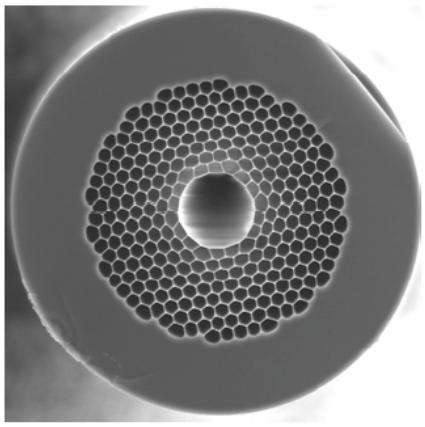

Fig 5-3 *SEM photograph of a holey fiber for the NIR. The air core diameter is 20 um*

Research is on the way to these fibers for the visible (http://www.crystal-fibre.com/products/airguide.shtm). Currently however, losses in the visible are still quite high, on the order of a few dB/m. Other problems to solve are the small passband (5 – 10 % of the central wavelength) and the tiny core diameters (5 – 20 um) of air-gap photonic fibers. While these problems do not hinder their use as fibers in communication applications, both are not compatible with use of this type of fiber as a broad-passband, large-etendue fiber feed. We consider it unlikely that it will ever be feasible to replace Silica fibers by air-core fibers in this application.

We have therefore explored an alternative way to feed CODEX. If OWL would have a Nasmyth focus, not more than 6 folding mirrors will be needed to deliver the light to an underground Coude focus. The two feeding schemes are represented schematically in fig. 5-5.

Commercially available broadband reflective coatings (overcoated silver or multilayer dielectric) have a reflectivity of 98.5% over the range 450 – 700 nm, and slightly worse in the 400-450 nm range. The efficiency of a such 6-mirror Coude feed will thus be in excess of 90%. Taking into account that there is also 1 telescope mirror less, this 5-mirror telescope design is about 2.5x more efficient at 450 nm than the 6-mirror design with 200 m fiber.

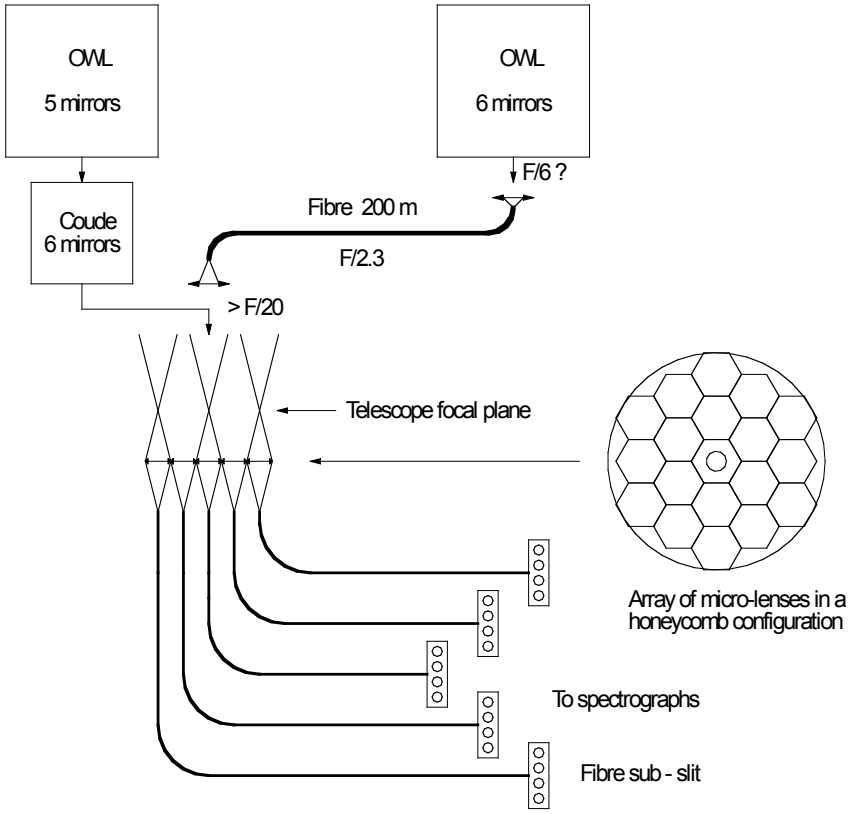

Fig. 5-5 *Schemes to feed CODEX in its underground facility. On the left side, a possible Coude focus feeds directly the lens array. On the right side a single 200 m fibre picks up the light of the target from the nominal focus. The output end of the fibre is projected on the lens array. In both cases, the ~1-arcsec image is dissected by an Argus-type array of lenslet and relatively short fibers that feed a number of unit spectrographs. The lenslet array can also be placed directly at the OWL F/6 focus; this does not change the losses in the Silica as the length of the path in Silica does not change.*

5.3.3 ADC and GLAO

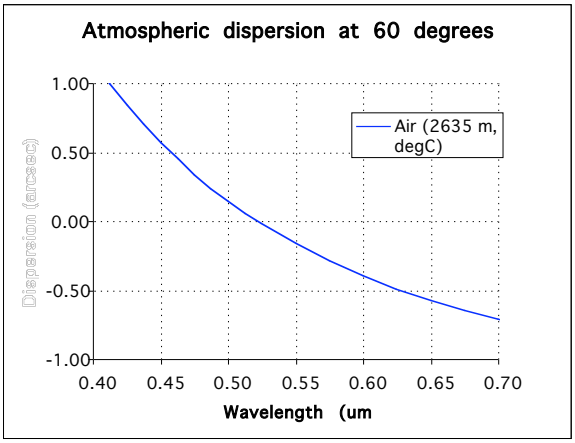

Fig. 5-6 *Atmospheric dispersion in the range 400 – 700 nm at 60 degrees Zenith Distance*

The atmospheric dispersion in the range 450 – 650 nm is 1.3 arcsec at a zenith distance of 60 degrees. An ADC is mandatory to avoid wavelength-dependent injection losses.

In case a general-purpose ADC is not available on OWL, a suitable dedicated solution is the ADC of the type used in X-shooter, which is a prism/lens that combines the function of image relay and ADC with only 4 air/glass surfaces. Such a design can be simple because it needs not be diffraction-limited. In view of the small field and wavelength range, with good A/R coatings the losses in such an ADC can be limited to 2-3%. Such a device can also be used to as a focal reducer to adapt the telescope beam Fno.

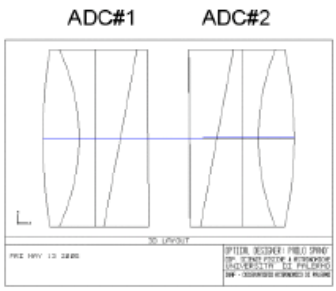

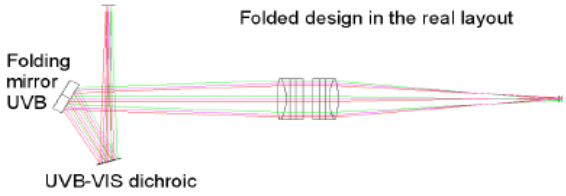

Fig. 5-7 *ADC system used in X-shooter. A similar design may be used on CODEX.*

Even if full AO is not foreseen for CODEX, the instrument will benefit from Ground layer Adaptive Optics (GLAO); if only for its image stabilizing effect that is necessary to reduce RV errors. Also the injection losses are reduced. Figure 5-8 was prepared using simulations by M. le Louarn for a 100-m telescope.

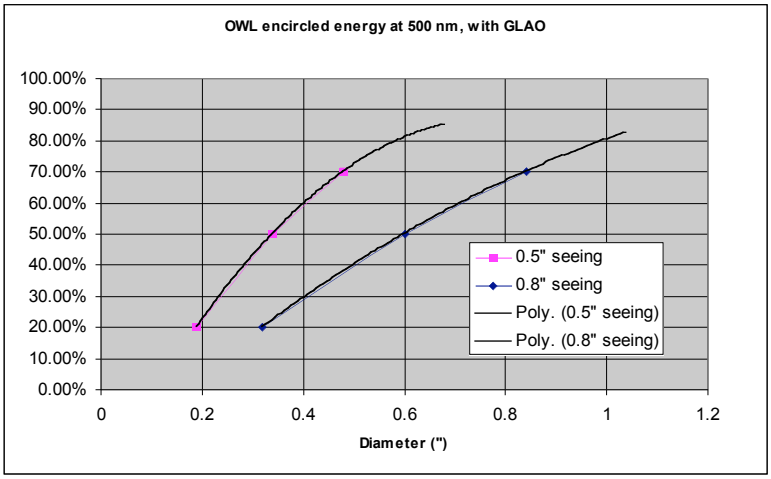

Fig. 5-8 *Injection efficiency into a circular entrance aperture at 500 nm, seeing 0.5 and 0.8 arcsec FWHM, with Ground Layer Adaptive Optics.*

The gain due to GLAO is largest when the aperture size is about equal to the seeing disk, while the current conceptual design assumes an entrance aperture of 1 arcsec. It may be possible to reduce this by 10 – 20% in order to reduce (by 20 – 40% the number of spectrographs and their cost. A detailed tradeoff study of cost vs. injection efficiency will be part of the next phase.

5.4 Fibre Slicer and scrambler

5.4.1 Slicer

The slicer was already indicated in fig. 5-5. It consists of a honeycomb lenslet array. Each lenslet captures part of the object light and guides it into its associated optical fiber.

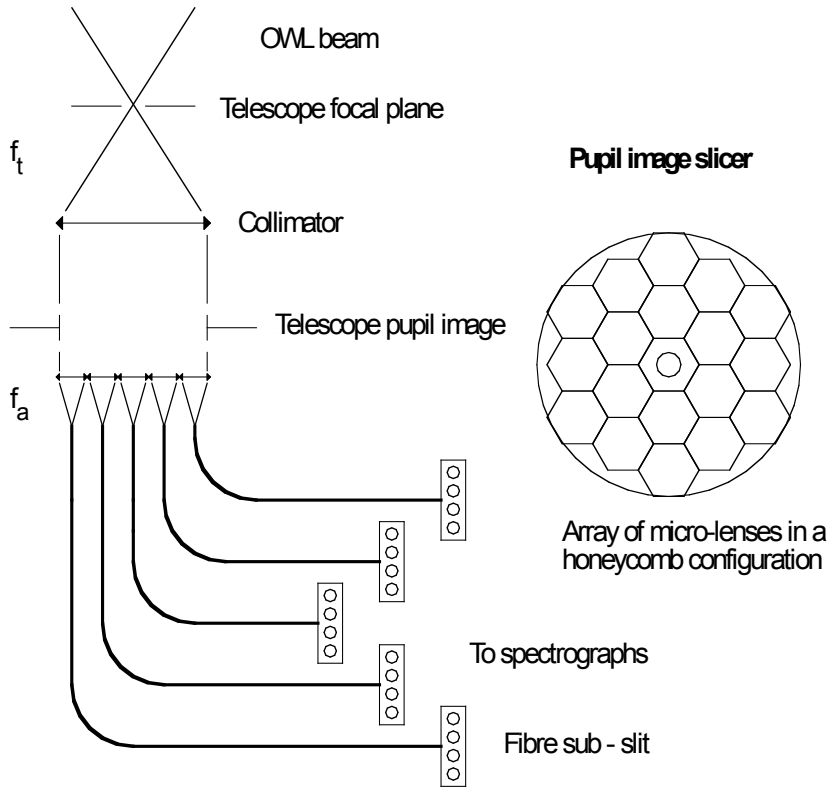

Figure 5-9. *Slicing the pupil of the telescope.*

In the telescope focal plane there is a tilted mirror with camera and detector for Acquisition and Guiding. It has a hole that acts as the entrance aperture of the instrument. Behind it, a lens collimates the light beam and places the image of the telescope pupil slightly in front of the mini-lenses, on their focal plane. The size of the image of the star on the fiber entrance is given by the ratio of the focal length of the mini-lenses and the collimator (f_a/f_t).

The image of the pupil for each fibre is at infinity and stable. Lateral displacements of the star in the focal plane of the telescope will be present in each sub-image on the fibres. These will be reduced by scrambling properties of the fiber; this is the reason why we have selected pupil slicing (see discussion in the next section). Another advantage of pupil slicing is that lenslets are allocated to a particular section of M1 area. While the telescope focal plane is being populated with mirrors, observations with a subset of the instrument may start. Note that this will require a pupil derotator.

For a unit spectrograph to achieve a spectral resolution of 150 000, the fiber core must be 120 um. For minimal focal ratio degradation (FRD), the beam launch aperture into the fibre has to be close to the numerical aperture of the fibre (typically 0.22 or F/2.22). We have defined a launch aperture of F/2.3 and a lenslet array containing 37 fibers. In the case of a 60-m OWL, the 120 um fiber core projects to 1.09 arcsec on the sky One lenslet is in the shadow of M2 (35% obstruction ratio assumed) and is unused. Each spectrograph will accept 8 fibers, so the number of spectrographs required is 5.

For a 100-m OWL, the core diameter of the fibers project to 0.65 arcsec[1]. The parameters of the lenslet array for these two cases are summarized in Fig. 5-10 and Table 5-2. Elsewhere in this document we discuss the need to perform prototype testing on the VLT. This is the reason why we have investigated a 3rd case, corresponding to a single CODEX spectrograph that can be fed by up to 4 VLT UTs. In this case the aperture on the sky is 1.34 arcsec.
Since in the case of the VLT there are only 4 fibers, the slit length is shorter than in the case of OWL.

[1] One can increase this to 0.96 arcsec by increasing the number of lenslets to 91; in this case 11 spectrographs are needed.

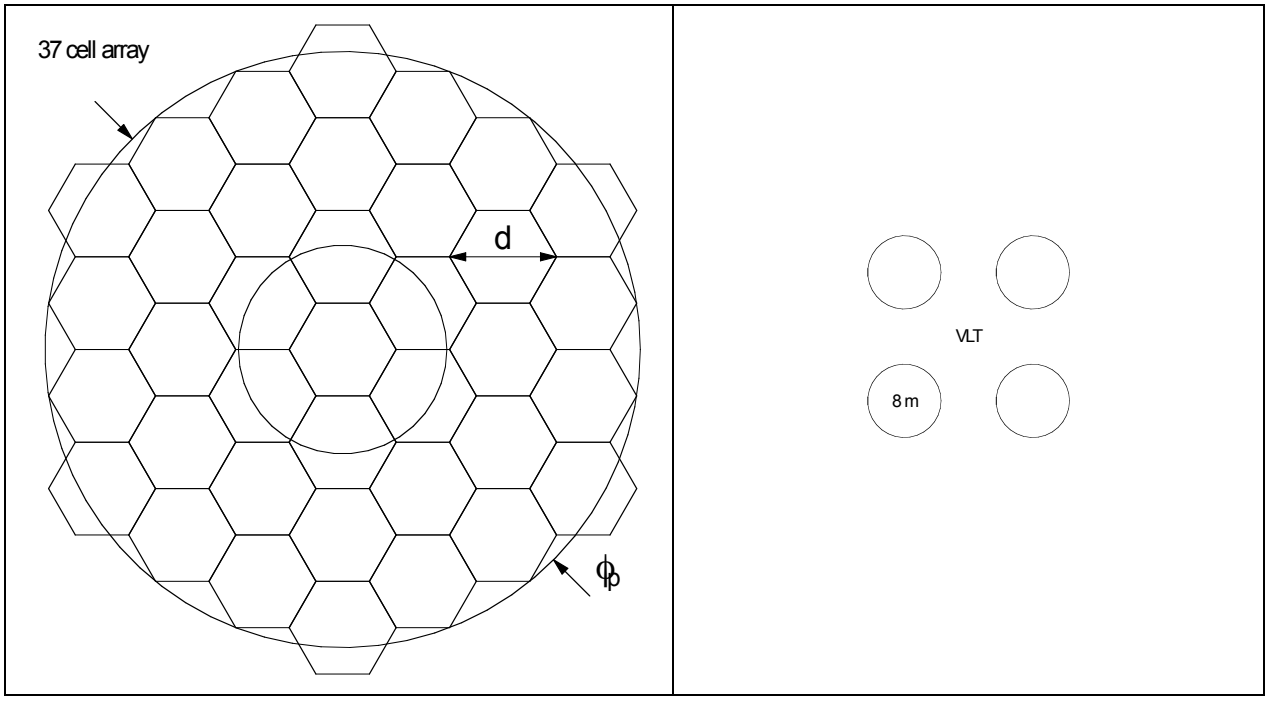

Fig. 5-10 *Projection of the pupil and central obstruction of OWL (left) and four VLT UTs (right) on a lenslet array. In the case of OWL, the projected size on M1 of the diagonal of a single lenslet is of 16.5m fot a 100m OWL and 10 m for a 60m OWL. The diameter of the central obstruction is 35 % of the pupil.*

Table 5-2. *Lenslet array and telescope parameters.*

Telescope diameter (m)	100	60	4 x 8
Diameter of entrance aperture (arcsec)	0.652	1.09	1.34
Assumed F/no in telescope focal plane	F/6		
Scale (mm/arcsec)	2.909	1.745	0.233
Lenslet diagonal in mm	5		
Fiber injection F/no	F/2.3		
Focal length of lenslet (mm)	11.5		
Focal length of collimator lens (mm)	181.9		30
Pupil projection on lens array (mm)	30.31		5
Projected lenslet diagonal on M1 (m)	16.49	9.90	8
Vignetting (light from the pupil missing lenslets near the edge in %)	6.6		0
Fibre diameter (core / cladding in μm)	120 / 132		
Number of active fibers and lenslets	36 (central lenslet is not used)		4 (one per telescope)
Fibres per fibre slit	8		4
Fibre slit length (mm)	1.032		0.528
Number of spectrographs required	5		1

Assuming that the light from the telescope is delivered (by Coude or fiber feed) to a suitable location in the facility, the length of fiber between the lenslet array and the output slits needs to be on the order of ~ 15 - 20 m minimum. Over this relatively length the transmission at 450 nm is still > 90%.

Referring to the discussion on feed schemes in the previous section, in case an all-fiber feed is selected, the lenslet array may be placed at one of the main telescope focal stations. In this case the required fiber length

is 300 or 200 m for the 100 and 60 m cases; the total length of 120 um fiber is then 26 and 8 km, respectively.

5.5.2 Scrambling and slit photocenter stability

The ideal fiber feed delivers to the spectrograph a beam with a perfectly stable PSF. Also the far-field intensity distribution must not be affected by guiding errors or seeing variations, since it can affect the PSF at the detector through second-order effects. To give an impression of the desired level of scrambling, a 10 cm/sec RV error corresponds to 5.10^{-5} of the instrument resolution, and corresponds to a shift of 0.6 nm in the location of the effective photocenter of the output of a 120 um fibre slit.

Fiber exit slit photocenter variations will be minimized in CODEX by a cascade of measures:

- Keeping telescope guiding and centroiding errors to the level of a few times 0.01 arcsec
- Use of a pupil slicer implies that the object is imaged on the entrance of each fiber and that best use is made of the scrambling properties of the fiber.
- Use of a light pipe at the end of the 8-fiber subslit. This type of device is found in every modern beamer to homogenize the beam at its output and make it insensitive to position instabilities of the arc of the projection light source. See fig. 5-11 Since the output distribution is the sum of light from 8 different fibers, there will be a statistical improvement as well.
- Optionally, a double scrambler can be inserted in each of the 40 or 88 fibers. This would only be done if laboratory tests show that the desired photocenter stability cannot be achieved

The operating principle of a light pipe in a beamer is shown in fig. 5-11. It is a usually a solid rod of glass with a rectangular or square cross section. Note that apart from its scrambling properties, a light pipe has other advantages that are further discussed in section 5.6.3.

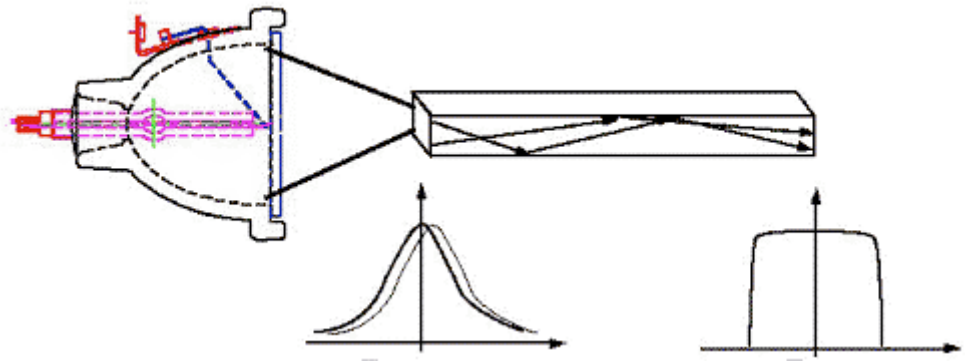

Fig 5-11 *Light pipe used in modern projection systems. Note the left curve is the cross section of the light levels entering the light pipe, and the right curve shows light levels leaving the pipe. Figure from "Arc Stabilisation for Short Arc Projection Lamps", H. Moench, G. Derra, E. Fischer and X. Riederer, Society for Information Display, 2000*

While in beamers a typical cross section is 10 x 10 mm, in CODEX it would need to be 0.12 x 1.03 mm. To improve manufacturability, handling and sensitivity to contamination of the external surfaces, the CODEX light pipe must be sandwiched between slabs of low-index glass. The fiber slit is cemented to the input side of the light pipe, as shown in fig.5-12.

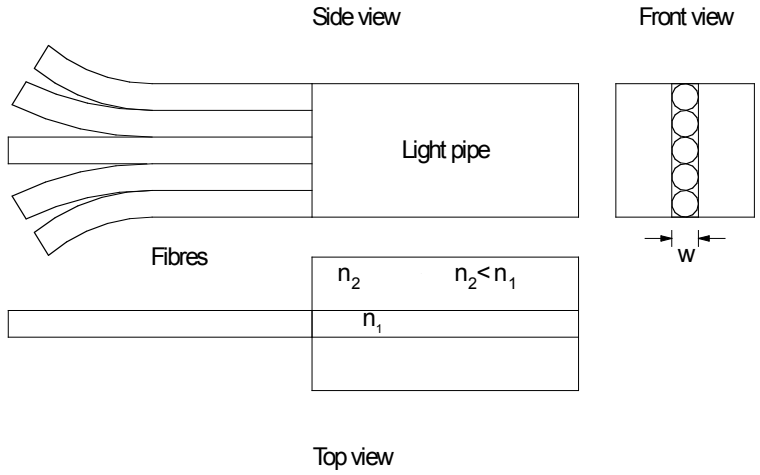

Figure 5-12. *CODEX light pipe mounted at the end of the optical fibers. The output slit will be uniformly illuminated.*

Fig. 5-13 shows a compact design of an image scrambler that can optionally be inserted in each of the 40 or 88 fibers between the lenslet array and the subslits. The device swaps the far and near fields between fiber 1 and fiber 2, so any residual photocenter variations that are present on the output of fiber 1 lead to variations in the far-field intensity distribution of fiber 2, which to first order do not affect the detected photocenter on the CCD. Similarly, the far-field intensity distribution of fiber 1, already quite stable since it corresponds to the telescope pupil, is imaged at the input of fibre 2 which performs further scrambling.

The device must be made to very high tolerances in order to keep losses at acceptable levels. To build 40 or 88 of them will also be costly. For these reasons we consider this an option, pending studies on the scrambling properties of fiber arrays and light pipes that are listed in the section on R&D at the end of this chapter.

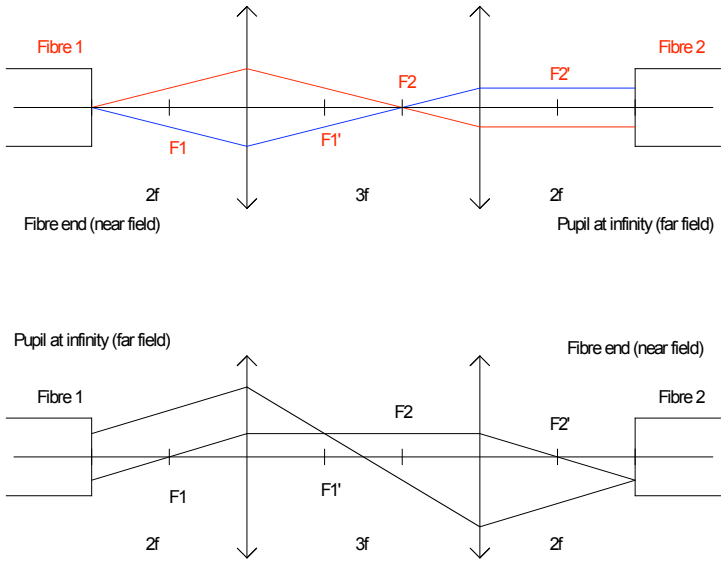

Figure5-13. *Double image scrambler*

5.5 Unit Spectrograph Design

5.5.1 Overall concept

We have designed the Unit Spectrograph with a wavelength coverage of 440 – 670 nm. It has a spectral resolution of 150 000 if fed with a slit of 120 um wide. The slit height is limited to about 1 mm. This slit is

imaged on the detector to a width of 60 um. We have assumed classical CCDs with 15 um pixels, so the sampling factor is 4.

In this preliminary design, the detector area measures 120 x 120 mm detector area, i.e. it is an 8K x 8K mosaic (four 4K x 4K or eight 2K x 4K).

A major design goal has been to limit the grating and optics size and exclude instruments that require square meters of grating. The overall design is shown in Fig 5-14; see its caption for explanation.

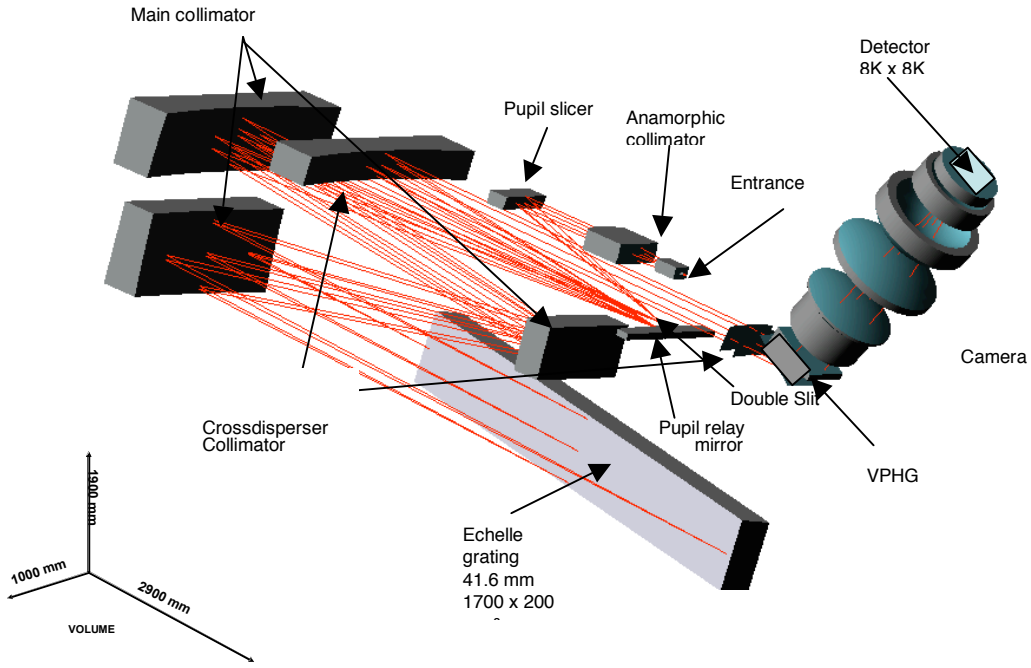

Fig 5-14: *Layout of CODEX Unit Spectrograph. Light from the fiber feed is injected at the entrance, then collimated to an elliptical beam with 4:1 axis ratio. The pupil slicer transforms this elliptical pupil to a 80 x 20 cm rectangular pupil and forms a double image of the entrance slit; one above the other. Then the light enters the main collimator(3-mirror anastigmat used in double pass) and is dispersed by the echelle. This is a white pupil design; an intermediate spectrum is formed on the pupil relay mirror. The crossdisperser (or pupil transfer) collimator produces a collimated beam on the VPHG which is also used as a 2.25 x beam expander to produce a 15 x 13 cm beam entering the camera. The detector size is 120 mm x 120 mm.*

The tools that are used in this design to limit the size of optical components are:

- Use of image slicing to reduce the effective telescope aperture “seen” by the spectrograph
- Use of an anamorphic beam (4 to 1) Since spectral resolution only depends on the illuminated length of the grating; not on the width, this helps to reduce the grating width, and the height of the optical components in the crossdispersion (vertical in fig 5-14) direction.
- Use of pupil slicing (2 slices). This technique creates a virtual grating with twice the length of the actual grating.
- Use of the crossdisperser VPHG as a 2:1 beam expander to expand the beam in the crossdispersion direction before entering the camera.

The result of these measures is that the grating in each spectrograph has a ruled area of “only” 1700 x 200 mm²; i.e. twice the length of a UVES grating. The size of collimator and camera optics are fully within today’s industrial capabilities

This design study is an “existence proof” that high-resolution, non-AO crossdispersed echelle spectroscopy is feasible on ELTs. We do not claim that it constitutes the optimum in terms of the selected slicing factors, number of spectrographs, cost of a unit spectrograph, its grating and detector size etc..

The following figure shows the evolution of the image and pupil sizes through the spectrograph. The object is assumed to be a single fiber.

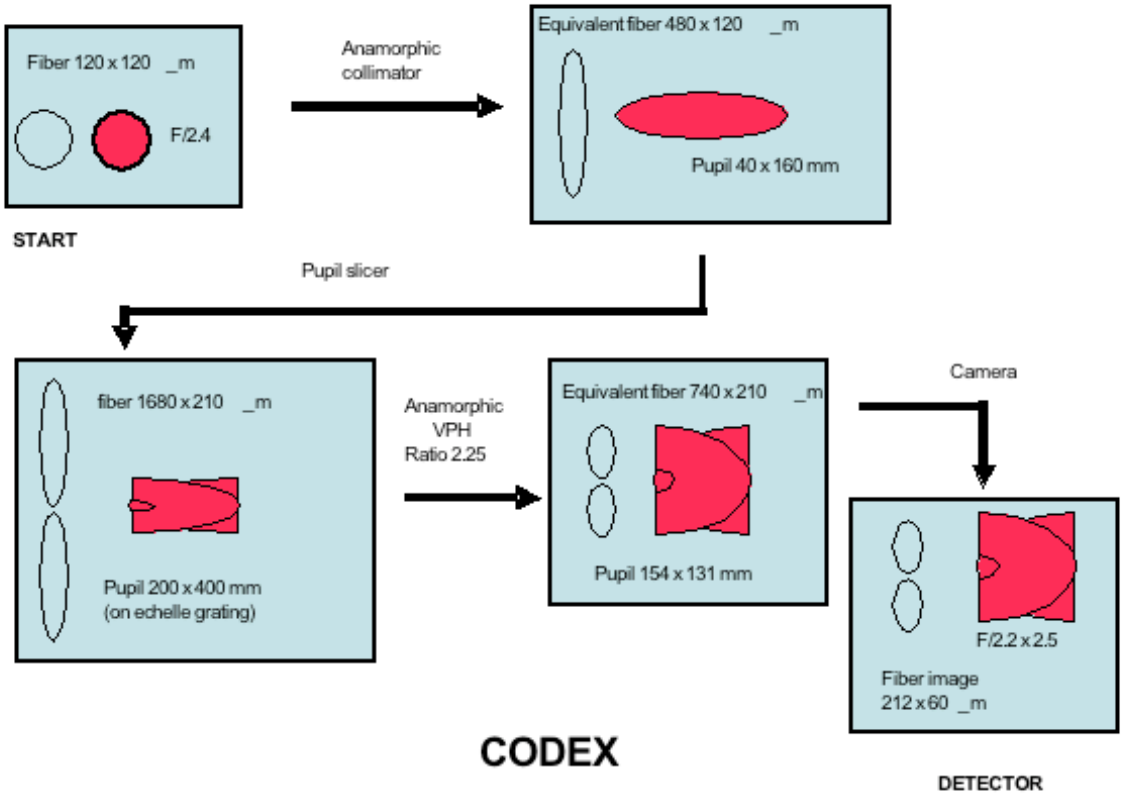

Fig 5-15: *Evolution of the image size (blue) of a 120 um fiber and of the pupil (red) through the spectrograph.*

The spectrograph is divided into 6 main units that will be described in more detail in the next sections:

- an anamorphic collimator
- a pupil slicer
- a main dispersion unit (collimator and grating)
- a cross dispersion unit (pupil transfer collimator and VPHG crossdisperser)
- a dioptric camera
- a detector unit

5.5.2 Anamorphic collimator

Since the resolving power of a grating is only determined by its length and not by its width, we use an elliptical beam to illuminate the echelle grating, in order to limit the width and so contain cost. This unit consists of two toroidal doublets that provide a parallel anamorphic beam of 40 x 160 mm. The collimator accepts a fiber output beam of F/2.4[2].

[2] This is at variance with the fiber F/no of F/2.3 assumed in the fiber/scrambler study; the difference is small and can easily be harmonized in one of the next iteration cycles.

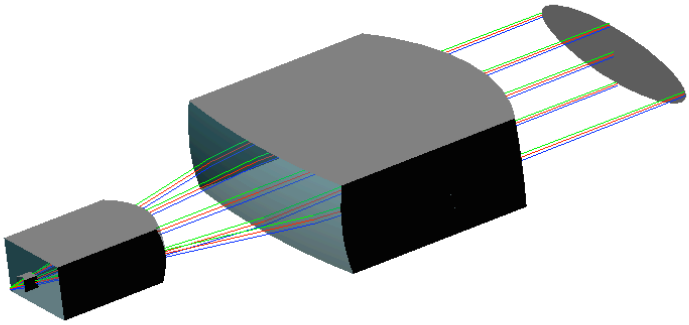

Fig 5-16: *3D view of the anamorphic collimator. Total lengths is about xxx mm*

5.5.3 Pupil slicer

The pupil slicer consists of two segments of an off-axis parabola that are tilted with respect to each other in order to create two images of the fiber slit, one above the other. Two tilted flat mirrors placed on the two slit images redirect the light to obtain superposition of the two half pupils on the grating. Each parabolic segment has a size of 24 x 85 mm.

Pupil slicing reduces the grating area by a factor two (200 x 1700 instead of 200 x 3400 mm²) for the same resolving power. The price to pay is a increase of a factor two in the required detector area, since the unit produces a double image of the slit.

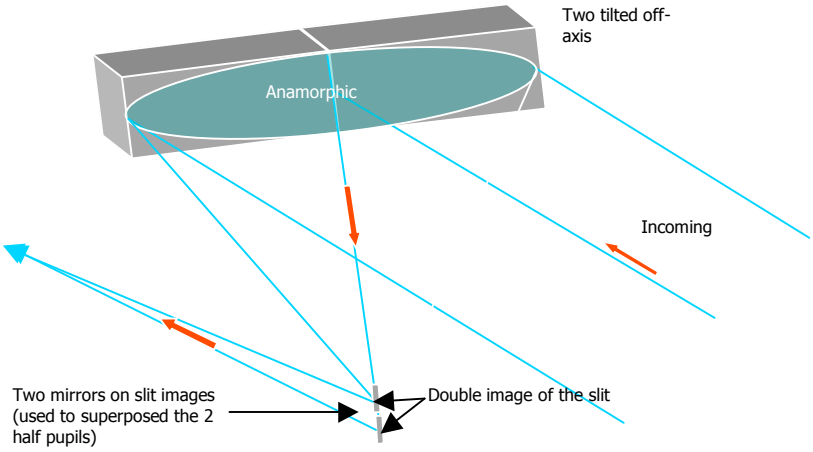

Fig 5-17: *3D view of the pupil slicer*

5.5.4 Main collimator and echelle

Even with pupil slicing, the collimated beam size remains very large (400x200 mm; rectangular see fig. 5-17). This excludes use of dioptric optics, so the main disperser collimator has to be reflective. A three mirror anastigmat used in double path has been selected; it delivers an intermediate spectrum with all orders superimposed at the intermediate spectrum mirror. This mirror acts as pupil transfer mirror i.e. it is curved to re-image the pupil. The width of the largest mirror is < 600 mm.

The grating is a 41.6 mm-1 echelle blazed at 76°. Its dimensions are 1700 x 200 mm² and consists of a 4 x 1 mosaic of 408 x 200 mm grating segments, with 10 - 14 mm dead spaces between segments The grating characteristics require the same master as was used to produce the UVES-blue echelles.

The UVES and HARPS echelles are copies of a 2 x 1 mosaic of precisely aligned submasters a single monolithic Zerodur substrate. At the time of replication the alignment of the submasters is “frozen into” the replica. Extending this technology to CODEX, which requires 4 x 1 mosaics, will be critical to the success of CODEX. This may require financing the extension of the mosaicking facility at a supplier, probably Richardson Grating Labs, similar to what was done for the UVES gratings.

Another solution is to mount two UVES-size gratings on a common substrate. A metrology and feedback system system must then be used in the spectrograph for in-situ verification and correction of the alignment of the segments. However, these solutions are intrinsically less stable and may suffer from PSF variations due to drifts or earthquakes.

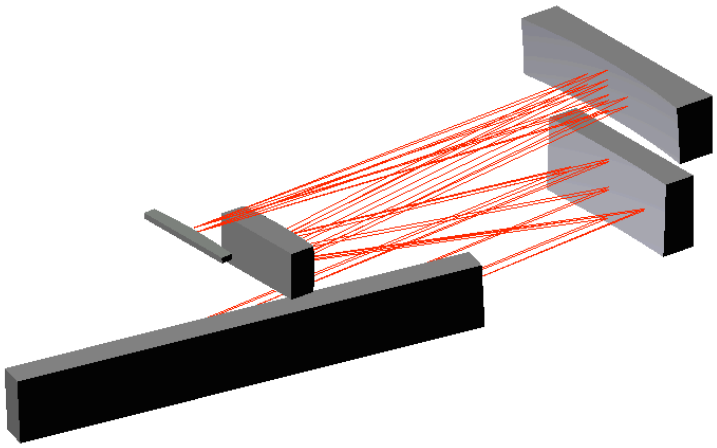

Fig 5-18: *3D view of the main collimator and grating. The overall volume of this system is 2400 x 600 x 600 mm*

5.5.5 Cross dispersion collimator and VPHG

The cross dispersion collimator is of the Maksutov type. It consists of a spherical mirror and a meniscus lens. This solution has been preferred to a dioptric collimator for its field curvature characteristics. The combination of residual field curvature of the main disperser, the pupil transfer mirror and the collimator offers a flat field in the parallel beam. The collimator has a focal length of 1050 mm.

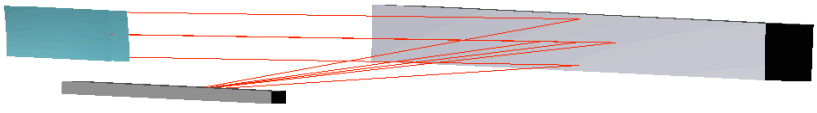

Fig 5.19: *3D view of the cross dispersion collimator and the crossdisperser*

The VPHG is sandwiched between two prisms. It is not only used to cross-disperse the orders, but also to expand the beam in the crossdispersion direction (figure 5-20).

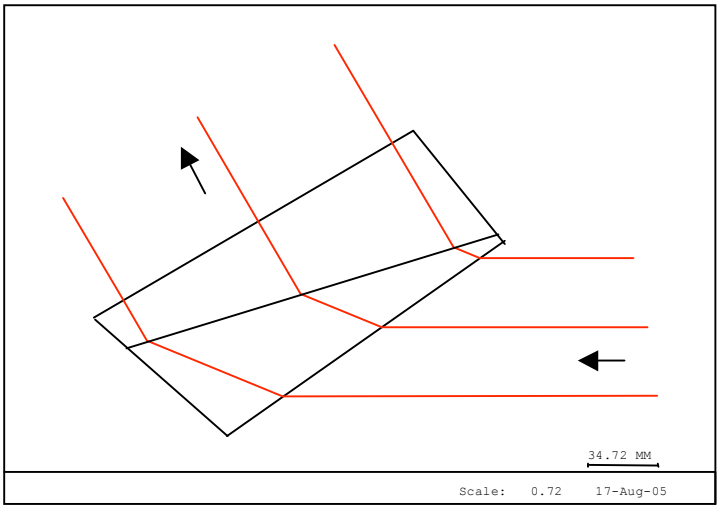

Fig 5-20: *Layout of the cross disperser VPHG.*

The VPHG is a 1500 mm-1 with slanted fringes which allow to operate it in a non-Littrow configuration. Combined with 2 prisms, the VPHG acts as a 2.25x beam expander in the crossdispersed direction. This reduces the size of the camera field in this direction by the same factor, which more than cancels the increase in detector area due to the pupil slicing. The prisms are made of NBK7. The various types of VPHG are shown in fig. 5-21.

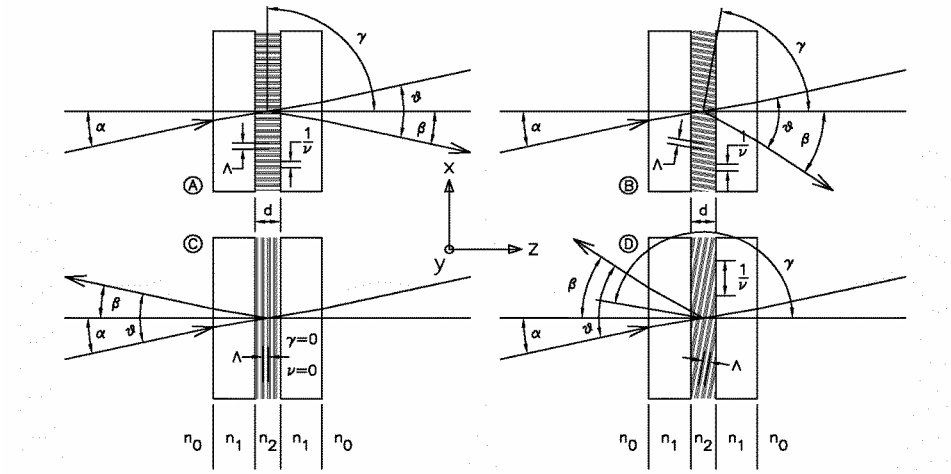

Fig 5-21: *Fringe orientation options for VPHGs. The one proposed for CODEX is shown in the top right hand panel. Figure from Arns, Barden et al, Proc. SPIE,3355*

First performance simulations kindly performed by A. Blanche at the Centre Spatial de Liege have indicated a peak diffraction efficiency in excess of 90%. The design requires further work since the unpolarized efficiency drops to ~55% at 450 and 650 nm. There are several ways to do this. Apart from increasing the □n of the Gelatin layer, we intend to use the prism parameters (angle and dispersion) to increase the bandwidth; we are confident that an efficiency of 70% over a bandpass of 200 – 250 nm can be achieved.

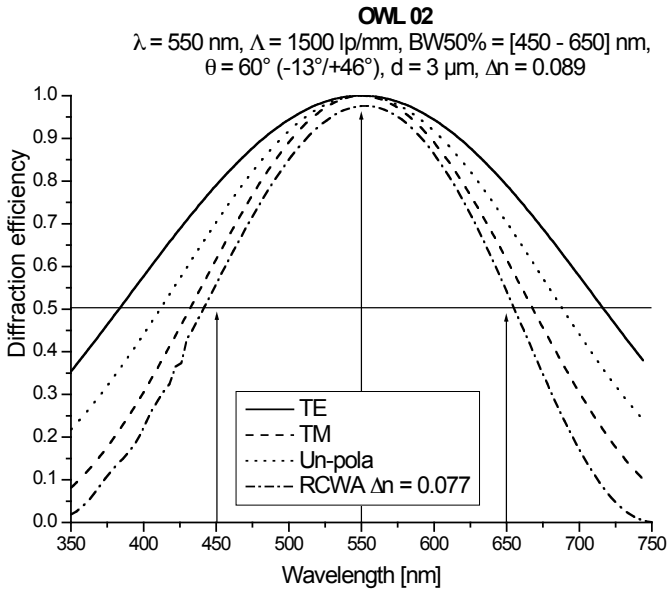

Fig. 5-22. *First results of RCWA simulation of the diffraction efficiency of a VPHG with slanted fringes (curve marked "RCWA"). Further optimization is needed to increase the bandwidth*

5.5.6 Camera and spectral format

The dioptric camera consists of 7 lenses in 6 groups, including the cryostat window. It already has encouraging performance of around 2 pixels. The only asphere is located on the surface of the first lens which is a CaF2 element. The total length of the camera is 730mm and the diameter of the largest lens is 350 mm. The camera is big and probably expensive, but feasible with present technology.

The spectral format is represented in fig. 5-24. The echellogram contains 35 orders between 446 and 671 nm. The minimum order separation is 2.3 mm (153 pixels) between orders 103 and 104. From Figure 5-23, the magnification in the crossdispersion direction is 1.77 (212/120). Allowing 10 pixels for interorder spacing, the input slit height can be up to 1.22 mm, which will accommodate eight 120 um fibers plus cladding.

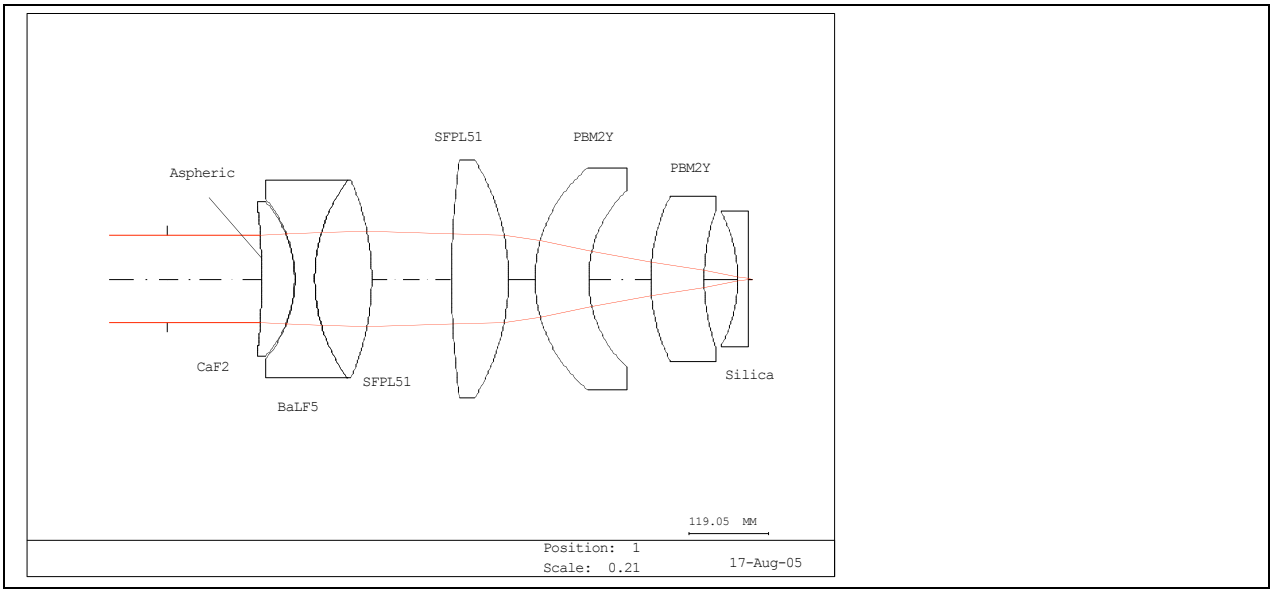

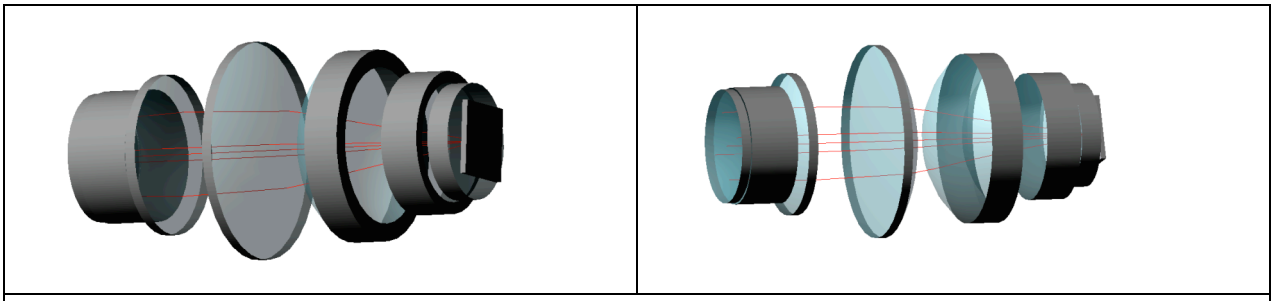

Fig 5-23: *Layout and 3-D views of the dioptric camera. The focal length is 333 mm. The F/no on axis is F/2.3; it covers a field of view of 120 x 120 mm²*

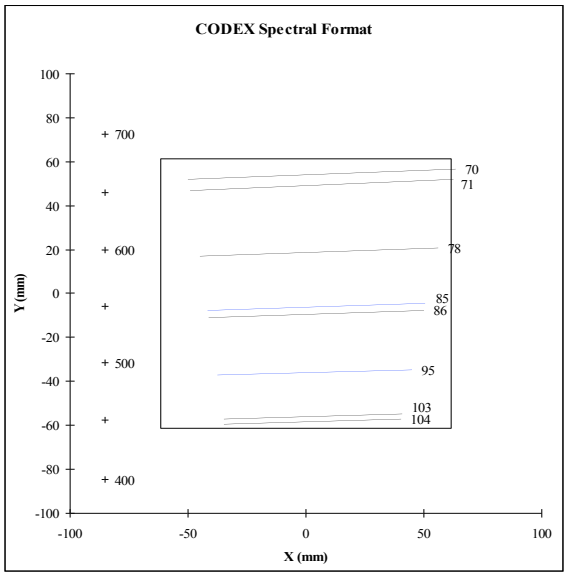

Fig 5-24: *Spectral format plot. The focal plane measures 120 x 120 mm*

The following table gives the energy concentration (80% EE in □m) corresponding to the left, center and right side of the FSR shown in the previous figure. The average EE for all field positions is 33 um, which already compares well with the projected slit width of 60 um. At the present stage the spectrograph is not fully optimized. A large contribution to the image defects comes from the anamorphic collimator. This will be the main focus of future design iterations.

Table 5-3.*Values of EE80 in um (fiber exit to detector plane)*

Order	*Left*	*Center*	*Right*
71	*55*	*32*	*19*
72	*54*	*30*	*19*
78	*41*	*23*	*30*
85	*34*	*26*	*43*
86	*33*	*28*	*45*
95	*30*	*22*	*46*
103	*51*	*28*	*12*
104	*55*	*33*	*11*

5.5.7 Detector array

Our baseline approach is to propose classical CCD detectors arranged in a mosaic. CCDs combine a number of properties that are not all found in other technologies like CMOS or L3:

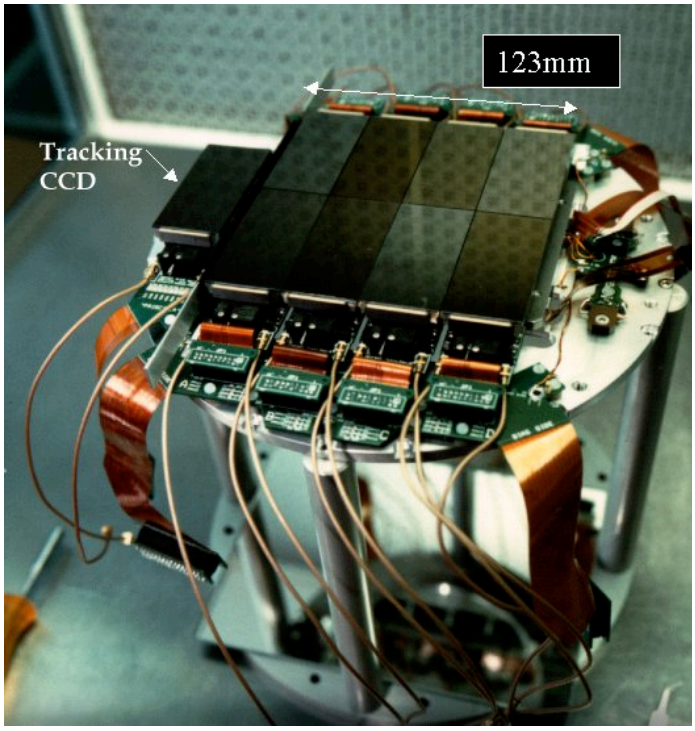

Fig.5-25. *Picture of the WFI 8K array which consists of eight 3-side buttable E2V CCDs of 2K x 4K each, plus one tracking CCD. The dimensions of the CODEX array will be similar to those of WFI (~120 x 120 mm). Similar to WFI, one or more "tracking" CCD might be used in CODEX to measure instrument drift during ongoing exposures.*

- Mature technology, RV suitability proven in HARPS
- Relatively low cost
- High QE over the wavelength range of interest
- Buttability
- Flatness of detector chips

The main drawback of CCDs is the read noise, where the current state of the art is a RON of 2-3 electrons. This will be examined in the next section.

The proposed array has 8K x 8K pixels; ¼ the area of the Omegacam array (Fig. 5-25).

The flatness that has been achieved on the Omegacam detector assembly is 50 um PV. This is adequate for the F/2.3 camera of CODEX.

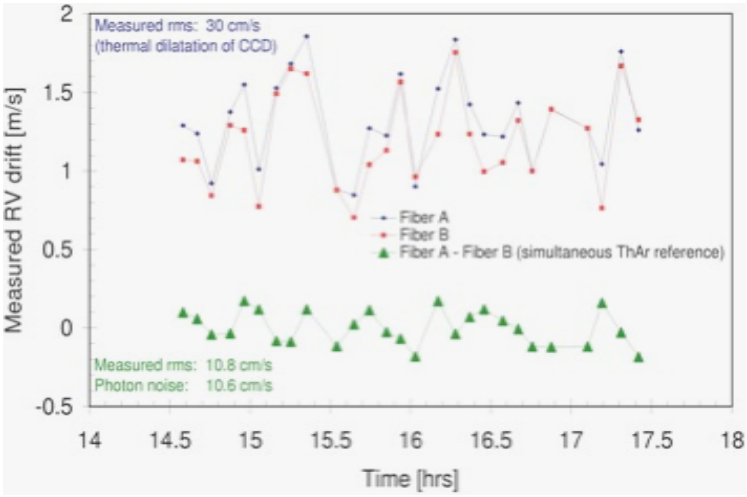

Fig. 5-26. *Periodic RV drifts measured in HARPS due to "breathing" of the detector assembly. From Rupprecht et al (2004), SPIE 5492. For further explanantion see text.*

In HARPS, the detector assembly has been identified as a major source of residual instrument instability. As can be seen in the upper curve of Fig. 5-26, the measured RV drift of HARPS undergoes a periodic variation every 30 minutes with an amplitude of ~0.5 m/sec (equivalent to a shift of 8 nm at the level of the CCD). The drifts are correlated with thermal dilatation of the CCD assembly with an amplitude of 20 mK and a displacement of the fixed point of the Aluminium CCD mounting plate by some tens of mm from the optical axis. The temperature variations are due to fluctuations (damped by the thermal braid) coming from the cold

plate to which the CCD assembly is coupled, and to the self-heating of the CCD chips during and after detector readout.

While this type of RV oscillation is quite acceptable in HARPS because it uses the simultaneous calibration technique (as shown by the lower curve of Fig. 5-26), it would not be acceptable in CODEX. For further discussion see section 5.6.3.

We intend to improve the stability of the CODEX CCD assembly by following measures:

- Design the CCD assembly for constant dissipation, regardless of its mode of operation (integrating, wiping, reading..) This can be achieved e.g. by adding surface heaters that inject the proper amount of heat, depending on the CCD operating mode.
- Improve the construction of the CCD assembly, by placing the effective fixed point in the center of the array
- Reduce the amplitude of the temperature “waves” originating by the cold plate and not fully damped by the copper braid that connects to the detector assembly. In HARPS, the cold plate is stable to about 1 K since its temperature is above that of Liquid Nitrogen and it is regulated by ON/OFF switching of the flow of cold Nitrogen gas. This is linked to the CCD detector assembly via a copper strap; the CCD has its own circuit, which stabilizes the temperature to ±10 mK. In CODEX, better stability could be achieved by adding an additional stabilization stage, or by maintaining the cold plate at the LN2 temperature.
- Use a material for the detector assembly with lower CTE. However, ESO has good experience with using Al in Omegacam for the mounting of large CCD mosaics. In the sum of its cryogenic properties (CTE, thermal conductivity, distortion during cool-down, stress relieving,.) Al will probably remain the best choice for the detector carrier material, despite its relatively high CTE.

By reducing thermal variations to 5 mK PV and placing the effective fixed point of an Al detector mounting plate within 10 mm of the optical axis, the predicted RV drift due to detector “breathing” reduces to 0.5 nm in the CCD plane (3 cm/sec).

5.6 Performance

5.6.1 Throughput

Below we compute the Detective Quantum Efficiency of the combination OWL + CODEX. Two cases are examined:

- Baseline design of OWL: 6-mirror design and fiber feed
- Alternative OWL design: 5-mirror design with Nasmyth focus, allowing a Coude mirror feed

In both cases we have used data for the reflectivity of the exposed telescope mirrors that were given to us by the OWL design team (protected Silver, aged 14 months, washed). We have assumed injection losses corresponding to GLAO on a 100-m telescope in 0.8 arcsec seeing and a 1 arcsec entrance aperture. Other assumptions see the table 5-4 and notes 1) to 8)

Table 5-4. *Calculation of overall throughput, from top of the telescope to detected photoelectrons*

6-mirror OWL and 200 m fiber

Wavelength	*1)*	*2)*	*3)*	*4)*	*5)*	*6)*	*7)*	*8)*	*DQE*
450	*0.57*	*0.40*	*0.80*	*0.70*	*0.78*	*0.65*	*0.70*	*0.85*	*0.038*
550	*0.67*	*0.65*	*0.80*	*0.70*	*0.78*	*0.65*	*0.85*	*0.90*	*0.094*
650	*0.67*	*0.75*	*0.80*	*0.70*	*0.78*	*0.65*	*0.70*	*0.90*	*0.090*

5-mirror OWL and 6-mirror Coude train

450	*0.62*	*0.91*	*0.80*	*0.70*	*0.78*	*0.65*	*0.70*	*0.85*	*0.096*
550	*0.72*	*0.91*	*0.80*	*0.70*	*0.78*	*0.65*	*0.85*	*0.90*	*0.142*
650	*0.72*	*0.91*	*0.80*	*0.70*	*0.78*	*0.65*	*0.70*	*0.90*	*0.117*

1) 6- or 5-mirror OWL coated with protected Ag aged 14 months, washed
2) Feed (intrinsic transmission of 200 m fiber or 6-mirror Coude; mirrors a 98.5%)
3) Injection losses (seeing 0.8", GLAO)
4) Slicer, FRD, lightpipe, scrambler
5) Spectrograph optics (20 air/glass a 99.5%, 10 mirrors a 98.5%)
6) Echelle (order center)
7) VPHG
8) CCD QE

The efficiency of the Coude feed is much better than the fiber-only feed. The efficiency gains at the 3 wavelength considered are 2.5, 1.5 and 1.3, respectively and translate directly into a time gain to reach a certain S/N in photon shot noise limited observations. We remind readers that a fiber length of 200 m considered here is probably an underestimate, especially for the 100-m case.

The predicted DQE is graphically represented it figure 5-27 below.

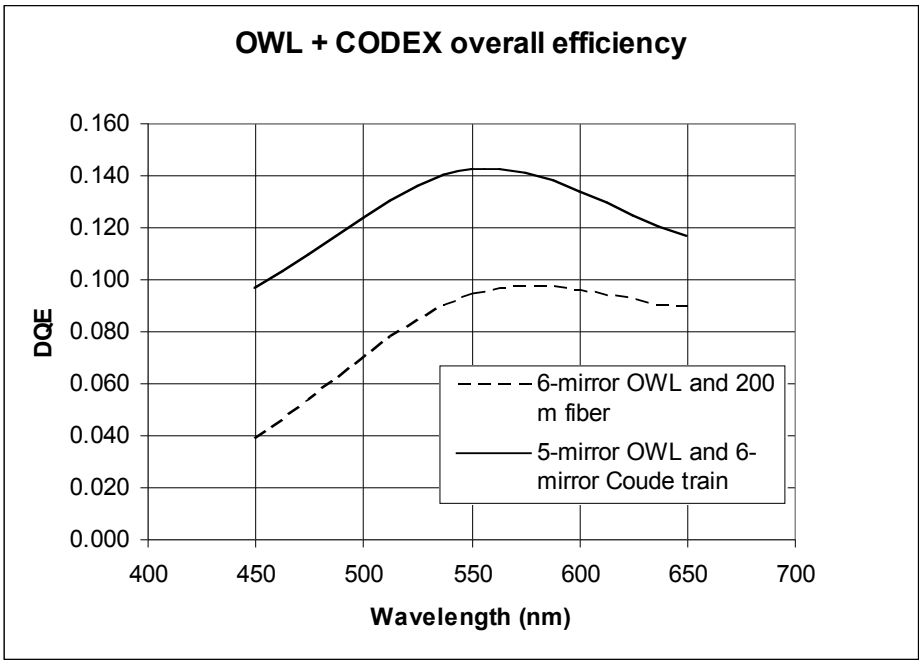

Fig 5-27. *Predicted DQE of OWL and CODEX (top of the telescope to detected photoelectrons). Shown is the efficiency at the order center, for order overage multiply with 0.8. Other assumptions see Table 5-4.*

5.6.2 Noise levels, signal addition

CODEX must be photon noise limited on a M_v = 16.5 QSO in 10 minutes. The light is spread over many spectra in different spectrographs that are co-added later on, so this requirement holds for every individual spectrum.

First we will investigate dark current. The count rate from an m_v = 16.5 object is 2.5 ph/m2/A/sec at 550 nm at the top of the atmosphere. With a telescope diameter of 60 m, a DQE of 10 % and a spectral bin size of 9.2 mA (R =150 000, sampling factor 4) the photoelectron rate will be 23400 e/h per spectral bin. We have 37 fibers, each producing two spectra, so the photoelectrons are distributed over 74 spectra. A spectrum is 110 um (7 pixels) high. Thus the count rate per pixel is 43 e/h/pix. This is two orders of magnitude larger than the CCD dark current (< 1 e/pix/h). We conclude that dark current will not be a limiting factor for any exposure time.

The situation is different for read-out noise (RON). In an integration time of 10 minutes one collects only 7 photoelectrons per pixel. If we demand that the impact of RON is a degradation of less than 12%, its variance must be < 25% of the number of photoelectrons per bin. With a RON of 3, this requires 5-fold binning along the spatial direction to collect 35 photoelectrons. A RON of 2 requires 3-fold binning. Due to lower count rates in some parts of the spectra or intensity variations between fibers, the actual required binning factors will be even higher.

5.6.3 Benefits of the light pipe

If one does not use the light pipe, the spectra of individual fibers were 110 um high (7-8 pixels) and not aligned to the CCD rows. Binning in the spatial direction would be limited to 2 at most in order to avoid pixelization effects.

Fig. 5-28 . *Light pipe made with high-efficiency mirrors. Glass rods with total internal reflection are also commonly used.*

The light pipe (fig 5-28) sums and mixes the light from the 8 fibers, providing an homogeneously illuminated slit. With a light pipe on the output of the 8 fibers, an echelle order will consist of a double spectrum, each about 70 pixels high. On a 16.5 magnitude object in 10 minutes of integration, each spectral bin willhave 390 photoelectrons evenly distributed over its height, equivalent to ~ 5.6 e/pixel.

The advantages of using light pipes in CODEX are:

- The light pipe acts as an efficient averager/scrambler.
- A light pipe allows large spatial binning factors, reducing requirements on detector RON Binning also leads to a reduction of data rates and file sizes.
- Simplification of data extraction. Per unit spectrograph, only 2 spectra must be extracted, weighted and summed, instead of 16. Spatial variations in the light intensity distribution are eliminated, which should simplify summing algorithms
- With a light pipe, one exposure meter per spectrograph will be sufficient. Without it, one probably needs one to determine the Mean Time of the Exposure (MTE) for each fiber spectrum.

In conclusion, for present-day CCDs with state of the art RON of 2-3 electrons, the light pipe is a key element to allow larger binning factors. In addition, light pipes provide scrambling, reduce data rate and simplify data extraction.

5.6.3 Instrument drift monitoring

With single fiber spectra there is still the possibility to assign one fiber to simultaneous calibration, although, as explained earlier, it would be very costly in terms of detector area required. Instead of performing *simultaneous* reference, we are considering several schemes which are more detector efficient, such as to interleave wavelength calibrations with the science integrations, or use of the tracking chips as with WIFI.

Interleaved calibration requires that the instrument drift during a 10-minute exposure is small or at least linear be smooth enough to permit modelling, in order to establish a sufficiently accurate RV correction to be applied to the Mean Time of the Exposure. To be on the safe side and sure that systematic effects are avoided, the RV correction must be accurate to the level given by the calibration photon noise; 10 cm/sec in the case of HARPS.

The HARPS drift curve shown in 5-26 exhibits in places slopes of 1 m/sec per 10 minute interval, and is not linear within such an interval. In case interleaved calibration is used, this will make it very difficult to establish instrument drift to the desired accuracy. Therefore, apart from reducing the amplitude of the drifts, also their frequency should be reduced. Meeting the drift requirement can be demonstrated with a technique similar to the one used to produce fig. 5-26 comparing two series of interleaved calibration exposures. This will be an essential test to perform on a prototype instrument.

5.7 Calibration

Light from the calibration source must be fed into the fibers at the instrument entrance, i.e. the telescope focal plane.

As stated in several instances in this report and discussed in detail in section 6.4.2, the Th-Ar lamps currently used for wavelength calibration are not the perfect solution, and they do not guarantee enough accuracy for our purposes. M. Murphy (IoA Cambridge) has proposed the use of a new system, based on laser frequency combs. This technology has been developed at the MPQ (Garching) and uses femtosecond pulsed lasers to create combs whose frequency can be anchored to a standard time signal (atomic clock or GPS) and be known with the same high accuracy of the clock itself, that is, up to a precision of a part in 10^{-14} – 10^{-15} The signal, passing through photonic crystal fibres uses the non-linear processes present in the fibres to extend the width of the original frequency spectrum, since in these fibres all combination of the original frequencies take place. The final result is a wide comb of equi-spaced emission lines with a frequency known with extremely high accuracy. This system has been developed for other purposes, and its adaptation to astronomical spectrographs will not be trivial. A number of problems exists, such as that the separation frequency which can be reached at the moment is only of 1 GHz, while 15 are optimal for our case. Another potential problem is the extension of the technique to wavelength as low as 400 nm, which has never been proven before. In order to overcome these problems and obtain a product that could be operated in an Observatory environment, ESO has launched a R&D program in collaboration with MPQ to produce a calibration unit based on this technique.

5.8 Data Rate

As far as data rate is concerned, again HARPS experience can be used a comparison. HARPS is equipped with a 4Kx4K detector, which produces 35 Mbyte each exposure. CODEX will have 100 of them, producing therefore 3.5 Gbyte each frame. With a typical integration time for the main program of 10 minutes/exposure, we expect a typical rate of 100 frames/night which shall be doubled when calibrations are taken into account. **A typical night is expected therefore to produce 200 frames or 700 Gbyte**. There will be occasions, however (studying stellar oscillations, searching for earth mass planets) when this data rate will be easily higher by a factor ten. **In these nights we do therefore expect up to ~1500 spectra or 5250 Gbyte/night.**

5.9 Research and Development

During an initial feasibility study, following hardware issues will be studied, prototypes made and tested:

General:

- Coude feed vs. fiber feed: efficiency/cost trade-off.
- Non-Littrow VPHG with slanted fringes: efficiency, bandpass optimization
- Echelle: 4 x 1 mosaicking technology

- CCD detector mosaic: temperature stabilization, constant-dissipation operation, central mounting of the detector assembly
- Laser comb calibration source

Fiber specific (studies mentioned below have partly been already started)

- Fibers: scrambling vs. length, diameter and feed mode (pupil or star on the entrance)
- Improving scrambling properties using controlled vibration or stress
- Improving scrambling using dual scrambling schemes
- Light pipes: photometric and scrambling properties, FRD, effects on data extraction and binning
- Lenslet array tolerances (image quality, fibre coupling efficiency, packing density)

Although specific issues may also be tested on HARPS, for example the improved stabilization of the detector array or interleaved calibration vs. simultaneous calibration, we still consider it essential to build a full-scale prototype of a Unit Spectrograph of CODEX for the VLT (CODEXino) prior to building a full-scale CODEX for OWL.

The reason for this is, that RV studies to this level of accuracy are unprecedented. To demonstrate that the desired performance can be attained, it will be necessary to integrate the technical solutions that were developed or tested stand-alone in a full-scale prototype. Because of the subtleties involved in attaining ultra-high RV precision, hardware, calibration, data reduction and operational issues are less easy to separate than in other instruments. This implies that the tests must be done with a view to end to end performance.

Based on the experience with CODEXino, a decision to proceed with CODEX can then be taken with confidence. Even after this decision is taken, CODEXino will be a useful test bed for e.g. new scrambling techniques, extraction algorithms or calibration procedures. The experience during this phase will ensure that CODEX can be operated in an optimum way directly after it has been installed.

The scientific merit of installing CODEXino on the VLT is discussed elsewhere in this report. Here we just note that only full science operation (not just for a single test run) will allow to evaluate its performance – especially stability and RV accuracy – over a longer time period. For this to happen, CODEXino should be fully integrated into the VLT operational and QA environment.

6. CODEX Performances Analysis

6.1 From HARPS to CODEX

The purpose of this chapter is to show that the measurement accuracy required by CODEX to attain the established scientific goals lies within today's technological possibilities. The final proof will not be provided here, because it would be close to impossible to establish a detailed and final error budget of an instrument, which has to deliver a precision 10 to 100 times higher than obtained with present instrumentation. Indeed, the goal is to attain about 1 cms^{-1} equivalent radial-velocity measurement precision, which has to be compared to the 1 ms^{-1} routinely obtained with HARPS (Pepe et al., 2005). Instead, we shall use the experience gained with HARPS to identify possible limiting factors, extrapolate them in terms of performance for CODEX, and issue advices for the design of CODEX and for operational aspects.

The following analysis has been divided in three parts:

1. Establish the maximum accuracy that can be achieved supposing a perfect instrument, i.e. compute the "fundamental" accuracy on a typically expected spectrum supposing that it is affected only by photon noise
2. Study the most limiting instrumental effects. This part includes also a discussion on the needed instrument calibrations and the requirements to them.
3. Discuss how the signal can be extracted from a measured spectrum or series of spectra

6.2 Achievable photon-noise error

6.2.1 Fundamental photon noise

The following computations have been based on four simulated spectra produced by the Trieste group within WP 2100. These spectra contain the Lyman forest of four real QSOs, and have been computed for every source at two different epochs separated by 10 years. The pixel size is 0.0025 Å, and the S/N is infinite. Table 6-1 gives the main characteristic of these spectra.

Table 6-1: Main characteristics of simulated QSO spectra

Filename	Nr. of pixels	Spectral range [Å]	Redshift
q0000spA.dat	284000	5385-6095	4.1
q0055spA.dat	276000	4900-5590	3.66
q0302spA.dat	232000	4415-4995	3.29
q1422spA.dat	228000	4920-5490	3.62

Figure 6-1 shows a portion of a simulated high-resolution spectrum convolved at various spectral resolutions. It can be seen that the Ly-alpha lines start to be resolved at R = 10'000. All the spectra have been sampled with a fixed "extracted pixel" pixel size of 0.0125 Å. Fixing the sampling has two advantages: First, the simulations become independent from the spectral format of the spectrograph and, at high S/N, also from detector noise. Second, at a given S/N the results obtained at different spectral resolution can be directly compared.

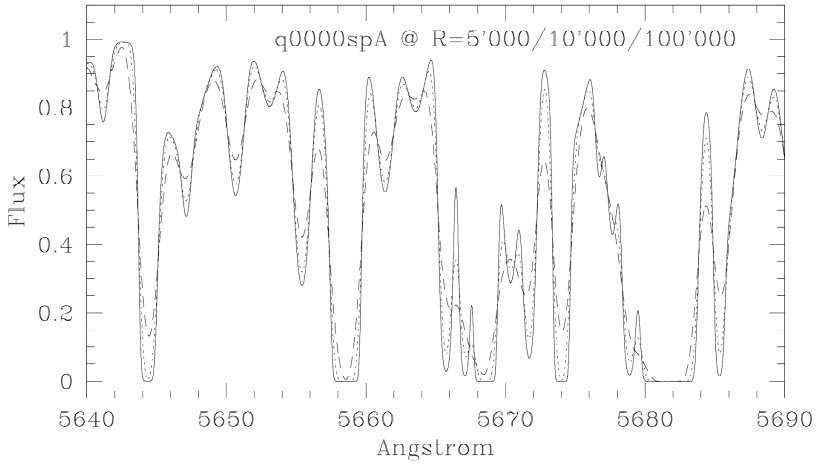

Figure 6-1: *Simulated target spectra at various spectral resolutions. The Ly-alpha lines start to be resolved at R = 10'000 already.*

In order to perform the simulations, the spectra have been added with photon noise to produce the desired S/N at continuum. Then, the technique described by Bouchy et al. (2001) has been employed to estimate the maximum radial-velocity information contained in the spectrum. The thus obtained values provide us with an upper precision limit, which can only be obtained if neither the source, nor the instrument, nor the data-reduction and analysis introduce any additional noise component or systematic error.

Figure 6-2: *Fundamental measurement accuracy as a function of spectral resolution*

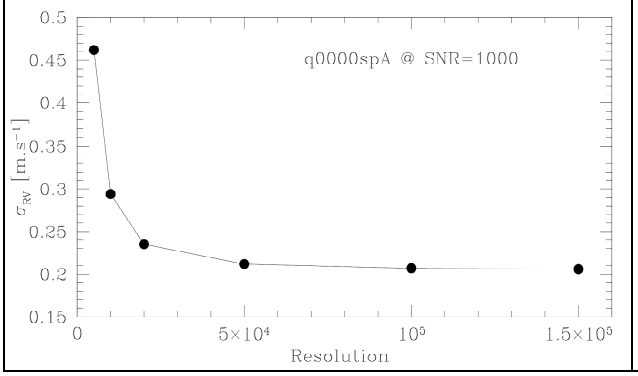

Figure 6-3: *Achievable measurement accuracy as a function of continuum S/N*

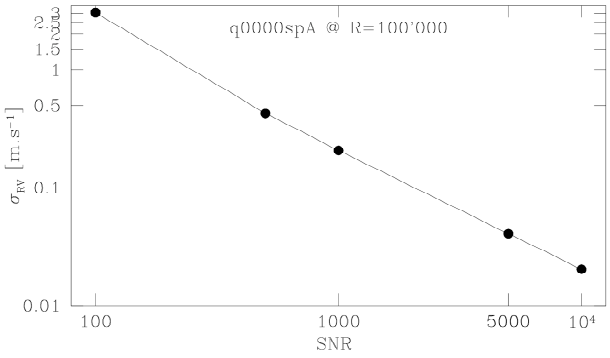

Figure 6-2 illustrates the results for q0000spA as a function of spectral resolution. Since the typical width of the Ly-alpha lines is about 1 Å, a resolution of ~30'000 is sufficient to resolve all the spectral lines. Therefore no gain on the photon noise precision is obtained when increasing further the spectral resolution. As we will discuss later, a high spectral resolution is needed, nevertheless, because of other reasons.

Figure 6-3 shows the same results, but plotted this time as a function of S/N at continuum. As expected, the measurement precision behaves proportionally with S/N, i.e. the photon noise error depends on 1/S/N. From this graph we see than a S/N of 20'000 is needed to obtain a photon noise error of the level of 1 cms^{-1} on one epoch spectra. Note that this result has been independently found by the analysis in section 3 and is perfectly compatible with eq. 3.13 .

Simulations have been repeated including in the simulated spectra the metal lines associated to individual Ly-α forests. The fewer but thinner metal lines contribute to the radial-velocity information at about the same level as the Ly-α forest lines, provided that they have been resolved by the spectrograph. Fundamental photon-noise computations performed on R = 100'000 simulated spectra show that the S/N needed to achieve a **1cms^{-1} precision** is reduced to **S/N = 13'600 (**for 1 epoch measurements and pixel size of 0.00125 nm**)**, i.e. precisely by a factor of 2 in equivalent flux or exposure time.

6.2.2 S/N computation

We show in Figure 6.4 the expected S/N ratio as a function of magnitude, as computed for a 100-m telescope and an overall optical efficiency of 10% (for comparison HARPS shows 6% efficiency, FEROS about 15%). The results are given for exposure times of six minutes, one hour, and one night. In the limit of pure photon noise (no read-out noise RON), i.e. for $m_v < 19$, we can apply the following simplified scaling formula

Eq. 1
$$S/N = 621 \cdot \sqrt{(T_{\exp}/10\mathrm{h}) \cdot 2.514^{(17.5-m_v)}} \ .$$

Considering the high number of spatial pixels the RON can be decreased considerably by spatial pixel binning, increasing the domain in which the measurement is photon-noise limited by several magnitudes, but, on the other hand, reducing the dynamical range of the detector.

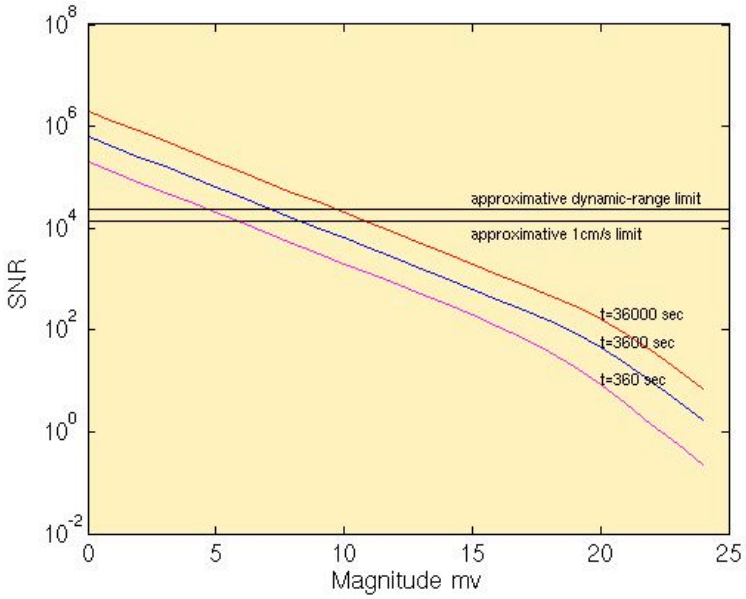

Figure 6-4: *Expected S/N at 550 nm as a function of object magnitude for several exposure times. We have assumed a 100-m telescope and a pixel sampling of 0.0125 Å. In order to estimate the influenec of RON we have assumed an echelle order width of 120 pixels and the spectra being distributed over 11 spectrographs simultaneously. The used value of 1e⁻/pixel for the RON assumes no binning*.

6.3 Instrumental limitations

In this section we shall analyze all instrumental effects (neither related to the source, nor to the data reduction and analysis), which can lead to systematic errors, non-Gaussian noise, and/or noise largely dominating the photon-noise. Only error source have been considered which cannot be “removed” by calibration. For these, we discuss first its nature, then we estimate the possible impact, and, if significant compared to the aimed precision, we shall indicated possible remedies.

6.3.1 Light-contamination of the scientific spectrum

The general statement we can make here is that contamination of the source spectrum by an external source is only dangerous if it contains spectral features. A spectral continuum, in the extreme case pure white light, will not affect the position measurement of the science object’s spectral lines. We will try to estimate in the next sections which kind of contamination source is potentially dangerous and to which extent.

6.3.1.1 Contamination by a spectral background continuum

We assume here that the contaminating spectrum does not contain any high-frequency feature but only slow chromatic flux variations. The spectral line shape of the scientific spectrum can indeed be changed, and thus its position would, if we superpose a continuum with a non-zero slope. In addition, it would affect all lines by the same systematic error.

For simplicity, we define the line position by means of its spectral photocenter. Considering a spectral resolution of R = 100'000 and the line stability requirement of 1 cm s^{-1} equivalent, we have to require that the photocenter of the line must not change by more than 1/300'000 of its FWHM. From a rough approximation we deduce that the flux in the continuum of the recorded spectrum must not change by more than 1/300'000 over a FWHM of the spectral line, or less than 1.5 ‰ per nanometer wavelength, or about 20% over the full CODEX spectral range. We have again to point out here that time-independent contamination will not have any effect, and that only slope variations of the contaminating spectrum would produce such an effect. We think therefore that this point can be neglected in the error budget.

6.3.1.2 Contamination by close-by objects

The point here is that we might have faint objects close to the scientific object, and that a part of its light falls on the spectrograph fiber and contaminates the scientific spectrum. Even worse, depending on the atmospheric seeing, the level of contamination might changes. Therefore, one should absolutely avoid scientific targets, which have a visible companion of any magnitude closer than typically 3 arcsec from the scientific object.

On the other hand, we cannot completely exclude that there are faint or unresolved objects within this field. We will therefore try to define a lower limit for the magnitude difference between the scientific target and the companion, above which the contamination will not produce any effect greater than 1 cm s^{-1}. In contrast to Section 6.3.1.1, where the error affects all the spectral lines in the same way, here we can assume that a spectral line position of the target is affected arbitrary by the contaminating spectral feature. The line position of the affected line is averaged with all the scientific lines. If we arbitrarily assume that the scientific spectrum contains about 1000 spectral lines, then we can afford that one single line is "distorted" by up to 10 m s^{-1} by the contaminating line, still lying within the required global 1 cm s^{-1} accuracy. Assuming worst case (i. e. the contaminating spectral feature is unresolved, shows the same contrast as the scientific line, and is just placed at about one FWHM from the line center) we compute the contaminating line should not be brighter than 1/300 of the scientific feature.

However, it is more likely to assume the presence of many contaminating spectral features distributed "randomly" over the spectral range of CODEX, affecting many spectral lines of the science object. We can think at the worst case, in which all scientific lines are affected by some random error described in the previous paragraph. The induced error decreases with the square root of the number of scientific lines N. If we take again our example with 1000 scientific lines, we can specify that the random error affecting one single line must be smaller than 30 cm s^{-1}, and that therefore the brightness of the contaminator spectrum has to be 10'000 times smaller than the science object spectrum.

The farer away the contaminator is located from the scientific target (in terms of astrometric distance) the fainter will be the contamination of the scientific spectrum. Let us assume a given magnitude difference and a given astrometric distance between the target and the contaminator. Let us also suppose that the scientific target is well centered on the fiber. We can then compute the part of the contaminator flux falling into the scientific fiber, and determine the level of contamination. Inversing the problem, we can require that the contamination level must be smaller than 1/10000, and compute the minimum allowed magnitude difference between target and contaminator, at a given distance. Figure 6-5 shows this relation for various seeing conditions. The minimum magnitude difference grows very rapidly with distance and becomes uncritical already at a distance of 2.5", even under seeing conditions of 1.5". It must be noted here, however, that the computation assumes Gaussian-shaped flux distribution. Therefore, some safety margin must be adopted.

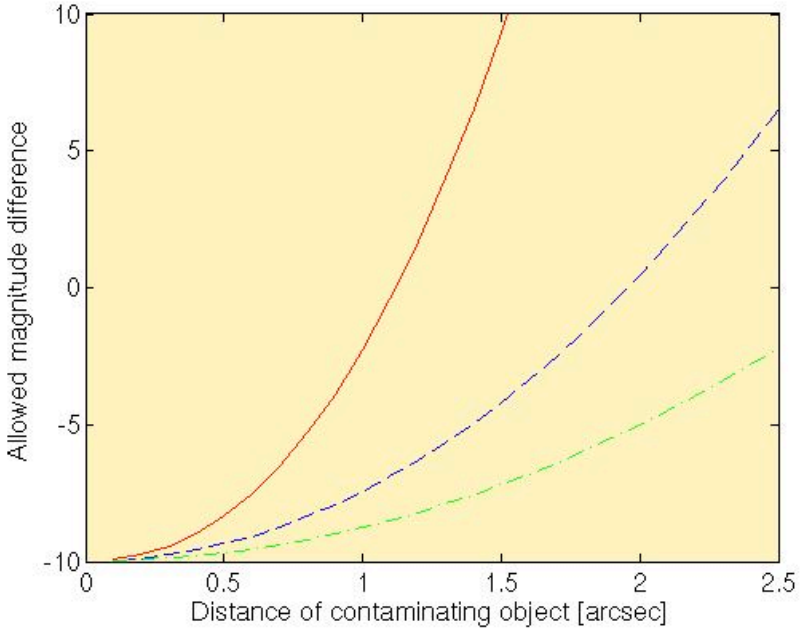

Figure 6-5: *The plot shows the allowed magnitude difference between the target (m_{object}) and a possible background or foreground object ($m_{contaminator}$), if one does allow a maximum contamination of the scientific spectrum by the contaminator spectrum by 1/10'000. We have assumed a fiber diameter of 0.7". The various lines show the results for different seeing conditions (red plain: 0.5", blue dashed: 1.0", green dotted-dashed: 1.5"). The worse the seeing, the larger must be the distance for a given magnitude difference.*

6.3.1.3 Contamination by Sun and Moon light

Along the same line as shown in the previous section, we have to avoid that direct or indirect Sun light reaches the detector with a contrast magnitude compared to the science target smaller than 10 (we can assume here the worst case, since the Sun spectrum is very dense). We propose following recommendations:

1. Avoid twilight observations
2. Avoid observations during full moon, or when target is too close to the moon
3. Avoid observations with cloudy sky and cirri
4. Investigate in more detail the sky brightness (diffused an reflected Sun light as a function of distance to the moon, moon phase, and sky conditions) as part of a preparatory program

6.3.1.4 Contamination by atmospheric absorption and emission lines

Although well known, atmospheric absorption and emissions lines cannot be "simply" removed from the scientific spectrum, because they are highly variable in intensity and position (up to 100 m s^{-1} variations). We therefore propose to take high-accurate atmospheric spectra as part of a preparatory program for OWL, and determine precisely the intensity of these atmospheric lines under bad atmospheric conditions.
Since correction or modeling of the atmospheric features is not foreseen (and in any case very difficult), the scientific data reduction will not use the spectral zones, which show the presence of an atmospheric line with intensity brighter than 1/10000 of the spectral line of the observed scientific target, and in particular avoid these zones for the velocity determination.

6.3.2 Chromatic flux variations in the target spectrum

A chromatic variation of the target flux might have two effects: First, a varying slope is introduced in the spectral continuum, producing a line-shape change as described in Section 6.3.1.1. Second, the weight of a single spectral line in the average of the positions over all spectral lines will change. If the line positions are affected by systematic errors, these errors will differently influence the mean radial-velocity value, depending on their weight. While the second effect can be avoided by a perfect wavelength calibration, the first can probably be minimized by appropriate data reduction. We should however aim at keeping these chromatic flux variations as low as possible. Considering what is said in Section 6.3.1.1, we propose to require that the flux ratio between the reddest and the bluest part of the spectrum does never change by more than ± 10 %.

The strongest chromatic flux variations are produced by the atmospheric dispersion combined with the varying seeing, as well as by varying atmospheric extinction. We propose therefore the following recommendations:

1. Use a continuous Atmospheric Dispersion Compensator (ADC)
2. Avoid observation during unstable astroclimatic conditions
3. Correct for varying continuum in the data-reduction pipeline.

6.3.3 Guiding, centering and focus stability vs. image scrambling

The problem of spectrograph illumination stability is probably, together with the wavelength calibration and the scientific source stability, one of the precision-limiting factors. Of course, one could argue that a self-calibrating system, such as the use of an iodine absorption cell, is conceptually able to remove this problem. In practice, the iodine absorption cell introduces other problems which are not easier to solve: contamination of the target spectrum, requires deconvolution and thus the perfect knowledge of the instrumental profile, requires extremely high S/N and a lot of computation time for the deconvolution process, etc. Despite its conceptual superiority, the iodine technique has not yet demonstrated to be able to reach a level below the 2-3 m s^{-1}.

On the contrary, the HARPS concept has demonstrated that on time scales of hours to nights, during which effects like bad centering or scrambling would appear, a performance of 20 cm s^{-1} rms can be reached. Nevertheless, we know that this system is not yet perfect, and that residual guiding errors exists at the few tens of cm s^{-1} level. These residual errors are due to the fact that the fiber scrambling is still not perfect, and that variations of the intensity distribution in the far and near field of the fiber exit still persist (despite the use of a 40-m fiber and a double scrambler). Errors in centering and focusing the star on the fiber entrance translate therefore in small shifts of the IP photocenter, which are in turn interpreted as a radial-velocity change.

A first analysis indicates that the 1 cm s^{-1} stability can be reached using the present HARPS concept (but applied on a fiber bundle), if a guiding-centering stability of the star on the fibers is better than about 0.02 arcsec. This number is only a rough estimate and depends strongly on many technical aspects. Given the employed technology (fibers, scrambler) these effects cannot be easily quantified at the moment. We propose therefore that this aspect should be part of a major development phase of the CODEX project, for which we would indicate following tasks:

1. Study the performance of a single fiber + slicer solution versus a solution using a fiber bundle, in particular with regard to optical efficiency and scrambling
2. Develop and test a fiber link and a “perfect” scrambler
3. Foresee a precise and fast guiding system with at least tip, tilt and focus control
4. Foresee to record and store for any exposure the integrated guiding image, which will allow to detect a posteriori potential guiding problems.

6.3.4 Instrument stability/environmental conditions

Introducing this section we must note that it will be impossible to manufacture a spectrograph, which guarantees that the recorded spectrum with an absolute drift of < 1 cm s^{-1} over 20 years, which is equivalent to a physical displacement of about 1 Å on the detector. It will be also impossible to model any tiny thermal, mechanical, pressure and material effect, or the combination of those, at this level of accuracy. We think therefore that the most realistic approach is to built an instrument as stable as possible with "reasonable" efforts, and to make sure that possible drifts are monitored by some "simultaneous or sequential referencing" technique, that is a comparison with an external standard. This corresponds exactly to the HARPS approach. Indeed, HARPS has demonstrated to reach absolute stability (prior to calibration) of 30 cm s^{-1} rms on short term (minutes to hours) and 1-2 m s^{-1} rms on long term (hours to months). We think that by applying minor technical improvements to the HARPS concept, the absolute stability could be increased further by a factor 5 to 10. Short-term stability of less than 10 cm s^{-1} can reasonably be aimed. For the long-term accuracy, some absolute calibration method must be foreseen, since one cannot guarantee that the instrument remains stable forever (earthquakes, failures, instrument changes, etc.).

The flux from the simultaneous reference is, regardless of its type, close to constant with time, while the flux from the astronomical object varies with time due to changing astroclimatic conditions. The consequence is that the Mean Time of Exposure *MTE*, as described in Section 6.5.11, is different for the target and the simultaneous reference spectrum. Thus, the drift measured by the reference spectrum might be slightly different than the drift suffered by the target spectrum. To avoid this discrepancy we have to make sure that the *MTE* for target and reference are identical, at least on a time scale for which the spectrograph does not drift by more than 1 cm s^{-1}. If the reference flux is controlled in closed loop with the target flux measured by the exposure meter, it should be possible to keep the flux level of the reference perfectly proportional to the target flux. This can be achieved e.g. by adjusting a neutral-density filter wheel position. We can then expect that the *MTE* for the reference will be identical to the *MTE* for the scientific frame, at least at the level of photon noise and control accuracy. We think therefore that a 1 s accuracy on the reference *MTE* can be achieved easily, as will be shown later for the scientific spectrum. Thanks to the HARPS experience, it looks fully realistic to suppose that the spectrograph will remain stable at the time scale of 1 s.

The proposed solution of controlling the lamp flux shows in addition the advantage that the integrated flux of target and reference will always have constant ratio. One has only to adjust the proportionality such that the RV accuracy is limited by the *S/N* of the target spectrum. A negative side effect is that the integrated reference flux will change as a function of sky conditions, and therefore will not have the exact value as during the preceding calibration exposure. Using a ThAr lamp as spectral reference becomes more difficult, because of the great dynamic range of its emission features. A laser comb source or a stabilized Fabry-Perot absorption spectrum would be much more convenient with regard to this aspect.

In conclusion to this section, we would like to summarize some requirements to the instrument concerning its stability and the drift measurement.

1. The instrument and the detector should be made as stable as possible within a reasonable costs. The instrument should have fixed optical configuration and orientation. Temperature stabilization at 0.01 K level and vacuum operation below 10^{-4} mbar seems feasible and thus mandatory. Detector temperature stability of 1 mK or better should be a goal.
2. Since instrumental drifts at the 1 cm s^{-1} level cannot be avoided, we will need one simultaneous reference fiber per spectrograph or a comparable calibration scheme. The spectral reference source is ideally identical to that used for the wavelength calibration although not mandatory. The only requirement is that always the same spectral source is injected in the reference fiber, i.e. during the wavelength calibration *and* scientific exposures.
3. The flux level of the reference source must be controlled in closed loop with the target flux measured by the exposure meter, e.g. by adjusting a neutral density filter.

6.3.5 Detector pixel sampling

In an ideal world, pixel sampling, i.e. the amount of pixels per spectral and spatial element, has to be chosen as large as possible, since it would allow to “measure” the line profile in great detail and increase the dynamic range of the detector. This is however in conflict with very practical aspects, such as detector space (costs) and increase of read-out noise (RON). Since the detector space is one of the most cost and complexity-driving factors, it is necessary to reduce the pixel sampling to a minimum without loosing signal. The loss in dynamic range can be compensated by a fast read-out at low RON, which allows us to make relatively short exposures with small overhead times.

Simulations show that the extraction of the spectral (and radial-velocity) information is optimum if one samples the spectral element with 4 pixels/FWHM at least. Reducing the sampling below 3 pixels will “flatten” the spectral feature and reduce the information content. An effective spectral sampling between 3 and 4 pixels/FWHM should be aimed. The pixel sampling in spatial direction is not relevant for this aspects, although it enters the discussion of detector area, dynamic range and RON. A large range of value can be covered without influencing the velocity measurement accuracy, and therefore the spatial sampling should be left as free parameter for spectral format optimization.

6.3.6 Detector and detector-pixel geometry

The exact knowledge of the detector geometry is at the basis of the experiment. The experience with HARPS shows that it is possible to measure the position of one single spectral line, covering the full detector dynamic range, with an accuracy of 1 m s^{-1}. Since the dynamic range of one CODEX spectrograph is about 30 times larger than for HARPS (larger spatial sampling) we can expect to achieve a precision of the extracted pixel geometry determination of about 0.2 m s^{-1}. Reversing the problem we can state that the mean geometric position of one pixel relative to another can be determined with about the same accuracy. If we suppose the use of a perfect calibration source (maximum density of equal spectral lines covering each the full dynamic range of the detector, and with perfectly known wavelength) we can determine the full detector geometry in one single calibration exposure, and each pixel position would be known sufficiently precisely to allow determination of the scientific spectral line position falling on it with an accuracy of better than 0.2 m s^{-1}. This random line-position error would finally average out with the square root of the number of lines, such than we could expect to reach the required 1 cm^{-1} level using 1000 spectral lines.

An ideal spectral source is essential for the measurement of the detector and pixel geometry. Such a source could be delivered for example by the stabilized laser comb or any stabilized Fabry-Perot spectrum. We think therefore that no critical accuracy limitation is set by the detector and pixel-geometry imperfections. In laboratory measurements (sufficient flux and integration time) it would even be possible to determine the intra-pixel response of every individual pixel by slowly scanning in wavelength the spectral source (laser or Fabry-Perot) and recording the spectra at each position (super-sampling).

6.3.7 Detector temperature control

Detector temperature changes will impact the detector pixel scale and have an effect on the absolute stability. Such a “detector breathing” has already been observed on HARPS, for which we have measured a instrumental drift of typically 3 cm $s^{-1}mK^{-1}$. The simultaneous reference is able to precisely track these drifts, but, there might be an operation scenario for which no simultaneous reference is used and a good short-term stability required. Despite the fact that the HARPS detector design is not perfect, a good stability could already be reached (~ ±0.01 K). However, improvement can be made in the mechanical support of the detector and its temperature homogeneity and control, to compensate for example increased thermal load on the chip during readout. We think therefore that a short-term stability about 10 times better than HARPS can be reached.

6.3.8 Detector read out

6.3.8.1 QE, RON and Speed

Detector Quantum Efficiency QE must be ideally close to 100% while the Read-Out Noise (RON) must be as small as possible. RON depends however on speed, at least for CCDs, such that low RON requires longer read-out times and thus longer overheads. It is therefore suitable to foresee at least two read-out modes, the first optimized for bright objects, high *S/N* and short exposure times, the second for faint objects, low S/N and long exposure times. Primary objective is to keep the measurements limited by photon-noise, secondary objective is to reduce the overhead times.

6.3.8.2 Bias and gain

Absolute BIAS and gain values are not critical for the RV measurements, but must be optimized for the expected signals. In particular the gain has to be chosen in accordance with the read-out mode. High-frequency (read-out time scale) variations of BIAS and gain would reflect in higher RON and must be avoided. Long-term variations (from one exposure to the other, and longer) of the BIAS can be detected, measured on each frame on the overscan zone and removed. Long-term variations of the gain must be avoided, but cannot be distinguished from flux variations. Since they affect the whole spectrum at once, both BIAS and gain variation are not expected to have any impact on the velocity measurement.

6.3.8.3 CTE and MTF

Charge Transfer Efficiency CTE and Modulation Transfer Function cannot be assumed to be perfect, and at the level of 1 cm s^{-1} accuracy, they will affect the Instrumental Profile (IP) and thus the spectral line shape. Consequently, they can introduce systematic effects on the line position. From HARPS we know however that this effect is lower than 1 m s^{-1} in absolute terms (prior to calibration). Furthermore, possible IP changes are determined and accounted for by the wavelength calibration procedure. Of course, the condition is that the IP does not change its shape between the calibration exposure and the scientific exposure. However this condition is relaxed when using the simultaneous reference, since the reference spectrum would suffer the same IP changes as the object spectrum. Therefore, we have only to make sure that the IP does not change differentially for the object and the reference fiber. Since the spectra of both fibers are recorded on the same detector simultaneously, there is no reason to think that MTF or CTE changes would affect the IP of the fibers differentially. For the sake of highest intrinsic instrument stability we suggest, nevertheless, that special attention is paid when specifying the CTE and MTF stability for the chosen detector, and that specific efforts are put to characterize them in detail. The only suggestion we want to make here is to align the orders along the direction of higher CTE. We note that, even if other type of devices may become available in the future, having attractive features, they shall be tested properly in all their aspects before becoming useful for CODEX.

6.4 Calibrations

6.4.1 Flat-fielding

In case of an echelle spectrograph, one has to carry out high-S/N *spectral* flat-field exposures (spectrum of a “white’ source), since standard flat-fields would not reflect correctly the chromatic response of each pixel. As a general rule the individual (relative) pixel response must be determined at least with a S/N much higher than the highest possible S/N obtained in a scientific exposure. Summation of multiple exposures might be necessary. The most important question in that respect is the stability of the flat-field, i.e. the time scale after which possible relative response changes of neighboring pixels become significant compared to photon noise. These time scales must be long compared to the time necessary to perform a complete set of flat-field exposures, and at least as long as the longest scientific exposure including the required calibration set.

In principle, there is, to our knowledge, no physical reason why the response of one CCD pixel should change relatively to the other pixels (in contrast to general BIAS or gain changes), but this might depend on the specific detector and should be investigated further.

One optical effect, which could introduce severe limitations on the flat-field stability, is the CCD fringing. The magnitude of this effect depends on the optical layout (long F-number are particularly bad) and on the color. Already at S/N of few hundreds this effect starts to dominate the flat-field pattern. The data reduction can flat-field this pattern and correct for it, provided that it is stable in time.

Collier-Cameron et al (2002) have already demonstrated, that photon-noise limit can be obtained for exposures with integrated S/N up to 10'000, by applying special techniques to remove any kind of systematics affecting the series of spectra. As mentioned before, time independence must be assumed. Our suggestion is therefore to avoid fringing (which is already reduced considerably by using a fast camera optics) and to investigate the magnitude and time-stability of the residual pattern.

6.4.2 Wavelength calibration

Wavelength calibration has two purposes:

a) provide an absolute wavelength scale as zero reference of the Doppler-shift measurement
b) provide a list of spectral lines with known wavelength relation in order to define the precise detector and pixel geometry.

The wavelength calibration is performed prior to the scientific exposure. It defines the relation between wavelength and pixel at the time of calibration exposure. Because of possible small instrumental drift, the absolute reference may drift in the time between the calibration exposure and the scientific exposure, and it becomes necessary to measure this drift by using a second fiber, which is illuminated all the time with the stable wavelength reference source (see Section 5.6.3).

In HARPS, these objectives have been achieved using a ThAr hollow-cathode lamp for both, wavelength calibration (absolute reference and geometry) and drift measurement. The ThAr lamp provides many thousands stable spectral lines covering the entire visible wavelength domain and allows us to associate the pixel space precisely with the wavelength space. This technique has demonstrated to be not only equivalent but even superior as the self-calibrating technique also an long-term. As an example we show in Figure 6-6 the residuals of the velocity measurements to the fitted orbital curve for *all* extrasolar planets discovered and published after 2004. Despite all the prejudices, only HARPS with its ThAr has been able to reach effectively the 1 m s^{-1} precision level.

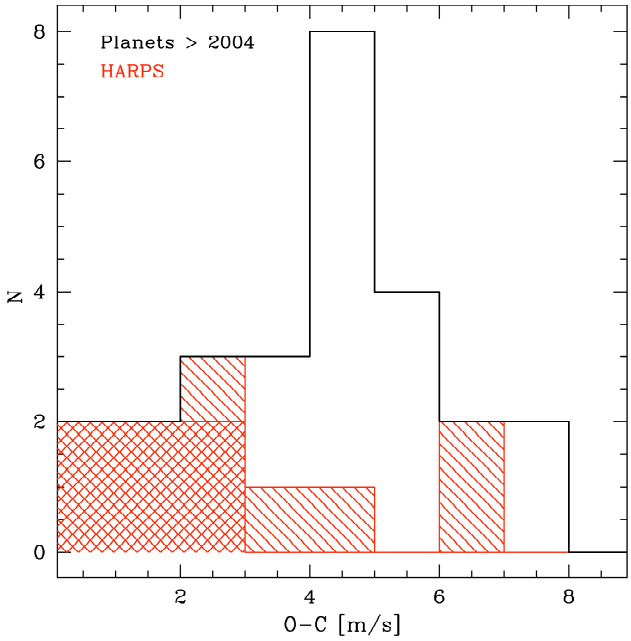

Figure 6-6: *Histogram of the of the residuals (O-C) on the orbits of all exoplanets detected since 2004 (start of HARPS operations). The planets discovered with HARPS are shown in red. The planets issued from the high-accuracy programme are represented by the cross-dashed surface.*

A study presently carried out by C. Lovis (private communications) of the Geneva Observatory shows, however, that the use of the ThAr is not yet optimum. In particular, the knowledge of the thorium and argon lines wavelength is not sufficiently precise and has to be improved. In addition, the argon lines depend strongly on the lamp pressure, and should therefore be avoided. C. Lovis has also demonstrated that some dependence on pressure and lamp current exists for the thorium lines. It seems that the present photon-noise limit of 10 cm s^{-1} can be reached using one single lamp and fixed operation conditions. It will however be very difficult to guarantee even this level of accuracy after replacing a lamp or changing its current.

Clearly, for an operation below the 10 cm s^{-1} accuracy level, more appropriate spectral references must be investigated. One of these, the laser comb, has been proposed by M. Murphy (IoA Cambridge) and is being studied by ESO. This kind of source provides a series of perfectly equidistant emission lines covering a large wavelength domain and perfectly stabilized at the 10^{-11} to 10^{-14} level. The advantages compared to the ThAr source are:

- Higher wavelength stability for absolute referencing
- Low dynamical range of the lines (all features have similar intensity)
- Perfectly known relation between the relative position of the emission features, which allows us to determine the detector and inter-pixel geometry with high accuracy
- Optimum Doppler-information density

Concerning this last point we are able to extrapolate, from the analysis performed by C. Lovis on thorium lines, that is will be possible to achieve a position accuracy of about 0.20 m s^{-1} per line on one single calibration exposure (photon limit). Considered the large amount of calibration lines, we expect that the 1 cm s^{-1} accuracy on the absolute zero-point reference can be reached already in one single calibration exposure.

Some disadvantages have also been identified for the laser comb solution, however. For example the laser lines do not show equal intensity, and the relative intensity might even change in times. As well, present system posses a line density which is too high to be resolved by a spectrograph with even R = 150'000. These problems could be avoided by using a simple Fabry-Perot illuminated in "white" light, provided that a sufficiently high stability can be guaranteed. In our opinion, this kind of solution should be considered as seriously as the laser comb.

Finally, we describe the characteristics for the ideal calibration source, which shall be converted into technical requirement:

1. The calibration source must cover the full wavelength domain of the spectrograph.
2. The line position and shape stability of all lines is better than 10^{-11} over the instrument life-time.
3. The lines are not resolved by the spectrograph, since otherwise information is lost, respectively we do not take full advantage of the spectral resolution of the instrument.
4. The line distance is perfectly stable (at the level of 10^{-11}) and ideally constant in $\Delta\lambda/\lambda$.
5. The line distance must be minimum 2 and maximum 3 FWHMs of the spectrograph IP.
6. No blends in the spectrum (separation between any two lines > 2 FWHM of the IP)
7. The relative intensity of any neighboring lines must be stable at 10% over time.
8. The dynamic range of line intensities over one order must be smaller than a factor 2.
9. The dynamic range of line intensities over the full spectral range of the spectrograph must be smaller than a factor 4.

Since line intensities can be included in the calibration model, the three last points are not strong requirements but for the moment rather a wish list. Data reduction and wavelength calibration will be the easier the more stable and homogeneous the line intensities will be. Precise numbers must be developed further.

6.4.3 Sky and atmosphere background correction

As mentioned in section 6.3.1.2, only background with significant spectral features is potentially dangerous for the velocity measurement. Depending on the ratio of line intensity of background and target, it might be useful, or even necessary, to determine the sky spectrum independently. For that purpose one could foresee one or more independent fibers, which, however, will consume a considerable amount of detector space and increase the total costs. If the relative brightness of the background can be kept low (ideally $\Delta m \geq 10$), no such correction is needed. We want finally suggest here that this domain should to be explored further, e.g. by direct measurements of the sky with the VLT, and simulate the possible impact of realistic background spectra on the synthetic scientific spectra.

6.5 Data-reduction aspects

In the following we shall very quickly review the possible data reduction steps and identify, whenever the case, critical aspects and resulting requirements.

6.5.1 Bias correction

The real BIAS can be directly measured on the overscan zone of each detector frame. Experience with HARPS has shown that the measured value can be subtracted directly detector-line by detector-line from the frame. The overscan zone can be chosen sufficient wide and can be integrated in order to avoid that noise is added by the subtraction. This step is not critical for the Doppler measurement.

6.5.2 Dark correction

Dark correction is only important for precise spectroscopic studies. Given the low level of dark current and the high measurement precision of it, we do not foresee any critical aspect or impact on the velocity measurement.

6.5.3 Localization

The quality of the order localization (position and shape) is very high and thus non critical, provided that sufficient flux is available in each order. The only problem encountered in HARPS with regards to this aspect

is that both the flux of white lamp (tungsten or xenon) and the instrument efficiency decrease considerably towards the blue wavelength range, resulting in low calibration flux in this wavelength region. Therefore, an adequate combination of flat-field source and filters must be found to ensure a more or less flat response.

6.5.4 Order extraction

The extraction of the echelle orders can be performed by means of various algorithms, e.g by simple pixel summation in spatial direction, or using the Horne algorithm for optimum (flux-weighted) extraction. The latter is particularly efficient for cosmics correction, but requires the knowledge of the expected order shape in spatial direction, which in addition must remain stable in time. Since one single order is composed of several optical fibers aligned along a “slit” at the entrance of the spectrograph, and since seeing effects make vary the flux in each fiber, one will have to expect the order shape to vary. A second effect is that the flux “seen” by the different pixels varies, and that systematic effects introduced by a specific pixel are weighted differently from one exposure to the other. The data reduction would hardly be able to work optimally under these conditions. Such flux changes should therefore be avoided. Several technical solutions exist. Simple examples are shown in **Error! Reference source not found.**, assuming the use of circular fibers fed with hexagonal lenslets. The use of rectangular-shaped fibers or light pipes should also be considered, and even a combination of several solutions is possible. A detailed solution should be studied in the frame of the fiber-scrambler developments, which have already been identified as one main critical aspects of the presented design.

We should mention here that a uniform and stable intensity distribution over the slit area has also two additional advantages: The first is that pixel binning can be performed in spatial direction without losing any information. The second is that only one exposure meter would be needed per spectrograph.

Finally we have to mention the problem of slit-image direction tilt. Ideally, the slit is aligned parallel to one of the pixel axis. Even if this cannot be perfectly achieved, a) the residual effect on the radial-velocity measurement is small and constant in time, and b) it would be possible to model the slit direction as a function of the position on the echelle order, and thus take into account this effect during order extraction. At present, no further details can be provided on this aspect, which should be subject of specific investigations.

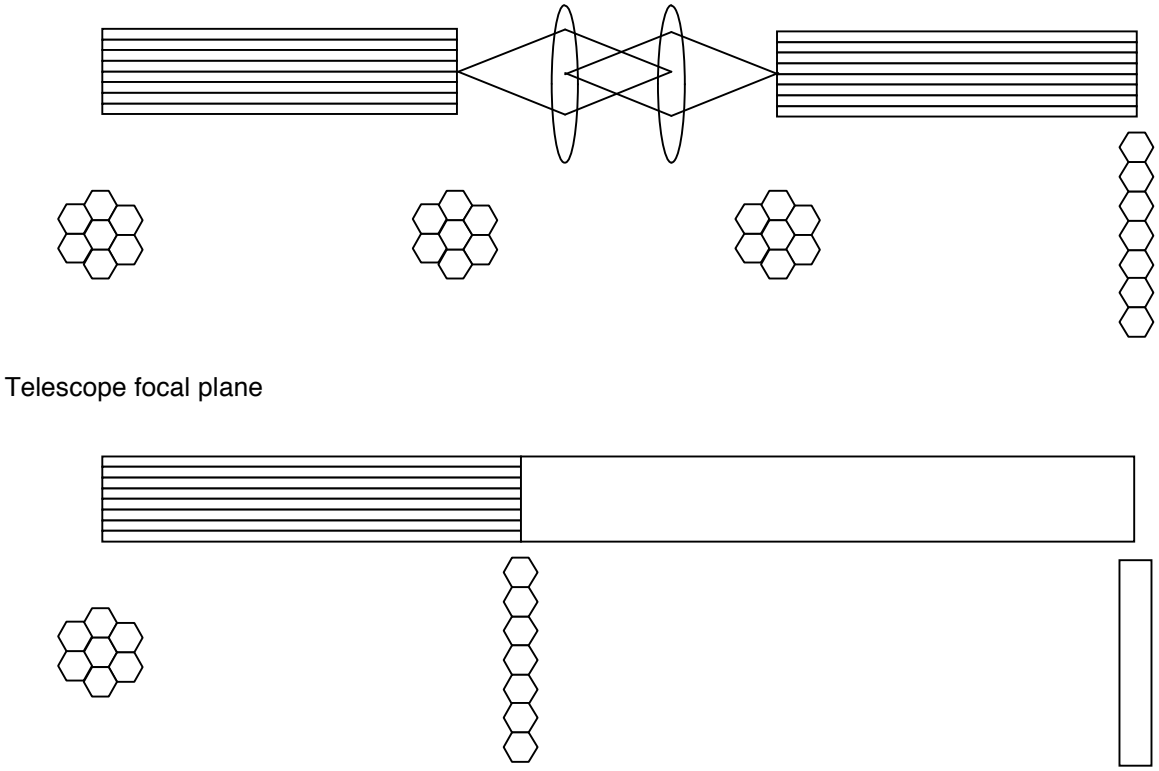

Figure 6-7: *Examples for solutions to ensuring homogeneous flux distribution and stable shape of the entrance slit. The upper example is a conventional symmetrical double scrambler as used for HARPS, but with scale factor 1 between far and near-field images. This solution has the advantage, besides redistributing the flux of one fiber over all fibers, to perform also exchange of far and near field. The disadvantage might be a small efficiency loss, because of imperfect filling factor. The second solution is the simple use of a light pipe. All the fibers coming from the telescope are glued on one end of the pipe. The other end of the pipe delivers then a rectangular slit, placed at the spectrograph entrance, with uniform intensity distribution***.***

6.5.5 Spectral flat fielding

For the spectral flat-fielding the same requirements apply as for the localization described in a previous section. We shall only add that the flux must be maximized in order to obtain the high S/N in short exposures, and that these frames have to be photon-noise limited. Varying flat-field response must be avoided at all costs.

Flat-fielding is performed routinely and without any major difficulty by the HARPS data-reduction pipeline. However, high S/N frames will require a different kind of approach not yet experience with HARPS. Specific high S/N observation and reduction approach must thus be developed for CODEX.

6.5.6 Cosmics correction

Cosmic correction is particular critical for long exposures at low S/N. If not removed, the cosmics would produce an error by many orders of magnitude larger than the signal to be measured. Since cosmics cannot be avoided completely, they have to be corrected in the data-reduction pipeline. A first step of cosmics correction is carried out within the optimum extraction algorithm (Horne). This algorithm applies particularly well to our case because of the large spatial width of the spectral orders. A second, very efficient “cleaning”

can be performed on multiple exposures, by building up an average and high S/N spectrum, and by removing the cosmics on the single spectra by comparison with the average spectrum.

6.5.7 Sky background correction

Because of lack of experience, we are not able to report any specific technique to correct for sky and instrument background (if significant and containing spectral features). Such a correction would aim at reducing the impact of this background, in terms of velocity measurement, below the 1 cm s^{-1} level. The currently proposed strategy is to avoid that kind of signal by adequate observation strategy. We are skeptical that an a posteriori correction can be carried out.

6.5.8 Wavelength calibration

The main difficulty of the present wavelength calibration algorithm in HARPS is to consider correctly and remove the effects of the large spectral line dynamical range and the many blends of the ThAr reference. Assuming a “perfect” spectral reference as described in Section 6.4.2, the calibration procedures reduces itself to the following (simple) steps on the extracted calibration frame:

a) Detect the spectral lines
b) Fit the lines parameters (position, amplitude, width) in the pixel scale x
c) Transform the pure (and abstract) pixel coordinates x of the frame into an effective (physical) position x’ of the line. This correction takes into account the detector and the pixel geometry. This geometry can be determined for the specific detector, e.g. during commissioning, provided that the pixel shape does not change in time (a time-dependent stretch or geometry change of the whole detector with low spatial frequencies is removed by the wavelength calibration). Slow wavelength scanning of the calibration source (laser, Fabry-Perot) could even be used to scan the intra-pixel response.
d) Identify the lines and assign an absolute wavelength according to a predefined table
e) Fit the relation $\lambda(x')$ using all the spectral line positions and wavelengths

Once the relation $\lambda(x')$ is known, it can be applied to all the following scientific spectra until a new calibration is performed. Note that for any frame the pixel position correction has to be performed *before* applying the wavelength calibration.

We have to point out that this calibration is as simple as described, as long as the wavelength reference is stable and fulfills the criteria described in Section 6.4.2. Any departure from these criteria (as for example the existence of line blends) will make the wavelength procedure much more complex and its quality less predictable.

Another important aspect to be highlighted is the importance of spectral resolution. Indeed, although spectral resolution might not contribute at increasing the measurement precision of the scientific target (e.g on the Ly-alpha forest), it remains of fundamental importance for the calibration procedure

6.5.9 RV extraction

Various ways of extracting the Doppler information from a spectrum are described in Section 6.6 and will not be discussed here.

6.5.10 Instrumental drift correction (non-Doppler drifts)

The instrumental drift is measured using the algorithm described in Bouchy et al. (2001). This simple and fast algorithm provides a direct measurement of the instrument drift expressed in Doppler shift and to be subtracted directly from the target velocity measured in the instrument rest frame before transformation into

the solar-system barycenter. This algorithm has proven to deliver fully photon-noise limited drift measurement at least to the level of 6 cm s^{-1}. At present, this drift measurement is averaged over the full wavelength domain (algorithm applied to the whole spectral domain at once). In principle, this use of the algorithm assumes that all instrumental drifts induce a Doppler-like shift of the spectrum (i.e. constant $\Delta\lambda/\lambda$). This is of course not the case for example for thermo-mechanical CCD drifts. To first order, it can be assumed however that the non-linear part averages out. Nevertheless, Bouchy's algorithm is easily improved to perform "local" drift measurement, i.e. determine and correct a drift value for small wavelength chunks independently.

6.5.11 Transformation of spectroscopic line shifts to the solar-system barycenter

The aim of this chapter is to describe the transformation of a spectroscopic shift z_{obs} measured by an Earth-bound observer to the corresponding barycentric shift z_B that would be measured by an observer at rest relative to the Solar System barycenter (SSB) and at zero gravitational potential.

In the frame of CODEX, the key problem is to know to which precision the transformation can be computed and what are the main factors limiting the accuracy. We emphasize that this chapter only discusses physical effects within the Solar System. In particular, movements of the SSB relative to the Galactic center and the Local group of galaxies are not considered here.

The general formula connecting observed and barycentric shifts is given by (Lindegren & Dravins 2003)

Eq. 2

$$1 + z_B = (1 + z_{obs}) \cdot \left(1 - \frac{\Phi_{obs}}{c^2} - \frac{\left|\vec{v}_{obs}\right|^2}{2c^2}\right)^{-1} \cdot \left(1 + \frac{\vec{k} \cdot \vec{v}_{obs}}{c}\right)$$

where

Φ_{obs} : gravitational potential at observer's location

$\vec{v}_{obs}$: velocity vector of the observer relative to the SSB

$\vec{k}$ ` : unit vector pointing from the observer to the target

Table 2: Sensitivity matrix of the accuracy of the barycentric correction with regard to their input parameters

Parameter	Induced error on the correction [cm s^{-1}]	Comment
Earth orbital velocity - *Solar system ephemerides*	 < 0.1	 JPL DE405
Earth rotation - *Geoid shape* - *Observatory coordinates* - *Observatory altitude* - *Precession/nutation corrections*	 ~ 0.5 < 0.1 < 0.1 < 0.1	 Any location in atm. along photon path may be chosen
Target coordinates - *RA and DEC* - *Proper motion* - *Parallax*	 ? ~ 0 ~ 0	 70 mas → 1 cm s^{-1} negligible negligible
Relativistic corrections - *Local gravitational potential*	 < 0.1	
Timing - *Flux-weighted date of observation*	 ?	 0.6 s → 1 cm s^{-1}

Table 2 lists the relevant input data needed to compute the transformation along with the accuracy to which they are presently known, expressed in velocity units. It can be remarked that already now the mm level of this correction can be reached. Nevertheless, two resulting requirements have to be pointed out here: First, we need to know the source coordinates with an accuracy of at least 70 mas, otherwise varying systematic errors on the line of sight and thus on the braycentric correction will be introduced. Second, the measurement time has to be known with an accuracy of better than 0.6 s. For an exposure of finite duration (typically minutes) this moment is not precisely defined, in particular at varying astroclimatic conditions producing flux variations. The Mean Time of the Exposure *MTE* is therefore not simply the arithmetic mean of the start time *TS* and end time *TS* + T_{exp}, but must be computed correspondingly to the formula

Eq. 3
$$MTE = TS + \frac{\int_0^{T_{\exp}} t \cdot f(t)dt}{\int_0^{T_{\exp}} f(t)dt} \approx TS + \frac{\sum_{i=0}^{N} \frac{T_{\exp}}{N} \cdot i \cdot f_{i,\Delta t}}{\sum_{i=0}^{N} f_{i,\Delta t}} = TS + \frac{\sum_{i=0}^{N(T_{\exp},\Delta t)} \Delta t \cdot i \cdot f_{i,\Delta t}}{\sum_{i=0}^{N(T_{\exp},\Delta t)} f_{i,\Delta t}},$$

where $f(t)$ is the flux measured at the time *t*. It becomes here evident that the stellar flux must be recorded with sufficient accuracy and resolution as a function of time. The second part of the equation just reformulates the formula assuming a discrete time resolution Δt and a total exposure time T_{exp}. *N* is the number of Δt-samples recorded during T_{exp}, and $f_{i,\Delta t}$ is the number of photon counts recorded in the bin *i* of duration Δt.

The goal of the following paragraph is to estimate whether we will be able to determine the *MTE* with sufficient accuracy, i.e. of the order of 0.6 s. To do so, we scale the count rate from the HARPS exposure meter to the case of CODEX. We obtain the values given in Table 3 with the counting rate *f* to be approximated by the formula $f = 21'600 \cdot 2.514^{(17.5-m_v)}$ cps. Since the typical photomultiplier noise is lower than 20 cps we assume here photon-noise limited measurements up to 23rd magnitude. Using the last part of the previous equation and assuming approximately constant flux samples $f_{i,\Delta t} \approx f_{\Delta t}$ (50% variations can be afforded), we can write the error for the *MTE* as follows

Eq. 4
$$\varepsilon_{MTE}^2 \approx \frac{\sum_{i=0}^{N(T_{\exp},\Delta t)} \Delta t^2 \cdot i^2 \cdot \varepsilon_f^2}{N^2 \cdot f_{\Delta t}^2} \approx \frac{\Delta t^2 \cdot N^3 \cdot f_{\Delta t}}{3N^2 \cdot f_{\Delta t}^2} = \frac{\Delta t \cdot T_{\exp}}{3 f_{\Delta t}} = \frac{T_{\exp}}{3f}.$$

In the last equation we have used the relation $f = f_{\Delta t} / \Delta t$, where *f* is simply the count rate per unit time. We deduce that for a given error ε_{MTE} the exposure time should not exceed $T_{\exp} < 3f \cdot \varepsilon_{MTE}^2$. We have to note that even in the case where we reach this maximum allowed exposure time, the RV accuracy obtained on one single frame can never reach the 1 cm s^{-1} (see previous sections). To illustrate that, lets fix the exposure

time to its longest possible value, i.e. one night or 36'000 s. Then, for magnitude 17, the obtained *MTE* accuracy corresponds to about 1 cms^{-1}, while the velocity measurement accuracy is of "only 17 cms^{-1}. We can generalize this relation by using Eq. 1 and Eq. 4 to compare the errors produced on the velocity measurement by the photon noise ε_{RV}^{SNR} on one hand, and by the error on the *MTE* ε_{RV}^{MTE} on the other:

Eq. 5

$$\frac{\varepsilon_{RV}^{SNR}}{\varepsilon_{RV}^{MTE}} = \frac{1\ \mathrm{cm\ s^{-1}} \cdot \dfrac{13600}{621 \cdot \sqrt{(T_{\exp}/36000\mathrm{s}) \cdot 2.514^{(17.5-\mathrm{m_v})}}}}{1\ \mathrm{cm\ s^{-1}} \cdot \dfrac{\sqrt{T_{\exp}/(3 \cdot 21600 \cdot 2.514^{(17.5-\mathrm{m_v})}\ \mathrm{cps})}}{0.6\ \mathrm{s}}} \approx \frac{635000\ \mathrm{s}}{T_{\exp}\ [\mathrm{s}]}$$

Even for the longest possible exposure time of about one night, this ratio remains always above 10, and gets even greater for shorter exposure times. Thus, we have always the situation where $\varepsilon_{RV}^{SNR} >> \varepsilon_{RV}^{MTE}$, where the final accuracy is not limited by the MTE accuracy. It is interesting to note that, because of Eq. 5, the radial-velocity error is *always* dominated by photon noise, independently of the magnitude and up to T_{exp} = 635'000 s. In order to avoid any possible systematic effect, we can, nevertheless, restrict the exposure time to the maximum allowed time, which still would guarantee an *MTE*-induced error smaller than 1 cm s^{-1}.

Source magnitude	**PMT count rate [cps]**	**Max. T_{exp} [s] for 0.6 s error on *MTE* (1 cms^{-1})**
m_v = 13	1'368'000	< 1'500'000
m_v = 15	216'000	< 237'000
m_v = 17	34'200	< 37'500
m_v = 19	5'400	< 5'960
m_v = 21	870	< 939

Table 3: *Expected CODEX exposure-meter count rate assuming a 100-m telescope and that 1% of the source light falls on the photomultiplier (PMT). The third column indicates the maximum allowed exposure time if we want determine the MTE at a level corresponding to better than 1 cm s^{-1}.*

We conclude that the required *MTE* can be reached and that the RV-measurement will never be limited by this parameter. We shall however issue following recommendations:

1. The object flux must be recorded precisely (photon-noise limited) and should not be contaminated by any external source (e.g. calibration source).
2. If the several field channels might suffer significantly different flux variations (e.g. when using a lenslet array on fiber bundle in the telescope's focal plane), one should monitor the flux of these channels independently. Note that in that case the maximum allowed exposure time is reduced approximately by the square root of the number of channels.
3. A possible exposure meter must cover the same wavelength range and "see" the same time-dependent object flux as the spectrograph. The best solution would of course be the use of a photon-counting scientific detector.
4. The sampling time Δt should be of the order of 1 s and *absolute* timing accuracy must be of the same order (~ 0.1 s).
5. All f_i data must be recorded (not only the *MTE*), in order to allow reconstruction and consider correctly also second order variations of the projected Earth's velocity, if necessary.
6. Nevertheless, the exposures should not be much longer than minutes to tens of minutes, in order to avoid complicate correction algorithms, too strong spectrograph drifts during the exposure time, and other (unexpected) second-order errors.

6.5.12 Correction of the solar acceleration in the galaxy

As seen , e.g. in Appendix 1 of section 3, galactic accelerations may be of the same order of the Cosmic signal that CODEX aims to detect. This applies also to the motion of the Sun in our Galaxy and to the acceleration induced by it, which can be estimated of the order of 0.6 cmsec^{-1}/yr. In principle, since the acceleration is along the galactic plane and will give a term varying with the galactic coordinates, it could be

measured by CODEX itself by choosing properly the targets distributed in the sky. While we shall distribute the objects in the sky in any case to monitor possible systematic effects, for this specific purpose the best answer will be provided by the GAIA mission. GAIA will indeed require this measurement, and by observing hundreds of thousand of QSOs it will be able to determine the solar acceleration in the Galaxy with an accuracy of better than 0.5 mm sec^{-1}/yr, (cf. GAIA Concept and Technology Report Study, ESA 2000 pages 110-115) that is about 10 times higher than the value itself and almost one order of magnitude more precise that the cosmic measurement. CODEX will be beautifully complemented by the superb performances of the ESA satellite.

6.6 Velocity extraction and analysis

6.6.1 Conventional approaches

There are currently in common use several approaches to the problem of extracting radial-velocity information from individual spectra:

- *Direct fit*: a parametrized functional shape of the spectrum is assumed, and its parameters are optimized to fit the observed spectrum. One of the parameters is the desired Doppler shift.
- *Cross-correlation*: The observed spectrum is cross-correlated against a 'template' spectrum. The template may be a simulation or an empirically observed spectrum. It may be a real-valued function of the wavelength (Tonry & Davis 1979), or a binary 0/1 mask (Baranne et al. 1996).
- *Fourier-domain analysis*: shift is sought for in the Fourier domain, where the shift is detected through analysis of the Fourier-transformed data (Chelli 2000).
- *'Optimal weighting procedure'*, where a velocity estimate is extracted from each individual pixel, and then averaged to produce a global velocity estimate (Bouchy et al. 2001).

6.6.2 Specific Challenges Ahead

CODEX has several specific features that the chosen technique will have to deal with:

- *Small effect: the Doppler-shift variation, over a period of several years, is unprecedently very small – a few orders of magnitude smaller than a pixel.*
- *High S/N: the S/N is assumed to be very high (in order to achieve the required precision).*
- *'Stretching': the Doppler shift is expected to vary among different spectral features, i.e., as a function of the wavelength ('stretching').*
- *Specificity: the relevant spectral features (the Ly Forest and the metal lines) are empirical and highly specific for the studied object.*
- *Blending: Ly-Forest features may be masked and blended with sharp metal lines associated with different redshifts.*

6.6.3 Suggested approach

The 'stretching', the specificity and the blending render all the current approaches insufficient to yield the desired output. Cross-Correlation, Fourier-domain analysis and the optimal weighting procedure are tailored for the simple case where the spectrum consists of one set of lines who undergo a single redshift.

In the field of double-lined spectroscopic binary stars several techniques emerged in order to deal with composite spectra. These are

- *Spectral Disentangling (Hadrava 2004)*
- *Tomography (Gies 2004)*
- *TODCOR (Zucker 2004)*

Basically they all rely on the same principles, applying some form of direct fit to the observed spectra, with different assumptions regarding prior knowledge. TODCOR assumes that the individual spectra are known in

advance, and only the redshifts have to be extracted. Tomography assumes that the redshifts are known in order to disentangle the unknown spectra. Spectral disentangling assumes neither the redshifts nor the spectra, but it practically relies heavily on good initial guesses for the optimization.

It seems that the best approach would be to generalize the case of the composite spectra of double-lined spectroscopic binaries to the case of the QSO spectra. The generalization will have to deal with two issues:

- *Dimensionality: currently, the techniques mentioned above analyze spectra of binary stars. Thus there are only two sets of spectral lines that have to be disentangled. Cases of triple and quadruple stars were already analyzed by simple generalizations of those techinques, but we have to seek ways to analyze efficiently the much higher dimensionality of the QSO spectra.*
- *The composite spectra in the case of binary stars are formed by simple addition: each photon arrives from one of the components of the binary star and the final measured flux is simply the sum of the two individual fluxes. In QSO spectra the combination of the individual features is multiplicative, since the various components contribute to the absorption of the radiation from a single source of radiation. This may be easily described by analyzing the logarithm of the fluxes instead of the fluxes themselves, but more work is needed in order to characterize this approach.*

Tomography and Spectral Disentangling as well as the latest version of TODCOR (Zucker 2003), are meant to analyze sets of spectra, in the context of orbital solution, i.e. time-varying redshift. This approach is also suited to the problem at hand, since the cosmic acceleration may probably be modeled as time varying redshift even more easily than a binary orbit. Thus, simultaneous analysis of multiple spectra measured along several years may provide better chances to detect an effect that may be undetectable with a single spectrum (Collier-Cameron et al. 2002).

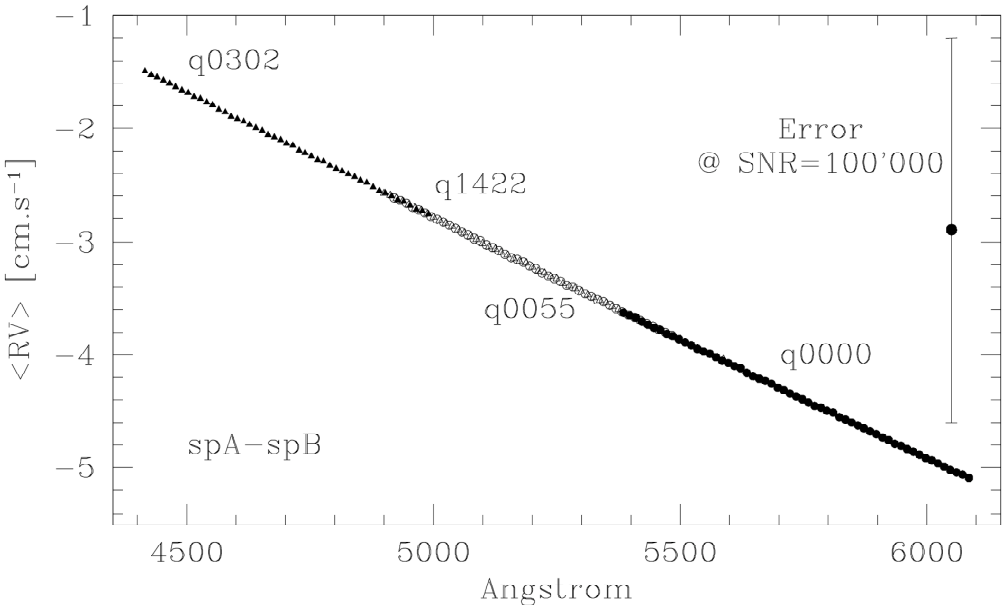

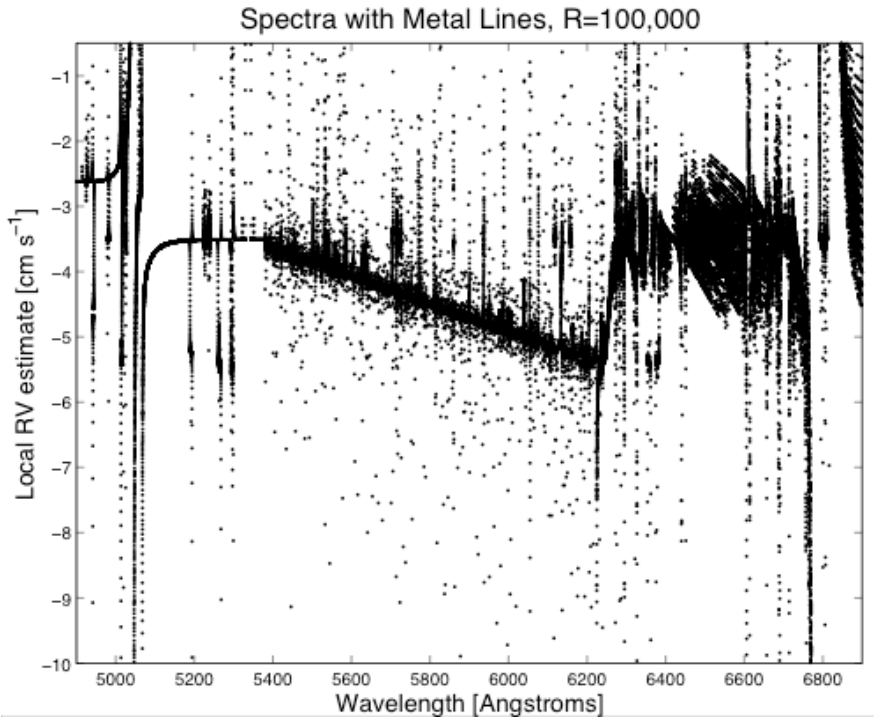

Figure 6-7: *Velocity variation between two epoch of the simulated spectra computed for small wavelength chunks individually using the optimum-weight approach (Bouchy et al., 2001). Top: Spectrum contains Ly-alpha forest only. Bottom: Metal lines have been included. They show different velocity variation compared to neighbouring Ly-alpha lines because of their association to a different redshift ż Line identification is required.*

6.7 Summary and suggestions from the performance analysis

In the present chapter we have tried to review all instrument and data-reduction aspects relevant to Doppler measurements of 1 cm s^{-1}-level precision. Reaching this precision is not an easy task, since it lies about 2 orders of magnitude below the performances reached routinely nowadays. We think, however, that there is no fundamental technical limit to reach this objective, provided that we put efforts in the development of some critical aspects described hereafter:

Guiding, centering and scrambling:
It is evident that the simultaneous reference, on which the instrument design is based on, delivers the required performance only if a change in fiber illumination does not cause a change in IP. It is therefore necessary to avoid, on one hand, any change in fiber illumination, and, on the other hand, ensure perfect scrambling. We suggest therefore to perform following developments:

a) Foresee in the instrument design an active and fast image correction (at least for focus, tip and tilt), which ensures that the star image is kept stable on the fiber entrance.
b) Investigate fiber scrambling, optical efficiency and focal ratio degradation as a function of fibre length, shape, material, connectors
c) Design, develop and test a “perfect” scrambling concept.
d) Prototyping

Wavelength calibration:
Wavelength calibration is probably one of the most limiting factors on HARPS. This calibration can be improved further, but the most serious limitations arise from the calibration source itself. These intrinsic limitations can be avoided by the use of a more adequate calibration source, and we are convinced that use of such a calibration source is mandatory for attaining the required precision level. The previously proposed laser comb is the most promising solution for our specific problem. We think therefore that development for the adaptation of this laser comb to our specific problem must be undertaken. The laser comb shows

however some disadvantages (e.g. line intensities, wavelength coverage) which are not present in a Fabry-Perot solution. The Fabry-Perot idea should therefore be investigated further. Prototyping of both solutions is unavoidable. Tests using HARPS should also be considered.

Finally, we would like to refer here to the various suggestions made in the preceding subsections for specifc improvements, investigations, or analysis.

6.8 References

- Baranne et al. 1996, A&AS, 119, 373
- Bouchy, F., Pepe, F. & Queloz, D. 2001, A&A, 374, 733
- Chelli, A. 2000, A&A, 358, L59
- Collier-Cameron, A. et al. 2002, MNRAS, 330, 187
- Connes, P. 1985, Ap&SS, 110, 211
- Gies, D. R. 2004, in *Spectroscopically and Spatially Resolving the Components of Close Binary Stars*, ed. R. W. Hilditch, H. Hensberge, & K. Pavlovski, ASP Conf. Ser., 318, 61
- Hadrava, P. 2004, in *Spectroscopically and Spatially Resolving the Components of Close Binary Stars*, ed. R. W. Hilditch, H. Hensberge, & K. Pavlovski, ASP Conf. Ser., 318, 86
- Lindegren, L. & Dravins, D. 2003, A&A, 401, 1185
- Pepe, F. et al. 2005, in preparation
- Tonry, J. & Davis, M. 1979, AJ, 84, 1511
- Zucker, S. 2003, MNRAS, 342, 1291
- Zucker, S. 2004, in *Spectroscopically and Spatially Resolving the Components of Close Binary Stars*, ed. R. W. Hilditch, H. Hensberge, & K. Pavlovski, ASP Conf. Ser., 318, 77

7. CODEX Feasibility, Costs and Planning

The technical sections have shown as the construction of CODEX is challenging, but no show-stopper exists to the feasibility of the project. Certainly a number of critical areas at present need to be clarified, some before PDR, others before FDR.

Thanks to its fairly well established design, it has been possible to prepare a broad development plan, shown in this section. We underline as the development and the use of a prototype is highly recommended, and the project plan includes therefore its development and construction.

In this whole section a 5-spectrograph cluster is considered, which, as explain in Chapter 5, corresponds to an aperture on the sky of 0.65 arcseconds for a 100 m. telescope or of 1 arcsecond for a 60 m. telescope

7.1 Feasibility

Critical areas to be sorted at latest at PDR:

1) Calibrations and Calibration Unit:

Understanding the best way of calibrating the observations and the instrument. Feasibility of the Frequency Comb Calibration Unit, or of an alternative method for improving calibration accuracy.

2) Fibre feed:
   a) Centering accuracy: even in presence of a scrambler, the requirement on centering are extremely demanding. Power of scrambling, effects produced by decentering in presence of seeing limited observations shall be studied and possibly prototyped for different solutions.
   b) Overall efficiency: If only fibres were used to bring the light from the focal plane to the CODEX slit, they were to be extremely long (about 300 meter). Over such a length, fibres are much less efficient than a coude' feed, especially in the Blue. While it is clear that the last part of the feed must be done with fibres for scrambling reasons, it is highly desirable that OWL is equipped with a kind of coude' feed to an underground stationary focus. Other type of fibres may require testing. All these aspects require clarification and tests.
   c) Light pipe

3) Being CODEX a seeing – limited instrument, the entrance aperture must be quite wide and the detector area correspondingly large. Current estimates for the overall silicon detector area reach up to 1 m^2. Regardless of how this area is split between separate cameras, with the actual costs of detectors at the level of 2-3 KE/cm^2, this voice could make the overall costs exploding. Ways of containing the detector costs shall be identified.

4) Fully realistic simulations, including the effects of sky and other source of noise; construction of a realistic and detailed 'mission plan' and observational strategy.

Critical areas to be tested before FDR

1) System Level: understand which are the limitations of the system, in particular in:
   a) Detector general characteristics, stability
   b) Mechanical stability, ability of recovering shifts
   c) Overall corrections during long exposures
   d) Light Injection in the spectrograph

   And their combination in the real observations.

2) Grating: a mosaic of two UVES gratings is required. One full grating shall be produced and tested to prove its feasibility and its mechanical stability.

3) CCD and cryogeny: show which level of stability can be reached for large detectors (or mosaics), this might be associated to a new continuous flow cryostat and should be prototyped.

4) Scientific applications: capability of eliminating stellar noise in the case of search for earth – size exo-planets

7.2 HW COSTS

HW costs have been divided in two main categories: Common Components indicate all components which will be common to all spectrographs, and whose cost will be largely independent of the number of units. Single Spectrograph Components indicate those components that will be cloned for the different units. Their cost is given for one unit.

Common Components:

COMPONENT	COST (KE)	Comments
Calibration Unit	450	
Acquisition-guiding system	350	
Fibre Fed (includes scrambler	350	
Transport & Insurance	450	
Integration & Test cost	500	
Travel & Miscellanea	700	
CODEX Lab and facilities	500	
TOTAL COMMON	3300	Includes 300K for prototype

Single Spectrograph Components:

COMPONENT	COST (KE)	Comments
Spectrograph Optics	1300	includes X-disperser
Echelle Grating	600	20x160 cm mosaic of 2 UVES echelles
Spectrograph Mechanics	400	Includes optical bench
Spectrograph Electronics	100	
Vacuum System	500	
Criogeny and CCDs	600	4 4Kx4K CCDs + Cryostat + Controller
TOTAL/Spectro	3500	

Grand TOTAL: 3500 KE/unit x 6 Units --→ 21000 + 3300 = **24300** KE
The sixth Unit being the prototype.
This estimate does not consider eventual savings coming from mass production (6 units). We may expect savings in the range of 10-15% of the single spectrograph cost, i.e. 2.-3 MEuro.
On the other hand the above cost estimate does not include contingencies. The HW costs should therefore be comprised between ~21 and 26.0 ME.

Breakdown of the HW Costs:
No preliminary enquiry has been done, but costs are quite realistic because they have been compared and scaled from other projects, in particular from UVES and HARPS, which have the closest characteristics (beam, vacuum vessel,) to CODEX.
The background of the costs estimate is detailed below.

Common Components Costs:

The cost of the common components include overall 300 KE for the calibration, acquisition, transport and fibre system of the VLT prototype.

a) Calibration Unit: A laser costs 160 KE, the rest is added as for a standard calibration unit. The prototype will use a laser developed under a separate project.
b) Transport and Insurance: this item will not be negligible; overall weight of the order of 40-50 Tons will be shipped and for a considerable insured value.
c) CODEX Laboratory: It is assumed that the OWL project will provide the laboratory with Service Connection Points, as well as the optical train up to the fibre input. While CODEX will provide the requirements for the Lab and the optical train, its realization shall remain with the OWL project. Additional costs will, nevertheless be required, to prepare the lab for CODEX, such as thermal control and air conditioning, rails for maintenance and special equipment.

Single Spectrograph Components Costs:

a) Optics: 2 times the price of the UVES optics, 5 times the cost of the HARPS optics; size of the collimator will be bigger, pupil slicer is a new feature.
b) Echelle: 2.5 the cost of a single 20x80 cm echelle; some extra cost must be added given the need of mosaicing and phasing the 2 UVES-type gratings.
c) Mechanics: Similar to UVES, overall size is comparable to UVES
d) Electronics: With a passive system, No major investment; lots of sensors, exposumeter. .
e) Vacuum Vessel: 4 times the price of HARPS; each CODEX unit will be larger than HARPS and vessel price will likely scale with volume (TBC)
f) Detector price: based on MUSE preliminary enquiry (present price for a 4Kx4K CCD: ~90 KE each)

If the prototype was just one of the units, **the overall cost of the prototype HW were estimated in 3500 + 300 : 3800 KE** . We note, however, that some of the R&D and industrial investments for the production of the other 5 units will have to be set upfront, and this will make the cost of the prototype effectively more expensive. One critical item, for instance will be the production of the gratings and crossdispersers; for which we estimate that **one additional ME should be added to the capital investments for the prototype.**

7.3 Project Plan and Schedule

The project will develop in the following phases:

7.3.1 Phase A

Goal: To set up a detailed project proposal, to carry out some preliminary tests, to identify sources of funds (for the prototype and to reach FDR) and individuate a Consortium suitable to complete the project.

The Phase A ends with a Review and a recommendation by STC to ESO management and Council.

Duration : 12 Months. + 3 months Review: ends **December 2006**

7.3.2 Preliminary Design Phase

Goal: Confirm results of R&D (cfr. Previous section), definition of the full CODEX project, preliminary design.

R&D: Results from Feeding System, Calibration Unit, Detector stability

Duration: 18 Months. Probably Optical FDR together with PDR or shortly afterwards.
PDR June 2008

7.3.3 Prototype Final Design Phase

Goal: Standard FDR for the VLT prototype

Duration: 12 months – **FDR Prototype June 09**
Optics procurement started in Jan 09

7.3.4 Prototype MAIT

Goal: Procurement, Integration and Tests in Europe of Prototype
Note that the development of certain components (e.g. data reduction SW) will be 'almost' final, in that it will not drastically change for the full CODEX instrument.

Duration: 18 Months - **PAE Prototype Dec2010**

7.3.5 Prototype Integration-Commissioning-Tests

Goal: Integration at telescope, Commissioning

Duration: 12 Months – **PAC Prototype December 2011**

7.3.6 Final Design Phase:

Goal: This phase is characterized by the final design of the whole CODEX. It is expected to last 3 years and it shall include all the experience gained by using and testing the prototype at the VLT. Optical FDR, optics procurement and procurement of other components in critical path (e.g. gratings, detectors) might start before FDR.

Duration: 36 months – **CODEX FDR Dec 2014**

7.3.7 CODEX MAIT

Goal: Procurement, Integration and Test of the 5 spectrographs. TBD if the work will be strictly sequential or, most likely, will run in parallel to gain time. The knowledge acquired with the prototype shall help to make this phase as automatic as possible.
Given the modularity of the instrument it might be decide also to ship it to the OWL observatory in parts.

Duration: 3 years – **CODEX PAE Dec 2017**

7.3.8 Integration, Commissioning at the OWL Observatory:

Duration: 18 months. **CODEX PAC June 2019**

7.4 Human Resources within ESO and the ESO Community

Even if the structure of the CODEX consortium is not yet known and it will be established during Phase A, we can already state that ESO and its community are extremely well equipped for building this experiment.

Thanks to the considerable experience developed in managing and executing large projects, very similar or larger than any single CODEX unit, all technical and managerial capabilities are available at ESO or in its community. Although system aspects should never be neglected, thanks to its modular concept, CODEX can be broken-down in its 6 subunits, each being smaller or comparable to typical VLT instruments.

The CODEX overall size is within a factor 2-3 comparable to large IInd generation VLT projects such as MUSE or K-MOS. 'Cloning' has been experienced with FORS, VIMOS and to a even larger extent (24 units) with MUSE.

The ESO detector group is engaged in comparable size projects (Omega Cam, MUSE).

ESO, and the ESO community (Geneve, Heidelberg, Padova, Munich Sternwarte, OHP) have developed a unique knowledge and expertise in fiber fed white pupil spectrographs from the extremely successful Delabre-Baranne concept with an impressive record of success and tailored to the highest accuracy in radial velocity measurements (UVES, FEROS, HARPS, GIRAFFE, VELUX, FOCES, SARG, CORELIE, plus all their copies and variations operated worldwide).

With HARPS, ESO and the Geneve Observatory have shown an example of instrument with end-to-end operations, where the user obtains the full data reduced with the highest accuracy from the pipeline. This point is of capital importance for CODEX and it is explicitly inserted in the project from the beginning. The use of an efficient archive and re-processing of the raw data is a must, and ESO is extremely well equipped for this task.

Manpower Estimate

Even without a detailed Work Break Down Structure, a broad estimate of the manpower required by the project is made. We have assumed:

a) ESO personnel: easy interfaces, no need for training, 40 Hs/week
b) Analogy with similar projects
c) Very limited used of internal workshop (e.g. most components built by industry on ESO design)
d) Existence of an OWL common SW, equivalent to the VLT SW
e) Does not include (as for all VLT instruments) DMD manpower

Phase	Manag/ System	Optics	Mech.	SW	Elect	DRS	Fibre Inc.R&D	Det	Integ.
Ph. A)	2	0.3	0.5	0.5		0.5	1.0	0.2	0.1
PDR	2	0.8	0.4	0.5	1.0	0.5	0.5	1.3	0.1
Prototype FDR	2	1.1	2.0	1.0	0.3	1.5	0.4	1.3	0.2
Prototype MAit	3	0.5	2.0	1.0	1.0	1.0	0.6	2.5	2.0
Prototype Comm.	1		0.2	0.5	0.2	1.0	0.1	0.3	0.5
Total up to end of Prototyp	**10**	**2.5**	**5.1**	**3.5**	**2.5**	**4.5**	**2.6**	**5.6**	**2.9**
FDR	6	0.5	1.0	1.0	0.5	1.5	0.5	1.3	2.1
MAIT	6	1.5	4.0	1.0	2.0	1.5	1.5	9	9.0
Int & Comm.	2		0.4	0.3	0.5	1.0	0.2	1.5	2.5
Total Main	**14**	**2.0**	**5.4**	**2.3**	**3.0**	**3.5**	**2.2**	**11.8**	**13.6**
Gran Total FTE	**24**	**4.5**	**10.5**	**5.8**	**5.5**	**8.0**	**4.8**	**17.4**	**16.5**

PDR and Full Prototype: **39.2 FTE**
FDR-PAE: **57.8 FTE**
TOTAL: **97.0 FTE**

The management/system box assumes the equivalent of two people, working part/fte or full/fte, depending on the project phases. In the detector it is assumed that NGC is used, and no controller development is required.
A few comparison numbers: both UVES and HARPS required about 30 FTEs. MUSE Detector system (same number of chips, 24 systems but no mosaic). manpower request is estimated in 13 FTEs. FTEs may be underestimated because of activities not included and because, given the long duration of the project, a 'minimum' threshold activity / person should be assumed, to insure continuity.

The project planning is summarized in Figure 7.1.

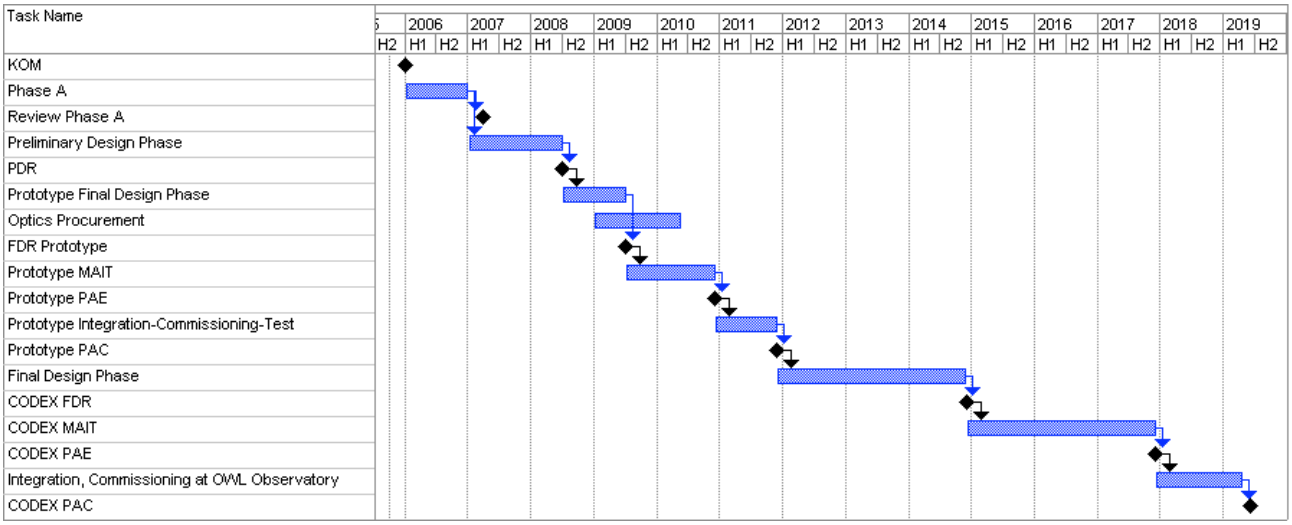

Figure 7.1: *Schematic project plan development for CODEX. Note that it includes the construction of a prototype for the VLT and its operations for three years during the Final Design Phase.*

APPENDIX 1 - Observing molecular absorption line systems with ALMA

1 Background

Molecular absorption occurs whenever the line of sight to a background quasar passes through a sufficiently dense molecular cloud. The molecular gas in nearby galaxies is strongly concentrated to the central regions, making the likelihood for absorption largest whenever the line of sight passes close to the center of an intervening galaxy. Molecular absorption in intervening galaxies can therefore be associated with gravitational lensing, with the absorption occurring in the lensing galaxy.

For molecular *absorption* the observable is the velocity integrated opacity $I_{\tau\nu} \propto N_{tot} T^{-1} \mu_0^2 (1 - e^{-h\nu/kT}) \approx (h\nu/k) N_{tot} \mu_0^2 T^{-2}$, where N_{tot} is the total column density of a given molecular species and μ_0 is the permanent dipole moment of the molecule. (Note: This expression is strictly speaking only true for linear molecules but represents a reasonable approximation for non-linear molecules as well).

The dependence on $(\mu_0/T)^2$means that the observability of molecular absorption lines increases with the strength of the permanent electric dipole moment and decreasing gas temperature. A situation which to a large extent is inverse to that of molecular emission. If multiple gas components are present in the line of sight, with equal column densities but characterized by different excitation temperatures, absorption will be most sensitive to the gas component with the lowest temperature. The dependence of the opacity on the permanent dipole moments also means that molecules much less abundant than CO can be as easily detectable. For instance, HCO^+ has an abundance about 5 x 10^{-4} smaller than that of CO, yet it is as easy, or easier, to detect in absorption as CO. This is primarily due to the much larger permanent electric dipole moment of HCO^+ compared to CO.

Absorption of molecular rotational lines have been observed in four systems at redshifts ranging between 0.25--0.89. The lines have velocity widths ranging from less than 1kms^{-1} to ~30 kms^{-1} and have been observed with standard equipment giving a velocity resolution of ~30 ms^{-1}. The center of the absorption line can, however, be determined with an accuracy much better than the actual velocity resolution (see Figure 1). Rotational molecular absorption lines thus has the potential to be probes of cosmic acceleration.

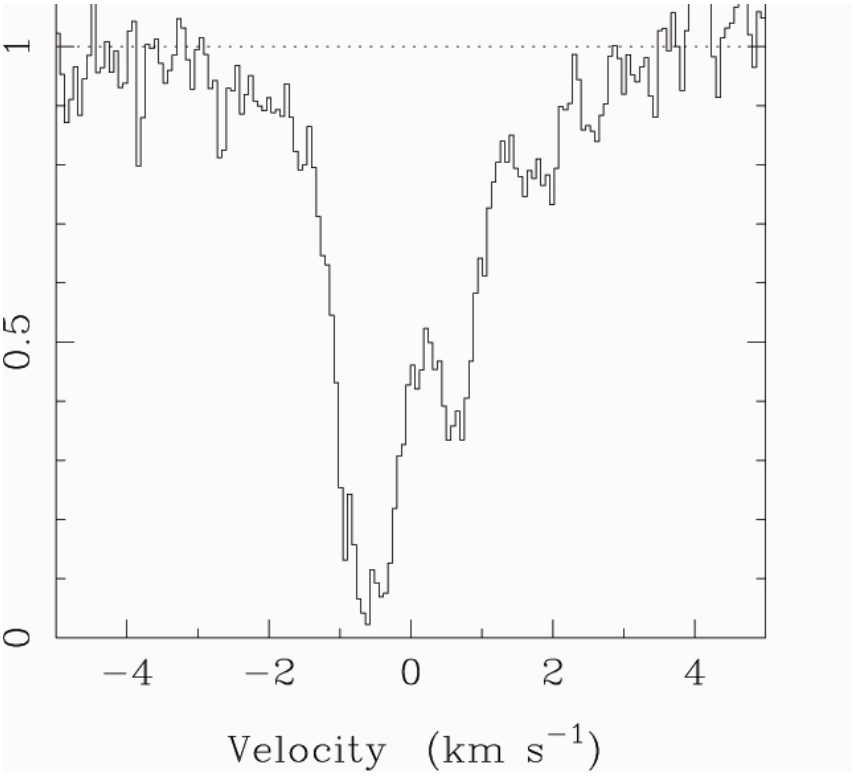

Figure 1: *A CO(0□1) absorption at z=0.24671 towards the radio source PKS1413+135. The velocity resolution is 60ms^{-1} and the velocity scale is heliocentric in the restframe of the absorbing gas. The continuum level has been normalized to unity.*

2 Observables and numerical values

In this section we present the formalism as well as numerical values of the effect of cosmic acceleration on the observables.

The observed frequency ν_{obs} of an object with restfrequency ν_{res} which is at rest in a comoving coordinate system is

$$\nu_{obs} = \frac{\nu_{res}}{1+z} \tag{1}$$

The change in frequency as a function of time, measured at time t_0 is thus

$$\left(\frac{d\nu_{obs}}{dt}\right)_{t=t_o} = -\frac{\nu_{res}}{(1+z)^2}\left(\frac{dz}{dt}\right)_{t=t_o} \tag{2}$$

where

$$\left(\frac{dz}{dt}\right)_{t=t_o} = \dot{z} = H_o\left(1+z-\sqrt{\Omega_m(1+z)^3+\Omega_k(1+z)^2+\Omega_\Lambda}\right) \tag{3}$$

Here we use:

$$\Omega_m = \frac{8\pi G}{3H_o^2}\rho_o,\ \Omega_k = -\frac{k}{R_o^2H_o^2},\ \Omega_\Lambda = \frac{\Lambda}{3H_o^2}, \tag{4}$$

describing the matter content (baryonic and non--baryonic), the curvature and, the cosmological constant, respectively.

In the following we will use $\nu_{res}=\nu$ for the rest-frequency, and ν_{obs} for the observed frequency at $t=t_0$. Using the above expression for ż we get

$$\left(\dot{\nu}_{obs}\right)_{t=t_o} = \frac{\nu_{obs}}{T_o}\left(1 - \frac{\sqrt{\Omega_m (1+z)^3 + \Omega_k (1+z)^2 + \Omega_\Lambda}}{1+z}\right), \quad (5)$$

Here we have used $T_0 = H^{-1}{}_0$ as a measure of time. T_0 has the numerical value T_0=13.04 h_{75}^{-1} ,Gyr (H_0=75h_{75} $kms^{-1}Mpc^{-1}$).

In Figure 2 $\left[\left(\frac{\dot{\nu}_{obs}}{\nu_{obs}}\right)_{t=t_0} T_0\right]$ Is shown as a function of redshift for four sets of Ω_m, Ω_k and Ω_Λ. In the case of a non-zero Λ term the observed rate of change will have an extremum at redshift z_{ext}

$$z_{ext} = \left(\frac{2\Omega_\Lambda}{\Omega_m}\right)^{1/3} - 1 \quad (6)$$

For Ω_m = 0.3 and Ω_Λ = 0.7, this occurs at z = 0.67 and for Ω_m = 0.15 and Ω_Λ = 0.85, this shifts to z = 1.25. This is where the cosmic acceleration will give the largest contribution to the observed rate of change of the frequency. The values depicted in the figures can easily be converted into Hz/year:

$$\left(\dot{\nu}_{obs}\right)_{t=t_o} = 7.7\left[\frac{\nu_{obs}}{100GHz}\right] f(z)(Hz/yr)$$

where f(z) is given by the lines in Figure 2. Hence, for the concordant cosmological model the maximum rate of change of the observed frequency due to cosmic acceleration will occur at z = 0.67 with an amplitude of 1.02 ν_{100} Hz/yr (ν_{100} is the observed frequency in units of 100 GHz), or 3.06 x 10^{-3} m/s/yr irrespective of the observed frequency. On a time scale of a few years, this is a factor ~ 10^4 smaller than the best velocity resolution achievable with present day instrumentation.

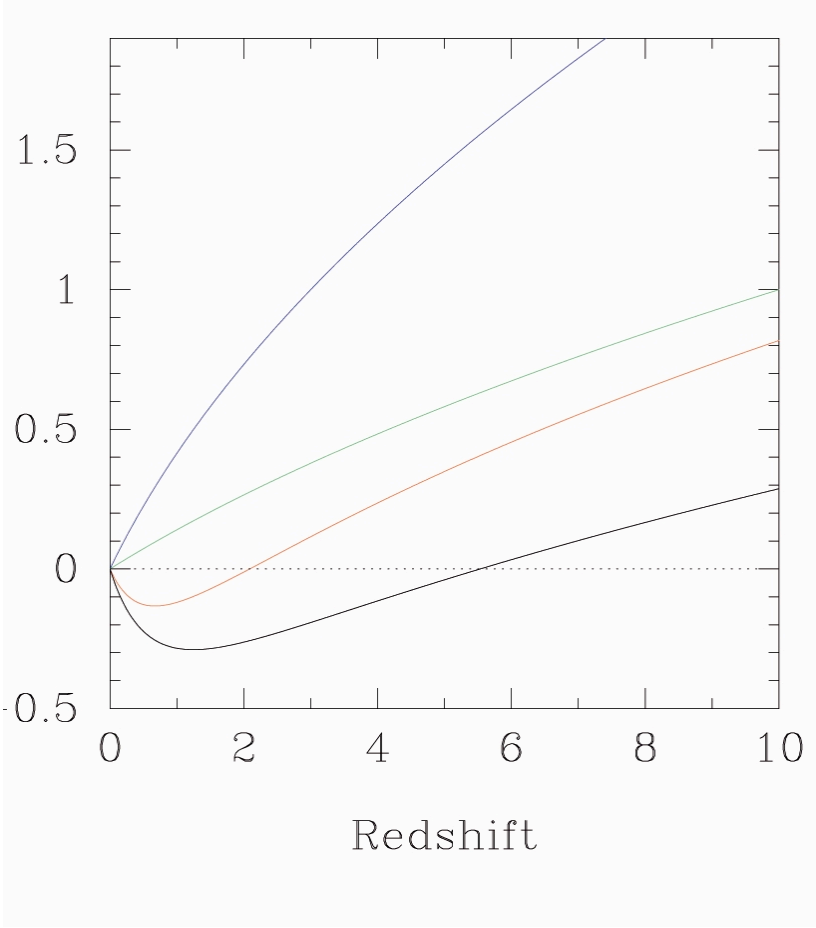

Figure 2: *The rate of change of the observed frequency $\dot{\nu}_{obs}$ times the ratio T_0/ν_{obs}; cosmic time and observed frequency, for 4 cosmological models:* ***Blue line*** *Matter dominated (Ω_m =1.0, Ω_k = 0.0, Ω_Λ =0.0),* ***Green line*** *(Ω_m = 0.3, Ω_k = 0.7, Ω_Λ = 0.0),* ***Red line*** *(Ω_m =0.3, Ω_k = 0.0, Ω_Λ = 0.7) and* ***Black line*** *(Ω_m = 0.15, Ω_k = 0.0, Ω_Λ = 0.85).*

3 Number of absorption line systems

A crucial parameter in using molecular absorption lines for a direct measurement of cosmic acceleration is the number of available and suitable systems. As mentioned above, there are four (possibly five) known molecular absorption line systems. These have all been detected by careful vetting of potential sources and not through an unbiased survey of a complete sample of radio continuum sources. The known number of molecular absorption line systems is therefore a lower limit to the actual number.

With its high sensitivity and wide instantaneous band width, ALMA is an excellent instrument for an unbiased survey of molecular absorption lines towards background radio-loud QSOs. There are two large unknowns in trying to estimate the number of systems that may be detected in such a survey: (1) the number of radio continuum sources available, and (2) the occurance of molecular absorption along the line--of--sight.

An estimate of the differential source counts at millimeter wavelengths can be done from detections and upper limits at millimeter wavelengths of sources selected at lower frequencies. From this one can derive the distribution of specrtal index and then extrapolate to higher frequencies and lower fluxes. This has been done by Holdaway & Owen (ALMA Memo 520) using data at 5, 8.4 and 90 GHz. The integrated source counts at 90 GHz are approximately N(>100 mJy) = 3.8 x 10^3, and N(>10 mJy) = 4.4 x 10^4 and N(>5 mJy) = 7.5 x 10^4, counting over the entire sky. For ALMA, we can use about 65-70% of these counts. A flux limit of 5 mJy is feasible but would result in somewhat lower quality absorption line profiles. We will therefore adopt a limit of 10 mJy. The number of available sources can easily be adjusted by a factor 1.7 if one would adopt a flux limit of 5 mJy, or by a factor ~0.7 for a flux of 20 mJy.

The number of these sources which will have molecular absorption along the line-of-sight is very uncertain. A rough estimate can be made from the number of detected sources (although this is drawn from a biased sample) and the estimated number of available continuum sources. Setting a continuum flux limit of 0.1-0.5 Jy for the already detected sample, the number of available sources are between 3800 and 500. Four molecular absorption line systems, found over ~65 % of the sky, gives an absorption fraction of 0.1--1.0 %, where the lower value has a higher weight due to the bias in the selection of the already detected absorption systems. Applying this to the estimated number of continuum sources available to ALMA at 90 GHz, we come up with 30-300 molecular absorption line systems detectable with background sources of flux densities S > 10 mJy. Again, the lower limit has a higher weight. Assuming that 50 molecular absorption line systems will be detected with ALMA, 5-10 of these will exhibit very narrow lines, again based on the biased known sample.

4 Caveats

4.1 Changes in the line--of-sight

There are three different effects in the line--of--sight (los) that can cause changes the shape and/or location of an absorption line.

(1) **Movement of the obscuring gas**.
Assuming that we are dealing with gas residing in a galaxy, the typical velocity perpendicular to the los can be ~300 km/s, which cause a shift in the position of the cloud of about 63 AU (Astronomical Units) per year, or 0.03 pc per 300 years. The observed size of substructure in the Galactic interstellar medium is less than ~2000 AU. Depending on the size of the background source, a different substructure of a molecular cloud can enter the los over a period of a few hundred years. However, absorption line measurements are biased towards excitationally cold gas, i.e. diffuse gas, which is less likely to show small scale gradients than are dense clumps.

(2) **Structural changes in the background continuum source**.

Flat--spectrum radio continuum sources are known to be variable on time scales of a few months. These variations are confined to the core and are believed to be associated with shocks propagating outwards along the inner part of the jet. The relativistic electrons quickly lose their energy and the spectral energy distribution (SED) of the jet becomes steeper further away from the core. The shift of the los due to such a propagating shock is unknown but could very well be of the order of a few tenths of a parsec. Hence, structural changes in the background source can cause a shift in the los which is greater than that caused by the intrinsic movement of the gas itself.

(3) **Changes in the physical conditions of the gas**.
The time scale for significant changes in the physical state of molecular gas (i.e. the excitation) is likely to be of less concern than the above two effects. The time scale for molecular gas to adjust to a change in the excitation conditions is essentially given by the inverse of the Einstein A-coefficient. For the most common molecules this time scale is between a few weeks to a year. The time scale for changes in the excitation conditions is, however, given by how fast shocks can propagate through the gas. The velocity dispersion in Galactic molecular gas is 6-10 km/s, and since this is much less than the rotational velocity of the gas, this is likely to be of little concern for measurements of the type discussed here.

4.2 Acceleration

We can express the rate of change of frequency due to cosmic acceleration (measured in ms^{-2}) by writing $\dot{\nu}/\nu$) c, where c is the speed of light in ms^{-1}. With 'ν_{obs} = 1 Hz/yr and ν_{obs} = 100 GHz the acceleration due to cosmic acceleration becomes 9.5 x 10^{-11} ms^{-2}.

In an order of magnitude estimation of the gravitational acceleration at large scales we can look at four scenarios, where the acceleration is simply evaluated as

$$a = -G\frac{M}{R^2} \qquad (7)$$

where G is the gravitational constant, R a `radius' encompassing a total mass M.

1. **Galaxy cluster** A galaxy residing in a rich cluster at a typical distance of 0.5 Mpc from the cluster center, where the mass enclosed by R is ≈ $10^{14}M_{\odot}$, will experience an acceleration of the order 10^{-11}-10^{-12} ms^{-2}. This is small in comparison with the acceleration caused by cosmic acceleration, but can become comparable if the galaxy is situated closer to the center of the cluster.

2. **Galaxy pair** For the typical separation of two galaxies in a loose group or pair we take the Milky Way and M31. The separation is 0.7Mpc and the galactic mass is set to 4 x 10^{11} $M_{\odot}$. This gives an acceleration of ~ 10^{-13} ms^{-2} and is clearly insignificant in comparison to the acceleration caused by cosmic acceleration.

3. **Galactic** An object in circular orbit in a disk galaxy will experience a centripetal acceleration which is a strong function of the galactocentric radius. Our own acceleration, at a galactocentric radius of 8.5 kpc, is ~2 x 10^{-10} ms^{-2}, where we assumed the mass interior to R to be 10^{11} $M_{\odot}$. This comparable in magnitude to the effect caused by cosmic acceleration.

4. **Local** A characteristic local acceleration can be estimated by assuming that an object is accelerated by a large mass concentration, $10^{7}M_{\odot}$, from a distance of ~500 pc. Although this is an exaggeration, the local acceleration is only of order 10^{-11}-10^{-12} ms^{-2}. This is likely to be insignificant in comparison to the effect of cosmic acceleration.

It is obvious that the galactic acceleration is the most serious effect. We can estimate the galactic acceleration better by adopting a mass model and derive the acceleration as a function of galactocentric radius. For a Toomre disk of order n=2, we get the surface density

$$\sum(r) = \sum_0 \left(1 + \frac{r^2}{4r_0^2}\right)^{-5/2} \qquad (8)$$

where *r* is the galactocentric radius and r_0 a characteristic disk scale length (c.f. Binney & Tremaine 1987, p.,44). The acceleration as a function of galactocentric radius is shown in Figure 3. In the central parts the acceleration larger than 10^{-10} ms^{-2}, which is comparable to the acceleration caused by the retardation of the universe. At larger radii, the galactic acceleration diminishes but remains significant out to R > 10 kpc.

4.3 Instrumental limitations

The receivers at millimeter wavelengths are of the heterodyne type, which means that a local signal is fixed close to the signal frequency. The two signals are mixed and the difference is extracted. The difference signal is subsequently amplified. The heterodyne method minimizes the noise introduced in the amplifying stage.

Standard oscillators will give a signal which is stable to approximately one part in 10^{12}, giving a frequency stability of ~1 Hz. However, this signal is multiplied in several steps and the final frequency stability will be considerably worse, exceeding the value of ‘ν caused by cosmic acceleration. It is, however, likely that this problem can be overcome by using custom designed oscillators with extremely good stability at high frequency (minimizing the multiplication process).

Another problem with the heterodyne system is that it is necessary to set of the local oscillator to compensate for the velocity of the telescope as it tracks a celestial source. The accuracy of this velocity correction is limited by high order nutation and precessing of the Earth's axis. With current software, the instantaneous velocity of the telescope is calculated with a precision of ~5-10 ms^{-1}. This should be compared with the expected velocity shift of a line due to cosmic acceleration of ~0.003 ms^{-1}per year. The precision for the telescope gets progressively worse with time, and over 10 years, the accuracy is only ~50-100 ms^{-1}. This is due to irregularities in the earths movement. This precision can be improved upon by using more accurate models of the various movements of the earth. Although it is presently unclear how accurate the models can be made.

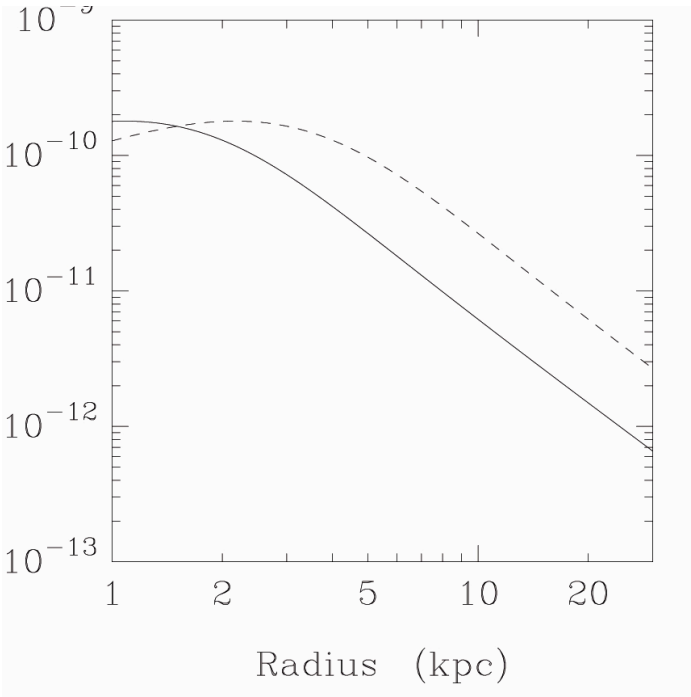

Figure 3: *The centripetal acceleration as a function of galactocentric radius in a galaxy characterized by a Toomre n=2 potential. The disk scale length is set to 2 kpc (full drawn line) and 4 kpc (dashed line). The central mass surface densityΣ_0 is set to 500 $M_\odot pc^{-2}$. The acceleration is directly proportional to Σ_0*

5 Summary and conclusions

From the above discussion it is clear that the most severe limitation to using rotational molecular absorption lines as probes of cosmic acceleration is the fact that they are located deep in the gravitational potentials of relatively large galaxies. The resulting gravitational acceleration exceed, or is of the same order, as the effect being measured. Other effects, including instrumental, have a smaller impact and do not exclude using rotational molecular absorption lines to measure cosmic acceleration.

TBased on estimates of the number of continuum sources with fluxes larger than 10 mJy at 90 GHz, and the number of molecular absorption line systems known today, it is likely that the number of absorption systems accessible to ALMA will be ~50, with 5-10 of these showing very narrow absorption lines. The number is not large enough to allow a statistical approach to overcome the effects of centripetal accelerations.

The integration time to reach sufficient S/N ratio at 1 cms^{-1} becomes forbiddingly large for continuum sources with flux levels below 10 mJy. Although this can be overcome by choosing only the strongest sources, it further limits the number of available absorption line systems and the ability to reach a statistically large sample in order to overcome the effects of centripetal accelerations.

The conclusion must therefore be that optical/UV lines offer a more viable strategy than molecular absorption lines to measure the effect of cosmic acceleration.

APPENDIX 1 - Observing molecular absorption line systems with ALMA

APPENDIX 2 - The Selection of the Quasar Sample

1 Véron-Cetty & Véron catalogue

The Véron-Cetty & Véron (2003) catalogue is the 11th edition of a compilation of known QSOs and active nuclei in the literature. It contains all the QSOs of previous editions, the final installment of the 2dF QSO survey (Croom et al. 2004) and the Data Release 1 of the Sloan Digital Sky Survey (Fan et al. 1999). This leads to a total of 48921 QSOs.

The first selection criteria we considered were based on the uncertainties pointed out in the Véron-Cetty & Véron catalogue. We omitted QSOs with inaccurate redshifts and coordinates and QSOs whose nature was doubtful. We then applied:

1 *The redshift criterion*: $1 < z_{QSO} < 5$;

2 *The magnitude criterion*:
we used the QSO magnitudes found in the Guide Star Catalogue II (GSCII, http://www-gsss.stsci.edu/gsc/gsc2/GSC2home.htm) and the SuperCOSMOS Sky Survey (SSS, http://www-wfau.roe.ac.uk/sss/) when available, as they are more accurate than the ones referred in the Vèron-Cetty & Vè'ron catalogue, otherwise we used the Véron-Cetty & Véron V magnitudes. The adopted magnitude criterion is redshift dependent in order to sample a region of the QSO spectrum redwards of the Lyα emission: for $z_{QSO} < 2.7$ we used B-magnitudes ≤18.5, for $2.7 < z_{QSO} < 4.3$ R-magnitudes ≤ 18.5, and for z_{QSO} >4.3 I-magnitudes ≤ 18.5.

As a result, from 48921 QSOs, 3271 satisfy the above selection criteria.

2 SDSS DR3

The SDSS DR3 is the most recent SDSS data release available, containing data taken up through 2003 June (Abazajian et al. 2005). It includes the objects found both in DR1 and DR2. We downloaded from the SDSS website (http://www.sdss.org/dr3/) all the objects spectroscopically classified as QSOs or high-redshift QSOs with no constraint on magnitude and position. On these 57027 QSOs found in the SDSS DR3, we applied:

1) *The redshift criterion*: $1 < z_{QSO} < 5$;

2) *The magnitude criterion*: we adopted a redshift dependent criterion by taking into account the definition of the SDSS photometric system (see Fukugita et al. 1996): for $z_{QSO} < 2.9$ we considered g-magnitudes ≤ 18.5, for $2.9 < z_{QSO} < 4.1$ r-magnitudes ≤ 18.5, and for $z_{QSO} > 4.1$ i-magnitudes ≤18.5.

As a result from 57027 QSOs, 2229 satisfy the above selection criteria.

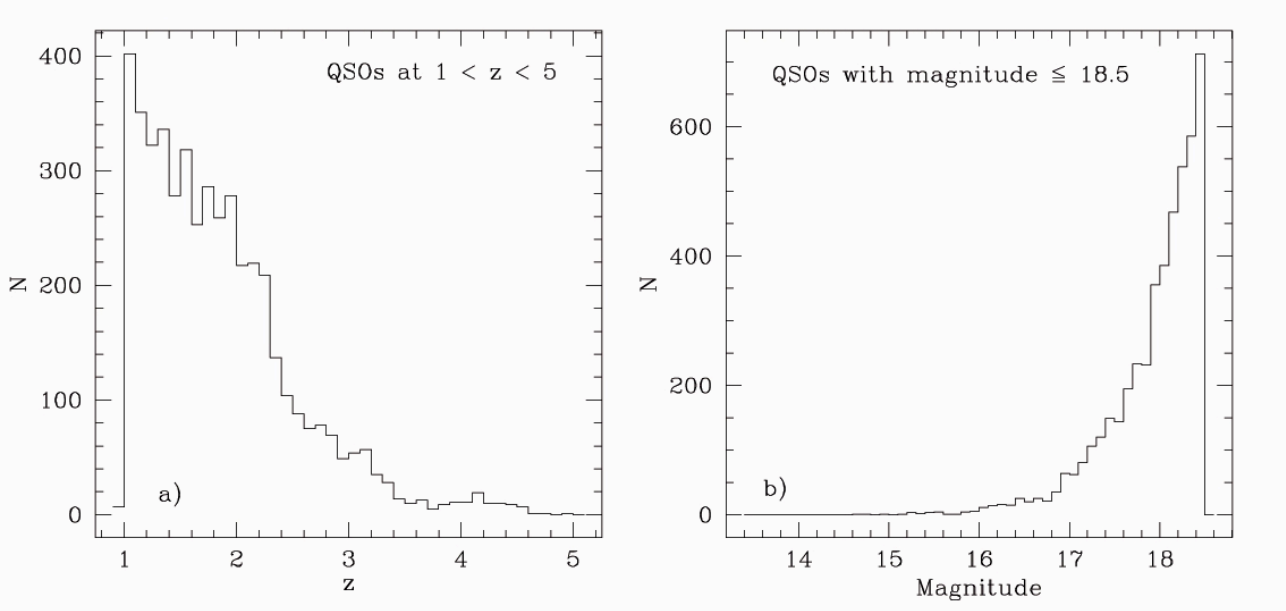

Figure 4: *The panels a) and b) show the redshift and magnitude distributions of the 4639 QSOs in our sample, respectively.*

3 The merged sample

We carefully looked for QSOs which might be duplicated in the two catalogues. To identify these QSOs we analyzed their coordinates and redshifts. We assumed that two QSOs having right ascensions and declinations within 3 arcsecs and redshifts within 0.05 are the same. After eliminating these QSOs, all others have their right ascensions and/or declinations separated by at least more than 1 arcminute.

We suppressed in this way 874 QSOs from the Véron-Cetty & Véron catalogue. We finally added 13 bright QSOs at z>4 presently unpublished (Cristiani, private communication).

In summary, a total of 4639 QSOs are a priori suitable for the CODEX experiment with redshifts between 1 and 5 and magnitudes ≤ 18.5. We show the redshift and magnitude distributions of this sample of QSOs in Figure 4 a) and b), respectively.

4 References

- Abazajian K., Adelman-McCarthy J. K., Agüeros M. A., et al. 2005, AJ 129, 1755
- Croom S. M., Smith R. J., Boyle B. J., Shanks T., Miller L., Outram P. J., Loaring N. S. 2004, MNRAS 349, 1397
- Fan X., Strauss M. A., Schneider D. P., et al. 1999, AJ 118, 1
- Fukugita M., Ichikawa T., Gunn J. E., Doi M., Shimasaku K., Schneider D. P. 1996, AJ 111, 1748
- Véron-Cetty & Véron P. 2003, A&A 412, 399

APPENDIX 3 - Precision Cosmology: present and future measurement of cosmological parameters

As discussed in the previous sections, the main goal of the CODEX experiment is a dynamic measurement of the expansion of the universe, i.e. an estimate of the time evolution of the Hubble parameter H(z). We have shown as the amount of the redshift variation (and consequently the expected signal for CODEX) depends on the main cosmological parameters, H_0, Ω_m, Ω_Λ, etc. Then an accurate a-priori knowledge of the range allowed for these parameters will be essential for extracting the signal of cosmic expansion in the CODEX experiment.

When the CODEX experiment is expected to be carried out, “precision cosmology” will be in its golden age, thanks to different projects now under study or construction: the expectation is that future results will allow a measurement of the main cosmological parameters with an accuracy of about few per cent.

This Appendix presents the various observables which can be used now and in the next future to put robust constraints. They are based on the cosmic microwave background, the Supernovae Ia, the Lyman-alpha clouds, the galaxy clusters and weak lensing. For each method, we discuss the basics, the underlying assumptions, the systematics, the accuracy of their estimates of the cosmological parameters as obtained up to now and as expected in the next few years.

1 The cosmic microwave background (CMB)

1.1 Method

The standard model of Big Bang predicts that our Universe was highly ionized until the recombination epoch ($z \approx 1000$) when neutral hydrogen formed from the combination of electrons and protons. After this moment the universe became transparent and the radiation, which before was tightly coupled to electrons via Thomson scattering, can propagate toward the observer, originating the CMB. Two different mechanisms are responsible for the anisotropies which are observed in the CMB. On large angular scales ($\theta \geq 1^o$) the anisotropies arise from the Sachs-Wolfe effect, i.e. from the fluctuations of the gravitational potential; this is directly related to the amplitude and slope of the primordial power spectrum, giving constraints on σ_8 and on the spectral index *n*. CMB fluctuations at smaller angular scales are the consequence of the acoustic oscillations of the fluid of matter and radiation hen they are causally connected. These oscillations have characteristic scales related to the size of the horizon at recombination, the maximum scale allowed for oscillations, creating prominent features called peaks. The study of the anisotropies on these scales gives information on the geometry of the universe thanks to the relation between angular separation and physical distance. Moreover, since the acoustic oscillations depend on the sound speed at recombination, one can obtain constraints on the matter content of the universe.

1.2 Present Results

The main problem in deriving the cosmological parameters from CMB anisotropies comes from their degeneracy: different combinations can produce almost identical CMB anisotropy spectra. In particular this problem is strong when studying the density parameters because the peak position is essentially a measurement of the geometry of the universe, i.e. of $\Omega_k = 1 - \Omega_m - \Omega_{\Box}$. At present the best estimates come from the analysis of the first-year data collected by the WMAP satellite (Bennett et al. 2003; Spergel et al. 2003). By assuming a flat universe with radiation, baryons, CDM and cosmological constant, and a power spectrum of adiabatic primordial fluctuations, the WMAP data only give $\Omega_m = 0.14 \pm 0.02\ h^{-2}$, $\Omega_b = 0.024 \pm 0.001\ h^{-2}$, $h = 0.72 \pm 0.05$, $\sigma_8 = 0.9 \pm 0.1$ and $n = 0.99 \pm 0.04$. By relaxing the flatness requirement, but including a weak prior $h > 0.5$, the WMAP data only suggest $-0.02 < \Omega_k < 0.08$ at 95 per cent level. Combining CMB data

with constraints from high-redshift supernovae, gives $-0.02 < \Omega_k < 0.06$ without prior, or $\Omega_k < 0.02 \pm 0.02$ including the HST KP estimate of the Hubble constant.

1.3 Systematics

The physical processes involved in the CMB anisotropies are based on the well known equations for the evolution of the perturbations of a matter--radiation fluid in the linear regime, which is quite robust. Data analysis can, however, suffer for some systematics. First, at large angular scales, the CMB power spectrum is strongly affected by the so-called cosmic variance, i.e. by the fact that they are not well sampled by the unique available realization of the universe. This problem strongly affects the determination of the amplitude and slope of the primordial power spectrum.

Second, the extraction of all parameters is done by assuming that the statistics for primordial fluctuations is gaussian, as expected by standard inflationary models. One more standard assumption is that primordial fluctuations are adiabatic, as suggested by preliminary results for polarization obtained by the WMAP team.

On smaller scales observational data can be strongly affected by contaminants, such as secondary CMB anisotropies (Sunyaev-Zel'dovich effects, Rees-Sciama effect, Ostriker-Vishniac effect, integrated Sachs-Wolfe effect, gravitational lensing, re-ionization, etc.), extragalactic sources (like radio sources, quasars, dusty galaxies, etc.) and galactic sources (Milky Way structure, compact stellar objects, dust): for this reason suitable algorithms for component separation, mainly based on numerical simulations, are required.

1.4 Future perspectives

The near future will be represented by the analysis of the data collected during the four years of operation of WMAP, possibly combined with high-resolution angular scale experiments (e.g. ACT and SPT), which hopefully could measure anisotropies up to l~2000, entirely free of any systematic errors over few per cent of the sky. Errorbars are expected to be reduced by a factor of 3-4 for the density parameters Ω_b and Ω_m, and for the primordial spectral index n. A further factor of 2 will be gained when the data of the first year of observations by the Planck satellite will be analyzed (in 2008-2009): the expectation is to have measurements of the CMB power spectrum to almost cosmic variance accuracy up to l~2500. Planck will be able to break the degeneracy between parameters by using the polarization observations.

Finally Planck will provide stronger constraints on the nature of primordial fluctuations in terms of gaussianity and adiabaticity.

2 The SNe Ia

2.1 Method

The most recent results (Riess et al. 2004), based on high redshift type-Ia Supernovae (SNe Ia) confirm the picture of a non-empty inflationary Universe that is consistent with a cosmological constant $\Omega_\Box \sim 0.7$. This implies that the expansion of the Universe is currently accelerated by the action of some mysterious dark energy. The firm determination of cosmological parameters with this method is based on the possibility of calibrating SNe Ia as standard candles. In this respect, SNe Ia are particular interesting because:

- they are very bright ($M_B \sim -19.5$ at peak);
- their absolute magnitude at maximum is well known;
- they are relatively common (in ~ 100 galaxies one may expect several SN explosions per year);
- they can be found in early and late type galaxies.

2.2 Properties of Supernovae Ia

The basic approach to determine cosmological parameters from SNe observations is contained in the relation between the apparent magnitude m, the absolute magnitude M, the absorption A due to dust extinction and the intervening luminosity distance d_L:

$$m(z) = M + 5\log_{10} d_L\,(z, \Omega_m, \Omega_\square, H_0) + 25 + A \qquad (1)$$

SNe Ia are not perfect standard candles: their absolute magnitudes correlate with second parameters, like rate of decline ($\square m_{15}$), light curve shape, SN color, spectral features (correlated with temperature) and Hubble type or color of the parent galaxy (Pskovskii 197, 675; Phillips 1993; Parodi et al. 2000). The second-parameter corrections are a serious problem because the nine calibrating SNe Ia have slower decline rates, are bluer and lie in later-type galaxies than the distant SNe Ia (Panagia 2005). As a result, current determinations of H_0 based on SNe Ia vary between 55 (Schaefer 1998) and 71 (Freedman et al. 2001).

2.3 High-z SN Ia and Cosmological Constant

With SNe Ia, one could measure the deceleration parameters without measuring H_0, assuming that the peak magnitude of SNe Ia is the same at all redshifts. Two international teams (Riess et al. 1998; Perlmutter et al. 1999) found ~100 SNe Ia at z>0.2 to study the cosmological parameters Ω_m and $\Omega_\square$. The first results indicated that, at high redshifts ($0.2 < z < 0.8$), distant SNe are dimmer than expected. R98, using a sample of 16 high-z SNe Ia, determined the likelihood for the cosmological parameters using a χ^2 analysis over the parameters Ω_m, H_0, and $\Omega_\square$, and found a best-fit result of $\Omega_\square = 0.68 \pm 0.10$ for a flat universe.

This result is consistent with an acceleration of the Universe ($\Omega_\square > 0$), but also with grey dust or monotonic evolutionary effects at high-z.

The SNe Ia evidence for acceleration was tightened up by the discovery and the study of SN Ia at redshifts higher than 1. Recently Riess et al. (2004) used GOODS data to discover 11 SNe Ia at z> 1, confirming the brightening of SNe at z> 1. A pure kinematic interpretation of the SNe Ia sample provides evidence for a transition from deceleration to acceleration at $z=0.46 \pm 0.13$ and is consistent with the cosmic concordance model of $\Omega_m \sim 0.3$ and $\Omega_\square \sim 0.7$, ruling out grey dust or monotonic evolutionary effects at high-z.

2.4 Systematics

The robustness of the $\Omega_\square > 0$ result depends on whether the intrinsic brightnesses of high-z SNe Ia are artificially affected by some unaccounted systematic effects:

- Extinction (host galaxy, IGM)
- Non-monotonic evolution
- Selection bias
- Sample contamination
- Lensing effect
- Second parameters (e.g., metallicity).

2.5 Two types of SNe Ia?

Mannucci et al. (2005) showed that there are two distinct population of SNe Ia, the “prompt” SNe, which dominates at high redshifts where the star formation is particularly active, and the “tardy” SNe, dominant species at lower redshifts where the SF is rapidly declining. In particular, in the local universe SNe Ia occurring in late type galaxies are systematically brighter than those occurring in early type galaxies (Filippenko 1989; Della Valle & Panagia 1992; Hamuy et al. 1996; Howell 2001). Extending this trend to all

redshifts, one would predict the alarming effect that SNe Ia at intermediate-z should be intrinsically dimmer than those at ≥ 1, mimicking the behavior of a cosmological constant (Panagia 2005).

3 Lyman-α

3.1 Methods

The Lyman-α forest is a unique probe of the dark matter power spectrum at scales corresponding to 1-40 h^{-1} comoving Mpc and at redshift z<6. Although several cosmological parameters can be estimated from the analysis of global statistical properties of the QSO spectra (see for example Bi & Davidsen 1997), all the present attempts to use the Lyman-α forest as a cosmological probe rely on the recovery of the linear dark matter power spectrum from the observed flux power spectrum $P_F(k)$

This method has been originally proposed by Croft et al. (1998) and has been subsequently improved by several authors (Croft et al. 2002; Gnedin & Hamilton 2002; Viel, Haehnelt & Springel 2004). It is based on the determination using hydro-dynamical simulations of a biasing function, b(k), which relates the flux and the matter power spectra $P_F(k) = b^2(k)P(k)$, at a given wavenumber k. Another alternative method is the one presented in McDonald et al. (2004), which relies on less computational expensive simulations run with the Hydro-Particle-Mesh technique (Gnedin & Hui 1998): an approximate method to simulate the low density intergalactic Medium. Since these simulations are a factor ~ 100 faster than full hydrodynamical ones, an exploration of a wide parameter space, that includes cosmological (shape and amplitude of the dark matter power spectrum) and astrophysical parameters (gas temperature, fluctuations in the UltraViolet Background, strong absorption systems, reionization....), is feasible. The first method has been applied to high resolution UVES spectra, while the second uses the low resolution SDSS QSO data set.

3.2 Results

We note that the recovered values of the slope *(n)* and amplitude (σ_8) of the primordial power spectrum we are going to discuss now do not depend on Ω_m, since in any popular cosmological model the value of Ω_m approaches one at high redshift. Moreover, the estimate is insensitive to the value of Ω_b, since the dependency on this parameter is cancelled out when normalizing to a given mean flux.

The Lyman-α forest dark matter power spectra recovered by Croft et al. (2002) and more recently by Viel, Haehnelt & Springel (2004) agree very well within the errors. The present uncertainties on the overall amplitude of the dark matter power spectrum are of the order of 25% (1σ) and the main contribution is that of systematic errors (see discussion in Section 3.12.3.3). The final results are more significant when combined with the large scales estimates of CMB experiments and can basically halve the errors on the values of n and σ_8 that are obtained from the CMB alone. When combining the WMAP 1st year data release with the Lyman-α forest dark matter power spectrum we get: σ_8=0.94 ± 0.08, n_s=0.99 ± 0.03 (Viel, Weller & Haehnelt 2004) . The same parameters, as recovered by the SDSS collaboration are the following σ_8=0.89 ± 0.03, n_s =0.98 ± 0.02 (Seljak et al. 2004). In addition, the two groups have found no evidence for a running of the spectral index n_s, as was claimed by the WMAP team (Spergel et al. 2003). Thereby, there is overall agreement on the recovered cosmological parameters obtained from two different QSO data set and with very different analysis methods.

3.3 Systematics and Improvements

Possible improvements for the estimate of the cosmological parameters using the Lyman-α forest rely almost entirely on the understanding of the many systematic effects.

In fact, there are a number of different systematics that contribute to the overall error on the rms fluctuation amplitude of the density field. The different systematic uncertainties, at the scales and redshifts considered here, are due mainly to the errors on the following quantities: effective optical depth measurement; interpretation of the data obtained with different numerical codes; poorly constrained thermal history of the intergalactic medium; effect due to the presence of galactic winds; metal contamination in the Lyman-□ forest.

In particular, the dominant contributions are the estimate of the mean flux (or effective optical depth) and the uncertainties in the numerical simulations modelling. At present the effective optical depth has an observational uncertainty of 10% which translates into a 7-8% uncertainty on the rms fluctuation amplitude of the recovered density field. The error introduced by different numerical codes has a similar contribution to the final estimate. Statistical errors seem to be less important and contribute up to 4% to the rms fluctuation amplitude.

A promising way of improving the estimate would be to extend the wavenumber range used in the analysis above. In particular, the largest scales are affected by continuum fitting errors, while the smallest scales cannot be used because of contamination by metal and uncertainties on the thermal state of the intergalactic medium. An estimate of how much the uncertainties in the measured cosmological parameters can be pinned down is difficult since an accurate modeling of the quasar continuum, the intergalactic medium thermal evolution and metal enrichment mechanism is needed.

It is not clear how much the estimates on cosmological parameters can be improved with future QSO data set, since statistical errors are subdominant compared to the systematic ones. The SDSS data set contains over 3000 QSO spectra at low resolution (20 times worse than UVES spectra) and the statistical error on the recovered power spectrum amplitude is of the order of 15%. A possible improvement could be in achieved by re-analyzing some of the SDSS spectra at higher resolution to have better estimates of the errors introduced by continuum fitting in order to extend the range of wavenumbers used. With a more accurate knowledge of the thermal state of the Intergalactic Medium it would be possible to decrease the error bar on the power spectrum amplitude σ_8 of ~5% percent.

Presently, the main limitations are on the theoretical side, and an ultimate goal which can be surely achieved within 5-10 yrs would be the full exploration of a wide parameter space using hydrodynamical simulations able to properly model the physics of the Intergalactic Medium.

4 Galaxy clusters

4.1 Methods

In the standard picture of structure formation based on the gravitational instability paradigm, clusters of galaxies represent the largest gravitationally bound systems in the universe. This is the reason for their cosmological importance. In fact, since the expected displacements from their primordial positions are much smaller than their typical separations, clusters retain the imprint of the main cosmological parameters, which can hopefully be constrained by studying their properties. In the past this opportunity has been largely exploited using cluster counts and their redshift evolution, obtaining tight constraints on the matter density parameter Ω_m and power-spectrum normalization σ_8.

The fundamental theoretical ingredient is the cosmological mass function, which, starting from the Press-Schechter formalism, has been calibrated by using the results of high-resolution N-body simulations (Sheth & Tormen 1999; Jenkins et al. 2001; Springel et al. 2005). However it is quite difficult to obtain a reliable complete sample of clusters with measured masses. Alternative methods make use of theoretical and/or observational relations between the mass and other observables, like the velocity dispersion and the X-ray temperature or luminosity. Since the range of masses is limited and the corresponding physical scales depend both on the mass and on Ω_m, by using the number density of nearby clusters it is possible to obtain

constraints only on a relation between the amplitude of the power spectrum σ_8 and Ω_m, unless one makes assumptions on the DM content of the Universe and, therefore, on the relation between the shape of the power spectrum and Ω_m (e.g. Schuecker et al. 2003). The only way to break the degeneracy is by studying the redshift evolution of the cluster population, taking advantage of the dependence of the linear growth rate of density perturbation on the matter and dark energy density parameters.

An alternative method to measure Ω_m is based on the baryon fraction f_b, which can be measured with X-ray observations. In fact the matter density can be estimated as $\Omega_m = \Omega_b / f_b$ if the baryon density Ω_b is known in an independent way (e.g. primordial nucleosynthesis and spectrum of CMB anisotropies). Furthermore it is possible to estimate the cosmological parameters by using the gas mass fraction for clusters at high redshift by exploiting its dependence on the angular diameter distance and assuming that the gas fraction remains constant with respect to the look-back time.

4.2 Results

By translating the temperature function of nearby clusters into a mass function, the obtained constraints are $\sigma_8 \, \Omega_m^{\,0.4\text{-}0.6} = 0.4\text{-}0.6$ (e.g. Henry et al. 2005, and references therein).

By analyzing the redshift evolution of the cluster abundances, by using velocity dispersion, X-ray temperature or luminosity, one obtains $\Omega_m \sim 0.3 \pm 0.2$, where the error must be interpreted as a combination of statistical uncertainties of each single analysis and difference among different analyses (e.g. Rosati, Borgani & Norman 2002; Voit 2005, for reviews). No useful information are instead obtained so far on the value of Ω_Λ.

From the measurement of $f_b \sim 0.15$, it is possible to show the consistency of Ω_m with a value of 0.3, when $\Omega_b h^2 \sim 0.02$ is assumed together with $h \sim 0.7$ (e.g. Allen et al. 2001).

Using the method based on the gas fraction in combination with a priori constraints on Ω_b (primordial nucleosynthesis) and H_0 (HST-Key project), Ettori et al. (2003) found $w < -0.49$; $\Omega_m = 0.34^{+0.11}_{-0.08}$ and $\Omega_\Lambda = 1.30^{+0.44}_{-1.09}$ when $w=-1$ is assumed; $\Omega_m = 1 - \Omega_\Lambda = 0.33^{+0.07}_{-0.05}$ for a flat universe (see also Allen et al. 2004).

4.3 Systematics

The theoretical interpretation of the mass function is well set, even if the application of the different proposed modelizations (i.e Sheth & Tormen vs. Jenkins et al.) can produce small differences in the high end of the mass function. Notice, however, that as all cosmological tests based on linear/nonlinear evolution of perturbations, also that based on the cluster mass function assumes primordial gaussian fluctuations, the only assumption for which a robust framework has been built so far.

As discussed in several papers (e.g. Borgani et al. 2001) there are large uncertainties in relating the theoretical quantity, the virial mass, to the observables, like X-ray temperature and luminosity. The scaling relations suggested by a simple model assuming spherical symmetry, hydrostatic equilibrium and isothermality of the gas, are violated at a 20-30% level, according to hydrodynamical simulations (e.g Rasia et al. 2004). Moreover the redshift evolution of such scaling relations, which is required when exploiting the different cluster evolution to break the degeneracy between Ω_m and σ_8, still requires a better calibration from observational data.

4.4 Future perspectives

In the next 10 years we foresee no significant observational progress in the X-ray band because of the absence of new financed projects for satellites. However, cluster serendipitous surveys, based on Chandra and XMM-Newton archives will represent true gold mines to increase the number of high-redshift galaxy clusters. A better knowledge of the physical properties of clusters (shape, density and temperature profiles, etc.), as currently obtainable from Chandra and XMM-Newton observations of nearby clusters, are potentially very useful to calibrate the uncertainties in the mass estimates.

A significant improvement can be provided by SZ surveys of galaxy clusters. Several different projects (Planck, ACT, ACBAR, AMIBA, AMI, APEX, CBI, BOLOCAM, SZA, etc.) will be able in the next future, thanks to the absence of cosmological dimming for the SZ signal, to identify clusters out to z>1. Since the SZ signal comes from a more extended region with respect to the X-ray one, cluster counts based on SZ are more dependent on the inner modelization of the cluster structure. A related problem is the accurate determination of the selection function for SZ based surveys, which must be taken into account in the statistical analyses. It is likely that the best strategy would be again to have surveys with X-ray selection, to have a selection function under control, with high--resolution SZ follow-up to estimate the cluster masses.

5 Weak Lensing

5.1 Method

The use of the weak lensing signal to constrain cosmological parameters is based on the measurement of the distortion of the galaxy shapes induced by mass inhomogeneities in the universe. The simplest statistics of the shear field, the two-dimensional power spectrum, is directly proportional to Ω_m and involves a line-of-sight integral of quantities related to the nonlinear matter power spectrum $P_{nl}(k)$ and angular-diameter distance, both strongly depending on the cosmological model. To compute $P_{nl}(k)$ one has to assume a linear power spectrum and makes use of analytical relations extracted from N-body simulation (Peacock & Dodds 1996; Smith et al. 2003). More computationally convenient statistics are based on integrated relations of the lensing power spectrum, like the shear variance or the aperture mass, or exploit the non-Gaussian aspects of the shear field, like the skewness of the converge field, the lensing bispectrum or the peak statistic. In this way it is possible to obtain from measurements of the lensing power spectrum estimates for Ω_m, Ω_Λ, σ_8 and Γ.

5.2 Results

By analyzing the VIRMOS-Descart data, van Waerbeke et al. (2004) found $\sigma_8=(0.83 \pm 0.07)(\Omega_m /0.3)^{-0.49}$, marginalizing the shape parameter of the power spectrum, Γ, in the range [0.1-0.3] and the mean source redshift in the range [0.8-1.0]. Combining their results with those from WMAP, they found that CDM models with Ω_m >0.5 are excluded at 3σ. Consistent results have been obtained by Hoekstra et al. (2003) from the Red-sequence Cluster survey. Jarvis & Jain (2004) and Jarvis et al. (2005), revisiting the CTIO lensing survey, found $\sigma_8=0.812^{+0.146}_{-0.100}$ (95% confidence level) when a Λ CDM with Ω_m =0.3 is assumed, or a (constant) dark energy equation of state parameter $w=-0.894^{+0.156}_{-0.208}$.

5.3 Systematics

The main limitation in determining the cosmological parameters from weak lensing measurements is the absence of a severe control of systematic effects, which have been listed and discussed by Refregier (2003). The most important for ground-based surveys is the large PSF ellipticity, which can be only limited in the future because of the finite surface density and signal-to-noise ratio of stars used for calibration. Other effects come from CCD nonlinearities or by possible overlap of galaxy isophotal contours creating spurious ellipticities. A further source of uncertainty is related to the lack of complete information about the redshift distribution of galaxies: this problem can be overcome only with dedicated spectroscopic surveys or by using accurate photometric redshifts. Systematic effects can be originated also by the existence of intrinsic alignments of the galaxy shapes, created by the tidal field, galaxy interaction or coupling of the angular momentum. Finally the necessity of correcting the matter power spectrum for the effect of non-linear evolution requires accurate analytical models extracted from N-body results. At present the accuracy of the predictions is below the 10% level.

5.4 Future perspectives

In the next future there are plans for different instruments dedicated to surveys and for which cosmic shear is a primary goal. Just to mention some of the ground-based ones: VISTA will cover 10000 sq. deg. by using a 4 meter telescope with a FOV of 3 sq. deg. (starting year 2007); Pan-STARSS will cover from 2008 31000 sq. deg. with four 1.8 meter telescopes, each of them with a FOV 4 sq. deg.; LSST from 2012 will use a 8.4 meter telescope with a FOV of 7 sq. deg. to cover 30000 sq. deg. From the space a large improvement in the quality and quantity of the data will come from the SNAP project: the plan is to have a wide-field survey covering one thousand sq. deg. in both northern and southern hemispheres resolving approximately 100 galaxies per sq. arcmin, for a total of more than 300 million galaxies. In this case, combining the weak lensing data to the SNe Ia results, obtained within the same project, the expected accuracy in the determination of Ω_m and Ω_Λ are 0.01 (assuming w=-1); assuming a flat universe the expected accuracy in the estimate of the parameters defining the dark energy equation of state is very good (0.05 for the present value of w and 0.11 for the redshift evolution).

An alternative candidate implementation of the NASA-DOE Joint Dark Energy Mission (JDEM) is JEDI (Joint Efficient Dark-energy Investigation), which is a 2 meter aperture space telescope capable of simultaneous wide-field imaging and multiple object spectroscopy with a field of view of 1 square degree. JEDI is expected to provide three independent ways to probe dark energy: distance-redshift relations of type Ia supernovae (SNe Ia), baryonic oscillations from a galaxy redshift survey, and weak lensing cross-correlation cosmography. In particular JEDI will conduct an ultra-deep survey of 36 square degrees over three years, yielding data simultaneously for the SN Ia, galaxy redshift, and weak lensing surveys. Because of its efficiency in making SN Ia observations, there is the option of devoting the third year exclusively to a wide survey (1000 square degrees) for galaxy redshifts and weak lensing measurements.

6 Conclusions

This short summary of the actual status and of the perspectives of precision cosmology clearly shows as this branch is extremely vital and is probably witnessing an un-precedent “golden age”.

In the next years we shall know with un-precedent accuracy the values of many cosmological parameters. However, as noted in section 1, all these measurements are geometric in nature, and, in addition, several require a number of assumptions on the evolution of the objects or are potentially plagued by biases and systematic effects. Making a parallel, we could say that in a few years we will be in a situation similar to the one of knowing perfectly the first Kepler law, but knowing nothing about the second one. We shall recall that if, and only if GR in its FWR formulation holds, then the dynamics and the geometry of the Universe are related in the way we expect. The dynamical measurement performed by CODEX is independent, clean, and it is unique.

In addition, all the other experiments will investigate the values of the cosmological parameters either at very high redshift (e.g. CMBR), or at redshifts <~ 2 (e.g. SNae, Clusters); CODEX will instead study the nature of these parameters in a redshift range ~2 to 4.5 , complementary to the other studies.

7 References

- Allen, S. W.; Schmidt, R. W.; Ebeling, H.; Fabian, A. C.; van Speybroeck, L., 2004, MNRAS,353, 457
- Allen, S. W.; Schmidt, R. W.; Fabian, A. C., 2001, MNRAS, 328, L37
- Bennett, C. L.; Halpern, M.; Hinshaw, G.; Jarosik, N.; Kogut, A.; Limon, M.; Meyer, S. S.; Page, L.; Spergel, D. N.; Tucker, G. S.; Wollack, E.; Wright, E. L.; Barnes, C.; Greason, M. R.; Hill, R. S.; Komatsu, E.; Nolta, M. R.; Odegard, N.; Peiris, H. V.; Verde, L.;Weiland, J. L., 2003, ApJS, 148, 1
- Bi, H.; Davidsen, A. F., 1997, ApJ, 479, 523
- Borgani, Stefano; Rosati, Piero; Tozzi, Paolo; Stanford, S. A.; Eisenhardt, Peter R.; Lidman, Chris; Holden, Bradford; Della Ceca, Roberto; Norman, Colin; Squires, Gordon, 2001, ApJ, 561, 13

- Croft, Rupert A. C.; Hernquist, Lars; Springel, Volker; Westover, Michael; White, Martin, 2002, ApJ, 580, 634
- Croft, Rupert A. C.; Weinberg, David H.; Katz, Neal; Hernquist, Lars, 1998, 495, 44
- Della Valle, M.; Panagia, N., 1992, AJ, 104. 696
- Ettori, S.; Tozzi, P.; Rosati, P., 2003, A&A, 398, 879
- Filippenko, A. V., 1989, PASP, 101, 588
- Freedman, Wendy L.; Madore, Barry F.; Gibson, Brad K.; Ferrarese, Laura; Kelson, Daniel D.; Sakai, Shoko; Mould, Jeremy R.; Kennicutt, Robert C., Jr.; Ford, Holland C.; Graham, John A.; Huchra, John P.; Hughes, Shaun M. G.; Illingworth, Garth D.; Macri, Lucas M.; Stetson, Peter B., 2001, ApJ, 553, 47
- Gnedin, Nickolay Y.; Hamilton, Andrew J. S., 2002, MNRAS, 334, 107
- Gnedin, Nickolay Y.; Hui, Lam, 1998, MNRAS, 296, 44 Hamuy, Mario; Phillips, M. M.; Suntzeff, Nicholas B.; Schommer, Robert A.; Maza, Jose; Aviles, R., 1996, AJ, 112, 2391
- Henry, J. Patrick, 2004, ApJ, 609, 603
- Howell, 2001, ApJ, 554, 193
- Jarvis, Mike; Jain, Bhuvnesh, 2004, astro-ph/0412234
- Jarvis, Mike; Jain, Bhuvnesh; Bernstein, Gary; Dolney, Derek, 2005, astro-ph/0502243
- Jenkins, A.; Frenk, C. S.; White, S. D. M.; Colberg, J. M.; Cole, S.; Evrard, A. E.; Couchman, H. M. P.; Yoshida, N., 2001, MNRAS, 321, 372 Mannucci, F.; della Valle, M.; Panagia, N.; Cappellaro, E.; Cresci, G.; Maiolino, R.; Petrosian, A.; Turatto, M., 2005, A&A, 433, 807
- Panagia, N. 2005, astro-ph/0502247
- Parodi, B. R.; Saha, A.; Sandage, A.; Tammann, G. A., 2000, 540, 634
- Peacock, J. A.; Dodds, S. J., 1996, MNRAS, 280, L19
- Perlmutter, S.; Aldering, G.; Goldhaber, G.; Knop, R. A.; Nugent, P.; Castro, P. G.; Deustua, S.; Fabbro, S.; Goobar, A.; Groom, D. E.; Hook, I. M.; Kim, A. G.; Kim, M. Y.; Lee, J. C.; Nunes, N. J.; Pain, R.; Pennypacker, C. R.; Quimby, R.; Lidman, C.; Ellis, R. S.; Irwin, M.; McMahon, R. G.; Ruiz-Lapuente, P.; Walton, N.; Schaefer, B.; Boyle, B. J.; Filippenko, A. V.; Matheson, T.; Fruchter, A. S.; Panagia, N.; Newberg, H. J. M.; Couch, W. J.; 1999, ApJ, 517, 656
- Pskovskii, Iu. P., 1977, Sov, Astron., 21, 675
- Rasia, Elena; Tormen, Giuseppe; Moscardini, Lauro, 2004, MNRAS, 351, 237
- Refregier, Alexandre, 2003, ARA&A, 41, 645
- Riess, Adam G.; Filippenko, Alexei V.; Challis, Peter; Clocchiatti, Alejandro; Diercks, Alan; Garnavich, Peter M.; Gilliland, Ron L.; Hogan, Craig J.; Jha, Saurabh; Kirshner, Robert P.; Leibundgut, B.; Phillips, M. M.; Reiss, David; Schmidt, Brian P.; Schommer, Robert A.; Smith, R. Chris; Spyromilio, J.; Stubbs, Christopher; Suntzeff, Nicholas B.; Tonry, John, AJ, 116, 1009
- Riess, A.G.; Strolger, L.-G.; Tonry, J.; Casertano, S.; Ferguson, Henry C.; Mobasher, B.; Challis, P.; Filippenko, A. V.; Jha, S.; Li, W.; Chornock, R.; Kirshner, R. P.; Leibundgut, B.; Dickinson, M.; Livio, M.; Giavalisco, M.; Steidel, Charles C.; Benítez, T.; Tsvetanov, Z., 2004, ApJ, 607, 665
- Rosati, Piero; Borgani, Stefano; Norman, Colin, 2002, ARA&A, 40, 539
- Schaefer, B.E., 1998, ApJ, 509, 80
- Schuecker, P.; Böhringer, H.; Collins, C. A.; Guzzo, L., 2003, A&A, 398, 867
- Seljak, Uros; Makarov, Alexey; McDonald, Patrick; Anderson, Scott F.; Bahcall, Neta A.; Brinkmann, J.; Burles, Scott; Cen, Renyue; Doi, Mamoru; Gunn, James E.; Ivezic', Željko; Kent, Stephen; Loveday, Jon; Lupton, Robert H.; Munn, Jeffrey A.; Nichol, Robert C.; Ostriker, Jeremiah P.; Schlegel, David J.; Schneider, Donald P.; Tegmark, Max; Berk, Daniel E.; Weinberg, David H.; York, Donald G., 2005, Ph.Rev. D, 71, 103515
- Sheth, Ravi K.; Tormen, Giuseppe, 1999, MNRAS, 308, 119
- Smith, R. E.; Peacock, J. A.; Jenkins, A.; White, S. D. M.; Frenk, C. S.; Pearce, F. R.; Thomas, P. A.; Efstathiou, G.; Couchman, H. M. P., 2003, MNRAS, 341, 1311
- Spergel, D. N.; Verde, L.; Peiris, H. V.; Komatsu, E.; Nolta, M. R.; Bennett, C. L.; Halpern, M.; Hinshaw, G.; Jarosik, N.; Kogut, A.; Limon, M.; Meyer, S. S.; Page, L.; Tucker, G. S.; Weiland, J. L.; Wollack, E.; Wright, E. L., 2003, ApJS, 148, 175
- Springel, Volker; White, Simon D. M.; Jenkins, Adrian; Frenk, Carlos S.; Yoshida, Naoki; Gao, Liang; Navarro, Julio; Thacker, Robert; Croton, Darren; Helly, John; Peacock, John A.; Cole, Shaun; Thomas, Peter; Couchman, Hugh; Evrard, August; Colberg, Jörg; Pearce, Frazer, 2005, Nat, 435, 629
- Van Waerbeke, L.; Mellier, Y.; Hoekstra, H., 2005, A&A, 429, 75
- Viel, Matteo; Haehnelt, Martin G.; Springel, Volker, 2004, MNRAS, 354, 684

- Viel, Matteo; Weller, Jochen; Haehnelt, Martin G., 2004, MNRAS, 335, L23
- Voit, M., 2005, Rev, Mod. Phys. 2005, 77, 20